Paul H. Jones

Geothermal and Hydrocarbon Regimes, Northern Gulf of Mexico Basin

Dr. Jones is professor of geology at Louisiana State University, Baton Rouge, Louisiana.

ABSTRACT

Geothermal heat flow in the Gulf basin is primarily a function of its hydrology. Water expelled from sediments with deepening burial and increasing overburden load escapes upward and toward the basin margin. Where it moves freely in the hydropressure zone, the basin is relatively cool; but where rapid sedimentation and contemporaneous faulting have retarded water loss from compacting sediments, the interstitial fluid pressure reflects a part of the overburden load, and the formation waters are superheated and geopressured. The geopressured zone is common below depths of about 3 km (9,600 ft) in the basin, beneath an area of 375,000 km^2 (150,000 mi^2), and extends downward perhaps 15 km (50,000 ft) to the base of Cenozoic deposits.

The upper boundary of the geopressured zone is the most important physical interface in the basin. Across it the head of formation water increases downward from a few hundred to several thousand feet above sea level; the geothermal gradient increases downward from 20° to 40° C/km to 100°C/km or more; the salinity of formation water decreases downward, commonly by 50,000 mg/l or more; and the porosity of shale and sand increases downward by 10 to 25 percent.

Petroleum matures in geopressured clay at 140° to 220°F. Montmorillonite is dehydrated at 180° to 250°F; fresh water released may equal half the volume of the mineral altered. Molecular solubility in fresh water of the hydrocarbons in Gulf basin crude, under geopressured zone conditions, could account for petroleum resources of the basin. Exsolution of petroleum hydrocarbons near the geopressured zone boundary could account for observed occurrences.

This geopressured zone is a natural pressure vessel from which superheated water of moderate salinity could be produced through wells, each yielding millions of gallons a day at pressures of several thousand pounds per square inch, and temperatures above 300°F, with considerable amounts of methane gas in solution.

CONTENTS

DISCLAIMER

FIGURES

TABLES

NOTICE

This paper was prepared with the support of the Geological Survey, United States Department of the Interior. This report has not been reviewed for conformance with Survey standards for stratigraphic nomenclature.

Inclusion of this paper in the *Proceedings of the First Geopressured Geothermal Energy Conference* held at The University of Texas at Austin was authorized by the Director, U.S. Geological Survey, on May 5, 1975.

ACKNOWLEDGMENTS

Ideas and interpretations presented in this paper are mainly those of the author, developed with the assistance of R. H. Wallace and J. B. Wesselman of the Gulf Basin Hydrogeology Project, Gulf Coast Hydroscience Center, Water Resources Division, at Bay St. Louis, Mississippi. Studies leading to this paper were based upon information received through many colleagues in oil company offices. Especially notable among these are T. D. Cook, C. E. Hottman, C. A. Stuart, W. C. Finch, and Gordon Rittenhouse of Shell Oil Co.; B. B. Mason, C. D. Jones, C. W. Holcomb, and R. E. Taylor, of Exxon Co., USA; H. R. Gould, P. H. Monaghan, and C. R. Hocott of Exxon Production Research Co.; W. A. Fowler of Phillips Petroleum Co.; G. W. Schmidt, C. H. Hedge, and R. W. Duschatko of Amoco Production Co.; R. S. Agatston, Rush George, R. O. McGinnis, and G. D. Roe of Atlantic-Richfield Co.; M. K. Horn of Cities Service Oil Co.; J. E. McCall, C. J. McGinnis, R. E. Murphy, and R. L. Woodward of Chevron Oil Co.; A. T. Hengle, A. G. Ostroff, and P. A. Mundt of Mobil Research and Development Corp.; J. A. Stone and C. H. Bruce of Mobil Oil Corp.; R. L. Layden of Sun Oil Co.; M. Rathke of Tenneco; V. O. Cook of Gulf Oil Corp.; J. G. McKelvey of Gulf Research and Development Co.; R. H. Valentien of Coastal States Gas Producing Co.; and M. J. Moore of George Coates Co. Without the advice, assistance, and encouragement of these and many others, the studies would not have been possible.

INTRODUCTION

Recent discoveries regarding the maturation, primary migration, and commercial accumulation of fluid hydrocarbons in geologically young, petroleum-producing basins of the world are keyed to the role of groundwater in the hydrothermal regime. These discoveries have resulted in new concepts in petroleum exploration, which are immediately applicable using data obtained by current exploration methods.

The rate of hydrocarbon generation from kerogen disseminated through clay deposits is temperature controlled. The chemical changes in clay minerals that release bound and crystalline water as free pore water at high pressure and low salinity are temperature controlled. The solubility of petroleum hydrocarbons in water increases enormously with rising temperature and fluid pressure. Groundwater is the principal factor in heat flow through sediments thus the hydrodynamic regime and the hydrothermal regime combine to determine the fluid hydrocarbon regime.

Hydrocarbons dissolved in superheated, high-pressure formation waters come out of solution—as petroleum and natural gas—wherever pressure is released and temperature drops, or where the salinity of the formation water is increased. Accumulation of the newly formed petroleum and natural gas occurs where the fluids enter suitable reservoir structures in the direction of decreasing hydraulic head. In the northern Gulf of Mexico basin some 90 percent of the commercial oil has been found in reservoirs in which the ratio of the fluid pressure to the pressure resulting from the weight of the overburden rock load (the geostatic ratio) is less than than approximately 0.7, and a majority of these reservoirs had pressures reflecting geostatic ratios greater than 0.5. This is the zone of maximum pressure differential in Gulf basin deposits. This is where the depth-pressure gradient of the geopressure zone grades into that of the hydropressure zone.

Degradation of petroleum at high temperature and pressure, in the presence of natural catalysts (clay minerals) in the geopressure zone, has resulted in the wholesale conversion of liquid hydrocarbon to methane gas. Less than 1 percent of Gulf Coast oil has been found in reservoirs at temperatures above 150°C (302°F). Because of the very high solubility of methane in low-salinity water at high temperature and pressure, many excellent structural traps in the geopressure zone have been found barren of fluid hydrocarbon. Where gas occurs in the vapor phase in such traps, the associated waters must be saturated. Appreciable reduction in reservoir pressure with production would cause exsolution of methane, replenishing the reservoir and reducing the rate of pressure decline.

The hydrothermal regime that governs the hydrocarbon regime of the northern Gulf of Mexico basin also describes its geothermal resources. The "floor" beneath which liquid hydrocarbons do not occur in significant amounts in the basin, marked approximately by the depth of occurrence of the 150° (302°F) isothermal surface, is the "roof" of the geopressured geothermal system. And beneath this roof another energy realm is yet to be developed. An entirely new technology will be required, not only for the exploration and appraisal of the geopressured geothermal resources, but also for their capture and use. Current misconceptions, incorrect inferences, and fundamental misunderstandings regarding deep sedimentary basin hydrology need to be identified, examined, and revised in the light of new knowledge.

Petroleum hydrocarbons and geopressured superheated water in Cenozoic deposits of the northern Gulf of Mexico basin make it one of the world's major energy provinces. No other petroleum-producing basin in the world has been studied more intensively with the latest and most effective methods in geology, geophysics, and engineering, using the most sophisticated instrumentation and analytical technology. Limitations on the effectiveness of these studies can be attributed to faulty or poorly developed concepts and to gaps in knowledge and misunderstanding resulting therefrom.

The synthesis of possible systems using information on the hydrodynamic, hydrothermal, hydrochemical, and hydrocarbon regimes of the basin can provide new insight into the commercial accumulation of petroleum hydrocarbons, as well as lay the basis for development of both geothermal resources and methane gas dissolved in the deep ground waters (usually saline) in the basin.

GEOLOGY

The Gulf of Mexico basin is one of the world's oldest ocean basins, having formed during the earliest phase of continental drift, some 160 million years ago (Dietz and Holden, 1971). The sediments that floor the basin are probably

of late Pennsylvanian age (Lehner, 1969), and although the Gulf is classed as an enclosed sea and is compared to the Black Sea and the North Sea, it appears to have had continuous, although for long periods restricted, connection with the World Ocean. Garrison and Martin (1973) state that the Gulf of Mexico basin " . . . is underlain by oceanic crust . . . depressed substantially below the levels of equivalent crustal layers in normal ocean basins," and ". . . has gained its present form wholly from a combination of sedimentary and intrabasin tectonic processes."

The area of the Gulf of Mexico is about 1.5 million square kilometres (km^2) (580,000 square miles). If the volume of sedimentary fill suggested in figure 1 is any indication, its present size is almost tiny by comparison with its original dimensions. Figure 1 is a regional profile of the earth's crust and upper mantle across the Gulf basin from East Texas to Yucatan. Important features of the basin include the patterns of sedimentary fill, the configuration of the Mohorovicic discontinuity (Moho), the thinning of the crust between the Oligocene trend and the Sigsbee Knolls, and the remarkable effects of salt diapirism. According to Worzel Watkins (1973), recent seismic refraction studies show that along Lehner's profile the continental crust thins gulfward and is absent beneath the Gulf Continental Shelf.

The Moho—the depth below the earth's surface at which ". . . the velocity of earthquake waves jumps from about seven kilometres per second to eight"—marks the top of the mantle and ". . . a change in the chemical composition or crystal structure rather than an abrupt transition from strong to weak material" (Anderson, 1971). The Moho is not an isothermal surface, and temperatures within the mantle differ markedly with depth, depending upon its composition. For example, the temperature at the Moho is estimated to be about 2,200°K (1,930°C) for "dunite" and about 1,500°K (1,230°C) for "basalt" (Lee, 1968), assuming constant pressure or depth of burial. Where the Moho occurs at depths less than 20 km (64,000 ft) beneath the Gulf Continental Shelf and less than 14 km (45,000 ft) beneath the Sigsbee Deep, the temperature is probably in the range of 1,300° to 1,500°K (approximately 1,000° to 1,200°C). In the Mesozoic rocks near the axis of the Gulf Coast geosyncline (Barton, Ritz, and Hickey, 1933), the temperature is probably greater than 500°C (932°F), indicated by the occurrence of serpentine pipes of mid-Cretaceous age in oilfield structures of the Gulf Coastal Plain (Raleigh and Patterson, 1965).

Cooling of upper mantle material immediately below the basin floor may have caused a sinking current in the mantle, accounting for progressive deepening of the basin since it was formed (Bullard, 1971). The oceanic crust beneath the Gulf basin ranges in thickness from about 5 to 10 km (16,000 to 32,000 ft). Deposits of late Pennsylvanian through Triassic age are generally less than 1 km (3,200 ft) thick beneath the deepest parts of the Gulf Coast geosyncline.

Immediately above the pre-Jurassic sandstone, shale, anhydrite, and limestone and extending throughout the Gulf basin, according to Garrison and Martin (1973), is the Jurassic Louann Salt. This "mother" salt bed has been thinned by diapiric flow and is almost absent in broad areas. It was squeezed gulfward by sand and clay deposits of prograding deltas, its remnants forming countless domes, ridges, and massifs. According to Hanna (1958), this occurred in three main cycles (fig. 2). In the East Texas salt basin and gulfward from the Eocene Trend salt diapirs have risen through the full thickness of overlying deposits. In the deepest parts of the basin, they penetrate up to 15 km (48,000 ft) of overlying sediments, some 12 km (38,000 ft) of which are upper Cretaceous, Tertiary, and Quaternary clastics. The tops of salt diapirs were

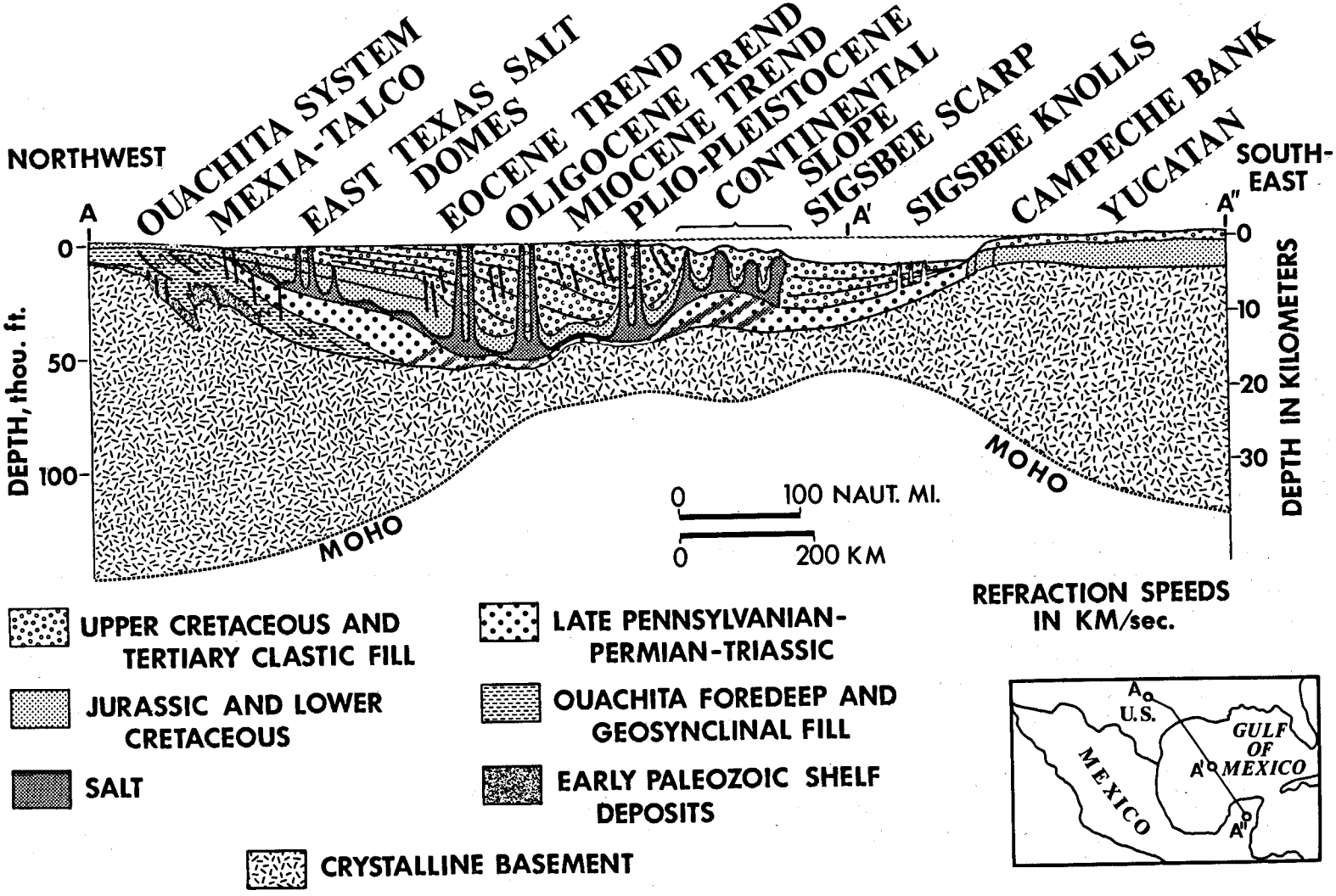

Figure 1. Profile section through the earth's crust and upper mantle from East Texas to Yucatan, showing sedimentary fill of the Gulf Coast geosyncline, effects of salt diapirism, and rise of the Moho between the Oligocene Trend and the Sigsbee Knolls.

commonly no more than a few thousand feet below the surface of deposition, and sometimes they rose above it.

The areal distribution of salt domes and inferred salt domes in the northern Gulf of Mexico basin is shown in figure 3. Not shown are the salt ridges and massifs beneath the outer continental shelf and slope depicted in figure 1. Widespread distribution and rather uniform scatter of salt domes is especially notable; only in the South Texas Coastal Plain and adjacent parts of the Gulf Continental Shelf are the domes few in number and widely spaced, probably because the mother salt bed was relatively thin in this area (Garrison and Martin, 1973).

The occurrence of a thick and extensive salt layer near the base of the sedimentary fill has had a marked effect upon the structural and depositional

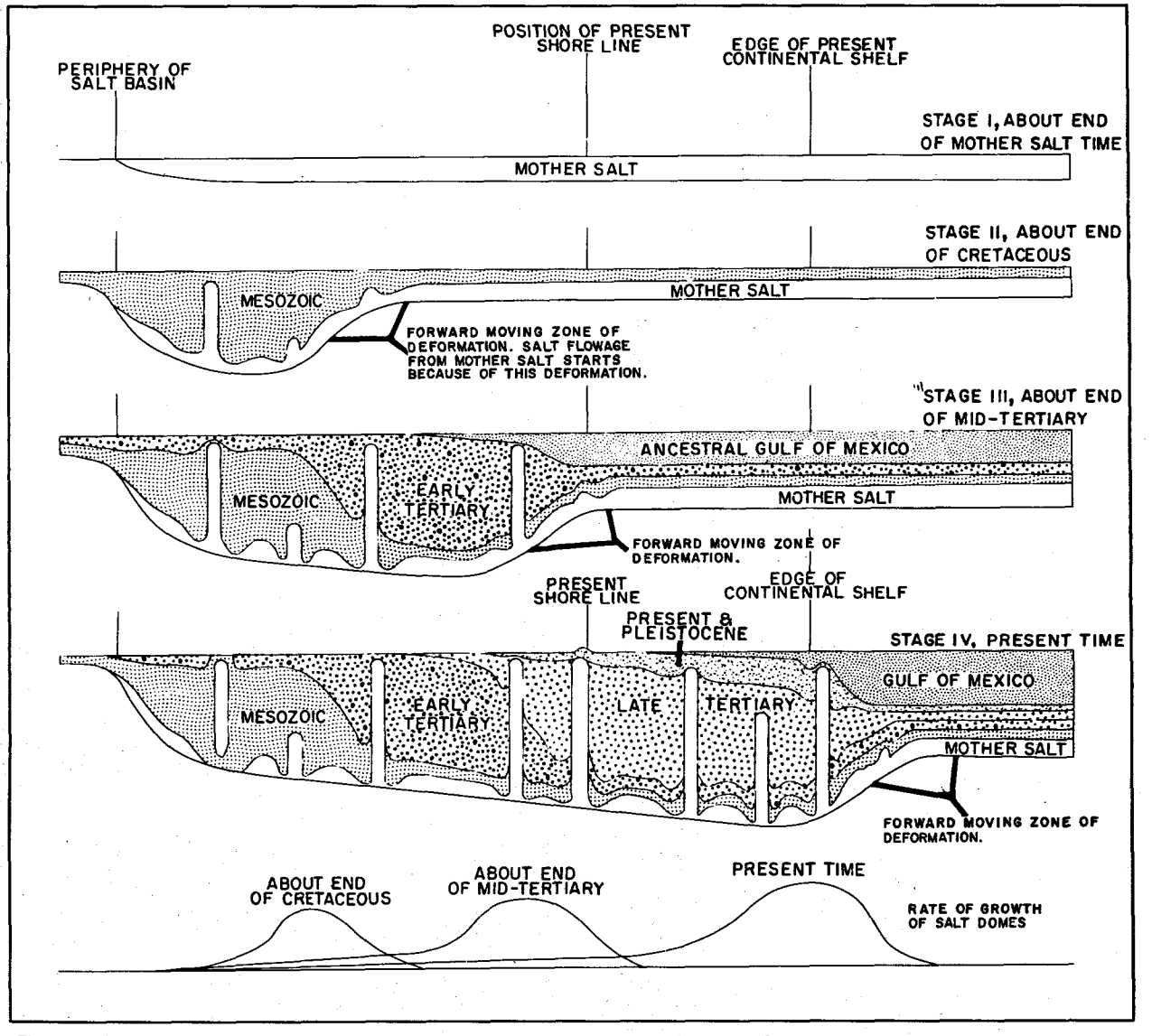

Figure 2. Idealized geologic sections, showing four stages in the development of the Gulf Coast geosyncline and their relation to flowage of salt and the rate of growth of salt domes, along the line of figure 1.

history of the basin since Jurassic time. This is due in part to the relatively low density, and in part to the thermophysical properties of salt. The thermal conductivity of halite (rock salt) is about 13 mcal/cm sec °C. At 200°C (392°F), salt is plastic in one direction; at 300°C (572°F) it is a perfect plastic, having only about 12 percent of its load-bearing strength at 25°C (77°F). Between temperatures of 300° and 800.8°C (572° and 1,474°F), at which it melts, the density of salt is less than 2.1. (See fig. 4.) Diapiric salt is a dominant factor in both the heat flow and structural evolution of the Gulf basin. Diapirism appears to have occurred at temperatures in excess of 300°C (572°F), because halite crystals show intense mechanical deformation with no evidence of strain (Balks, 1949, 1953), except near the margins of the domes, where cooling effects are apparent (Clabaugh, 1962).

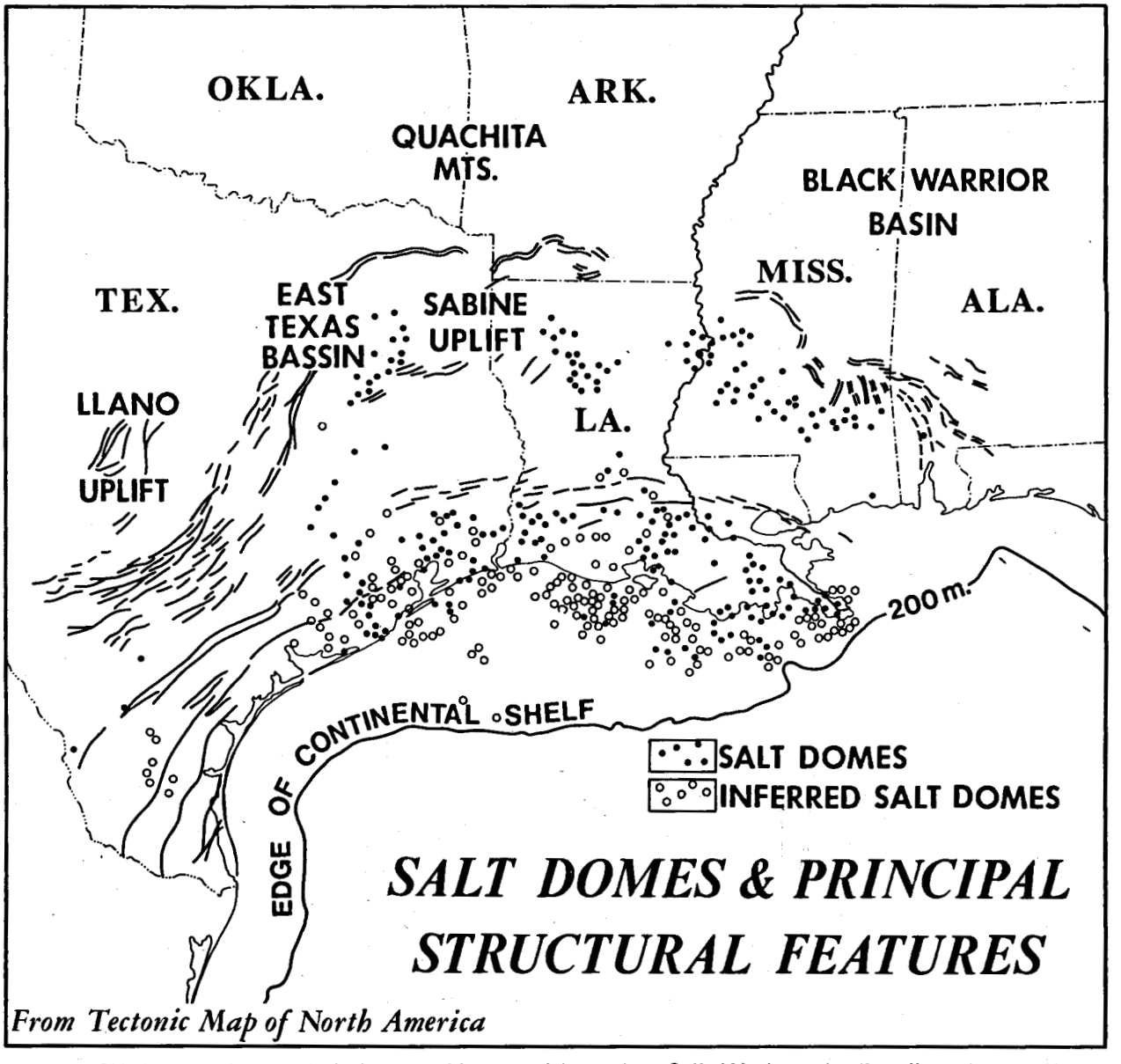

Figure 3. Salt domes and other principal structural features of the northern Gulf of Mexico region (from Tectonic map of North America).

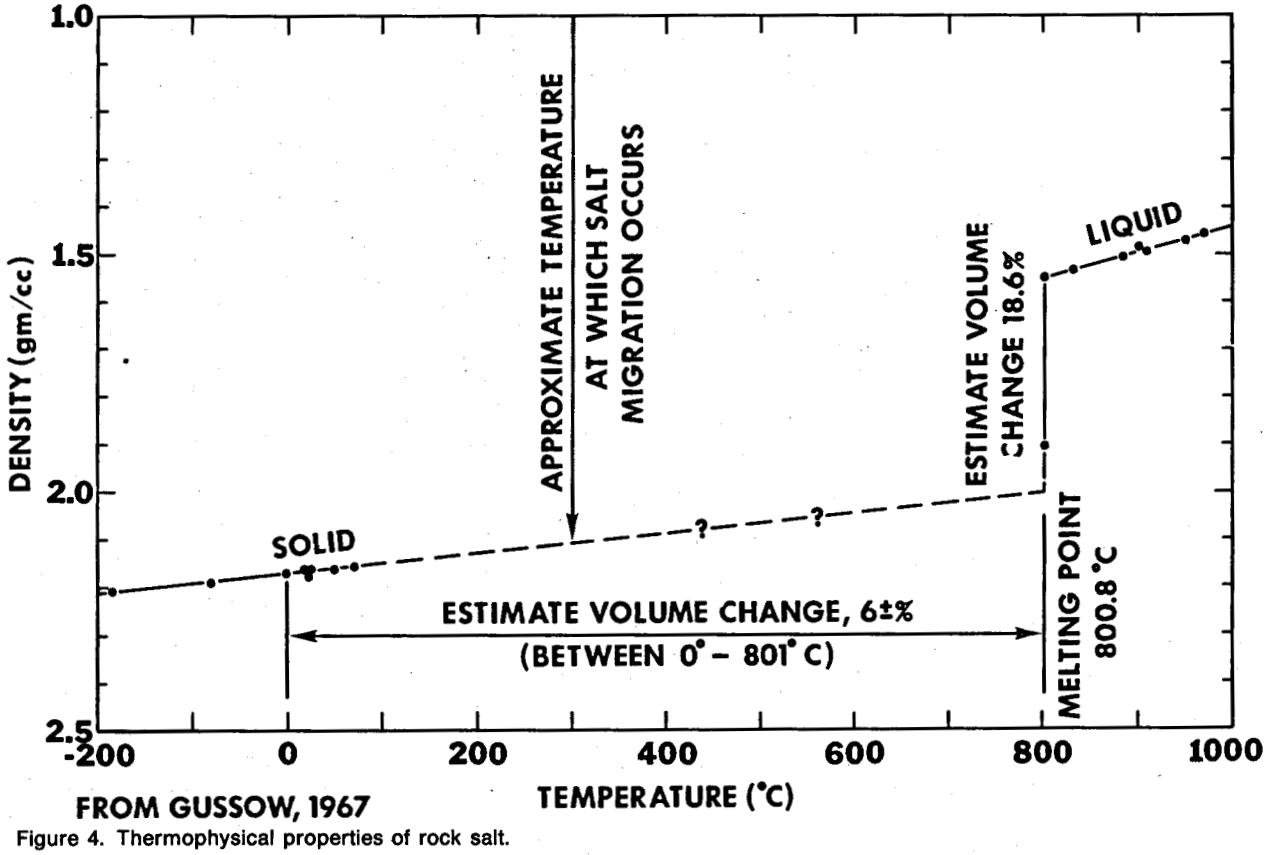

Figure 4. Thermophysical properties of rock salt.

The Louann Salt was blanketed by shale and limestone as subsidence of the floor of the Gulf basin began; according to Wilhelm and Ewing, (1972), "extensive regional subsidence of more than 10,000 ft (more than 3 km) during Cretaceous time" produced the basin, and "isolation came about by continuous contemporaneous carbonate growth of the Florida and Yucatan platforms." The thickness of deposits along the northern margin of the basin at the end of the Cretaceous time is shown on the north-south profile, figure 5, which also shows effects of rapid filling by noncarbonate clastic sediments during Eocene, Oligocene, and Mio-Plio-Pleistocene time. Collapse of the salt bed and its thin limestone cap beneath prograding sediments was accompanied by growth faulting in the overlying sand and clay deposits, progressive gulfward flowage of salt, and intrusion of overlying sediments by diapiric salt.

With the Laramide uplift of the Rocky Mountain area a great flood of noncarbonate clastic sediment spread across the plains and spilled into the deep waters of the Gulf. These Cenozoic deposits completely fill the Gulf Coast geosyncline, along the northwest margin of the basin, and have a volume exceeding 4 million cubic kilometres (a million cubic miles). According to Hardin (1962), the aggregate thickness of the deposits exceeds 15 km (about 48,000 ft) in the deepest parts of the geosyncline. The form of the geosyncline and the thickness of Cenozoic deposits as described by Hardin, are shown in figure 6. Meyerhoff (1968) indicates that the aggregate thickness of deposits of Vicksburg (Oligocene) and younger age is greater than 17,600 metres (58,700 ft) in coastal Louisiana, and 9,300 metres (31,000 ft) in coastal Texas. This enormous mass of sediments was formed in some 37 million years.

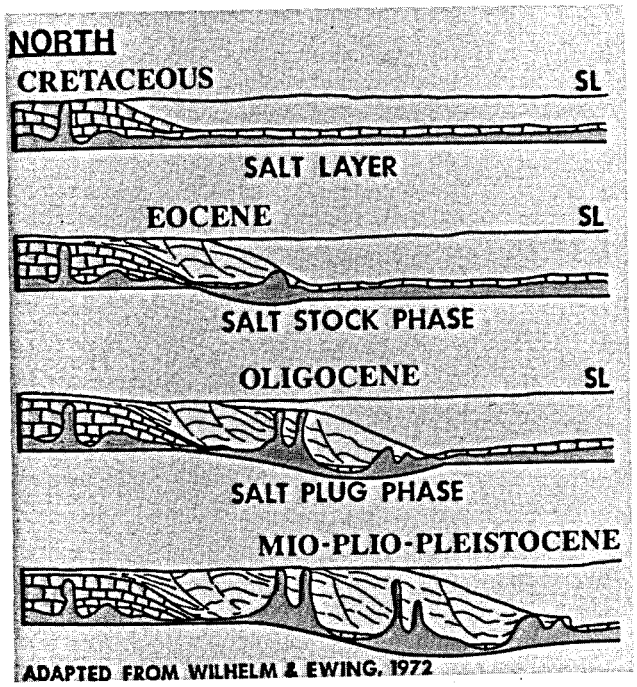

Figure 5. Idealized geologic sections, showing the effects of Cretaceous carbonate rocks on the structural evolution of the Gulf Coast geosyncline, along the line of figure 1.

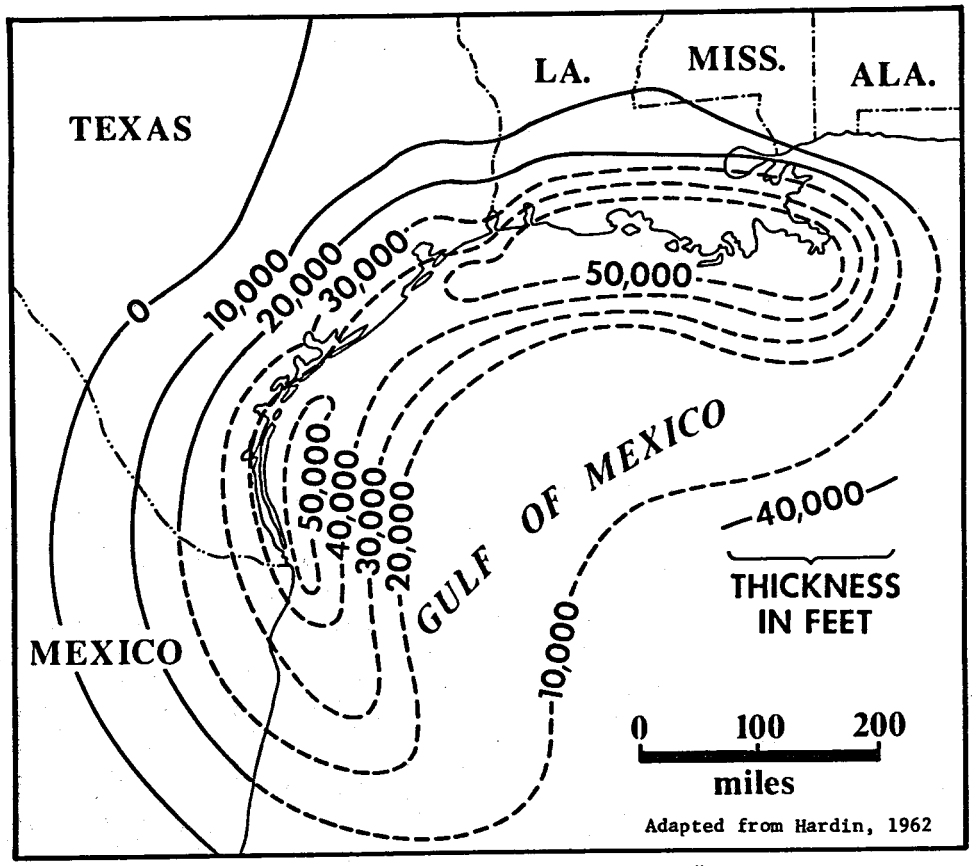

Figure 6. Thickness of Cenozoic deposits in the Gulf Coast geosyncline.

The sediments carried to and deposited in the Gulf basin during the Cenozoic were primarily clay and sand: the clay is largely of montmorillonite with lesser amounts of illite, kaolinite, and chlorite; the sand is mainly quartz of many varieties. These are evidently the end products of rock weathering in a temperate climate, regardless of the mineralogy of the parent rocks (Milne and Earley, 1958). The principal site of deposition during the early Cenozoic is now known as the Texas Coastal Plain and adjacent Gulf Continental Shelf, and the rivers that accomplished the fill ranged widely between the Sabine Uplift and the Rio Grande. Since early Miocene time, the principal site of deposition is now known as the Louisiana Coastal Plain and adjacent Gulf Continental Shelf.

The filling of the Gulf Coast geosyncline was accomplished in eight major cycles of prograding sedimentation, corresponding to eight major deltaic systems and their marine derivatives. These are shown schematically in the profile, figure 7, adapted from Bruce (1973). This profile crosses the South Texas Coastal Plain near Corpus Christi, and accordingly shows no effects of salt diapirism. Each younger deltaic system overrides its predecessor, forming a

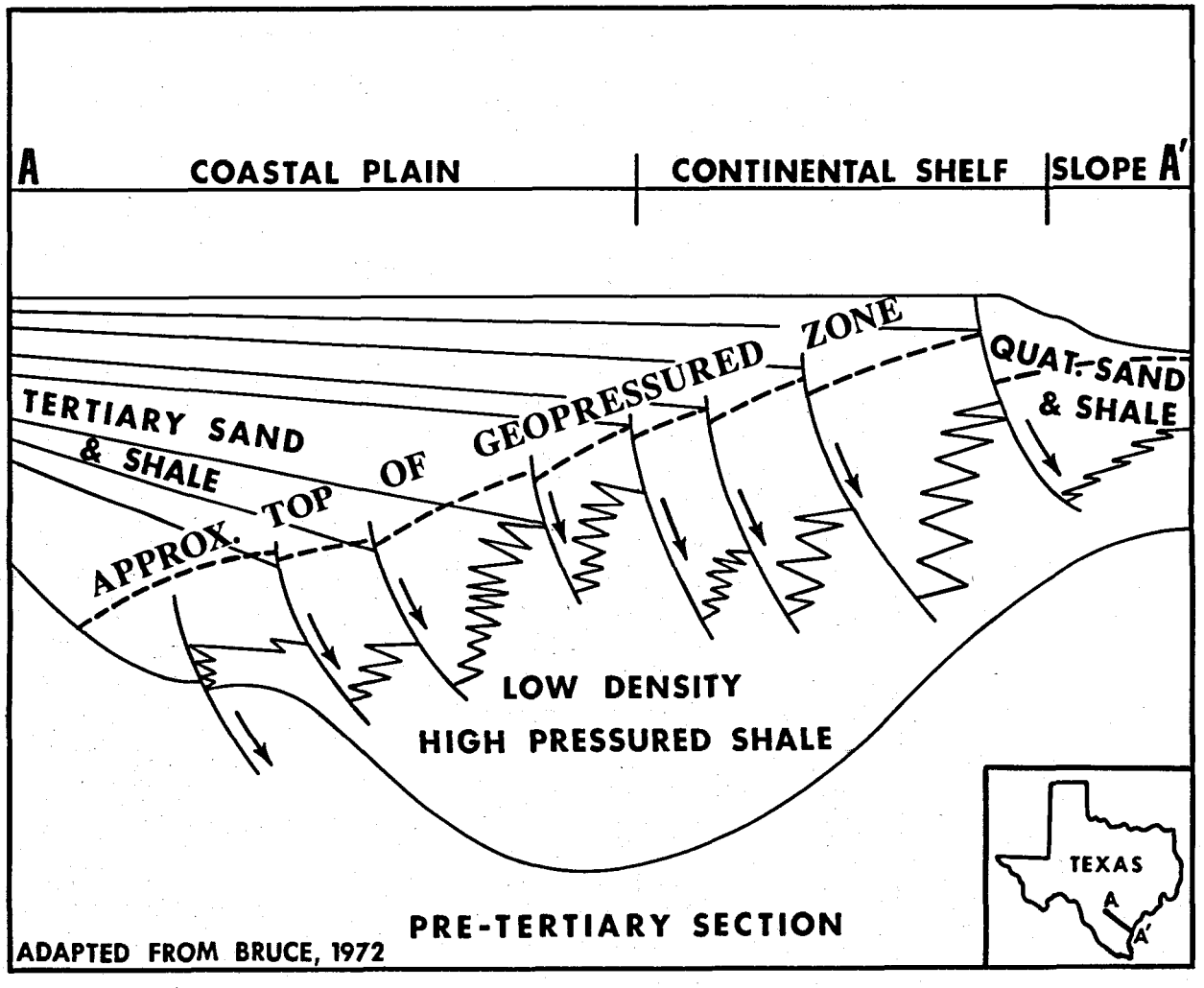

Figure 7. Geologic dip section across South Texas Coastal Plain, showing growth-fault systems in major Cenozoic delta deposits and their relation to the top of the geopressure zone.

wedge of deposits that gradually thickens gulfward. At the gulfward extremity of each wedge, a downward-thickening mass of sandy sediments has formed along a shear zone that cuts deeply into prodelta and marine clay deposits of older deltaic systems. This shear zone dies out at depth in geopressured shale (Bruce, 1973).

Prograding sandy deposits caused the shear zone to develop by overloading undercompacted shale and draining it like a filter press; increasing mass was accommodated by progressive subsidence. When the resistance to water expulsion from deposits below and within the "filter press" resulted in abnormally high fluid pressure, the subsidence rate was reduced or temporarily stopped. This cycle of deposition, water expulsion, downwarp, shear, and progressive rotation of deposits into the fault plane (with resulting reversal of dip) and stabilization (at least for a time) characterizes the contemporaneous fault zones of the Gulf basin. Locally, these faults are called "growth faults" (Ocamb, 1961). The cycle was repeated at differing scales in the distal parts of each major delta system, and the depositional processes define the geometry of sand-bed aquifer systems in the down-thrown blocks. In the geopressured section, the master faults shown in figure 7 have been and continue to be the major avenues of water discharge (Hubbert and Rubey, 1959). These fault planes receive flow from an infinite number of branch faults in the down-thrown block until one or more of the branch faults grows upwards and reaches the hydropressure zone in the resulting collapse belt (Bruce, 1973). Sand beds in the down-thrown block drain adjacent clay beds and discharge water at high pressure into the planes of the master faults. Drainage is accompanied by compaction, and the resultant losses in permeability gradually shut off the flow.

As shown in figure 7, the top of the geopressure zone in the Teritary deposits slopes landward from the Gulf shoreline. This is because the drainage of the younger Tertiary growth-faulted deposits is less advanced than in the older deposits, and the volume of the deposits formed in the younger cycles was progressively greater. The top of the geopressure zone in Quaternary deposits may be very shallow or very deep, depending upon sediment facies. Drainage is at a very early stage, the size of the depositional mass is very great, and the relative amount of coarse-grained material is large.

In plan, growth fault zones of the northern Gulf basin trend roughly parallel to the modern shoreline, as shown in figure 8 for the early Eocene Wilcox group in Texas. Also mapped on figure 8 is a system of faults which formed during post-Wilcox time; these faults cut and displace Wilcox beds without change in thickness across them, but show growth-fault characteristics in the overlying Yegua beds. Structural effects of both fault zones on Wilcox deposits are shown in the four dip sections, *A–A′* (fig. 9), *B–B′* (fig. 10), *C–C′* (fig. 11), and *D–D′* (fig. 12), the locations of which appear in figure 8. Whether or not the Wilcox post-depositional faults continue downward into Paleocene marine deposits is not known.

The areal distribution of sediment facies in lower Wilcox deposits is shown in figure 13 and in the upper Wilcox in figure 14. These maps, based on unpublished data provided by the Texas Bureau of Economic Geology, were used for identification of lithologic types shown in the cross sections, figures 9 through 12.

In the section shown in figure 9, which roughly parallels the axis of the Rio Grande embayment, Wilcox deposits show almost no growth faulting but are cut by many post-depositional faults in the gulfward half of the section. As the deposits shown were largely formed in sediment-starved coastal barrier or

shelf environments, the absence of loading effects is not surprising. The only notable fluvial channel meander belt deposits occur in the upper Wilcox, and they have excellent continuity to depths greater than 1.3 km (4,200 ft).

In the section shown in figure 10, which closely follows the axis of the San Marcos Arch, growth faulting effects are apparent in the middle and upper Wilcox deposits. A narrow belt of post-depositional faults has effectively flattened the apparent dip immediately gulfward from the massive lower Wilcox delta plain deposits.

In the section shown in figure 11, which trends southeastward into the Houston embayment salt basin, structural deformation is related to deep salt

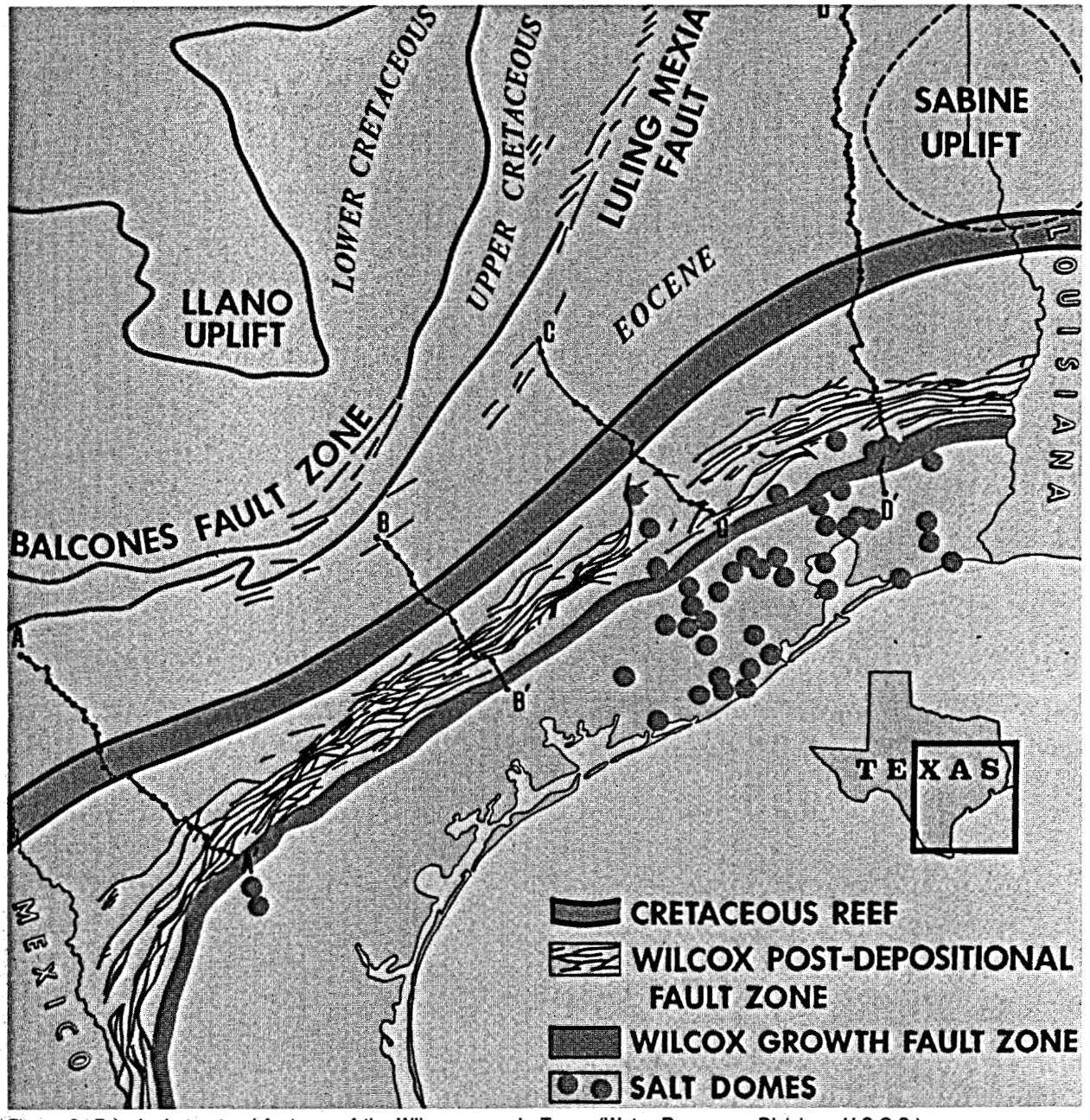

Figure 8. Principal structural features of the Wilcox group in Texas (Water Resources Division—U.S.G.S.).

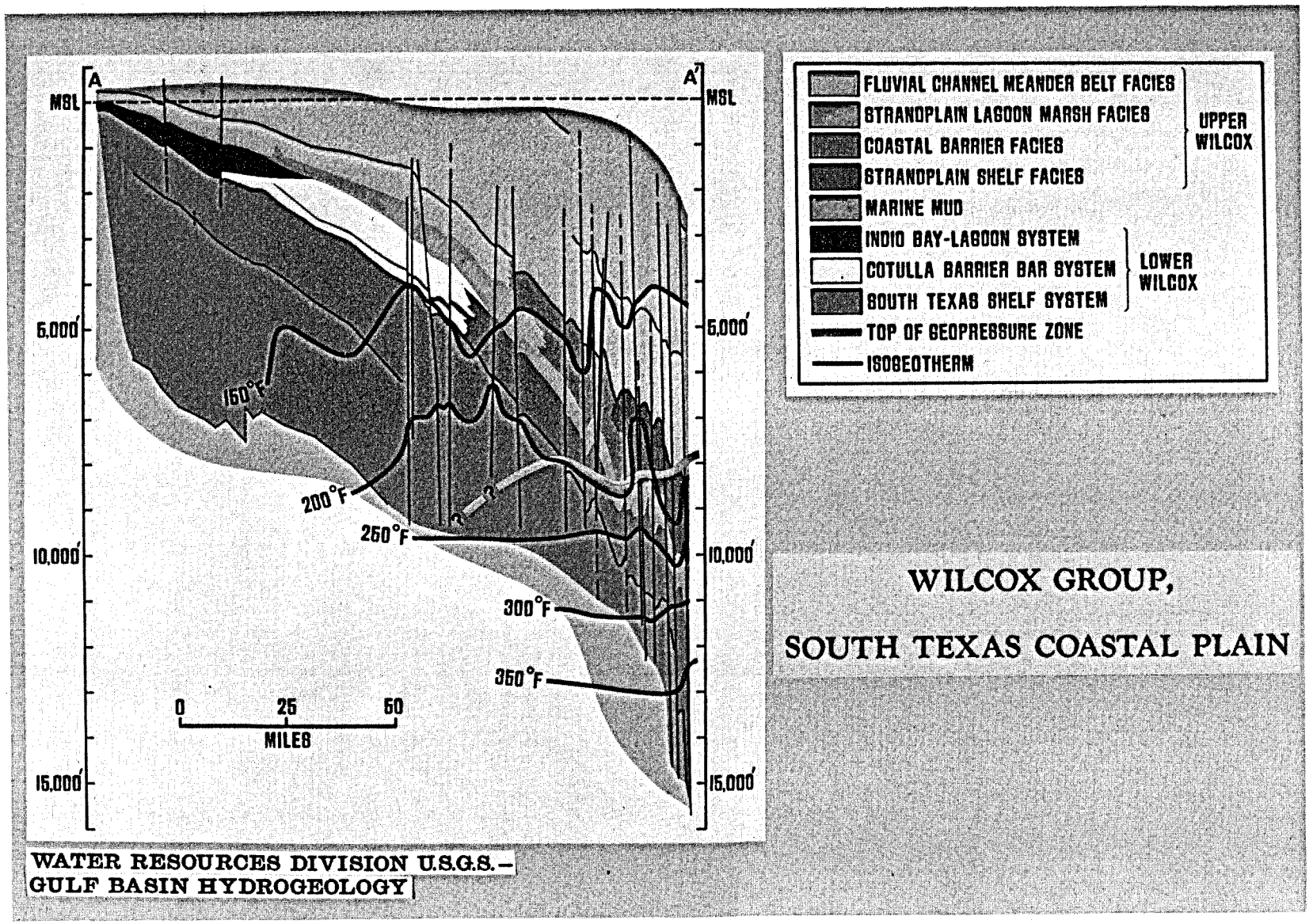

Figure 9. Geologic section across the Texas Coastal Plain along line *A–A'* on figure 8, showing sediment facies of the Wilcox group, major faults, the top of the geopressure zone, and five isotherms.

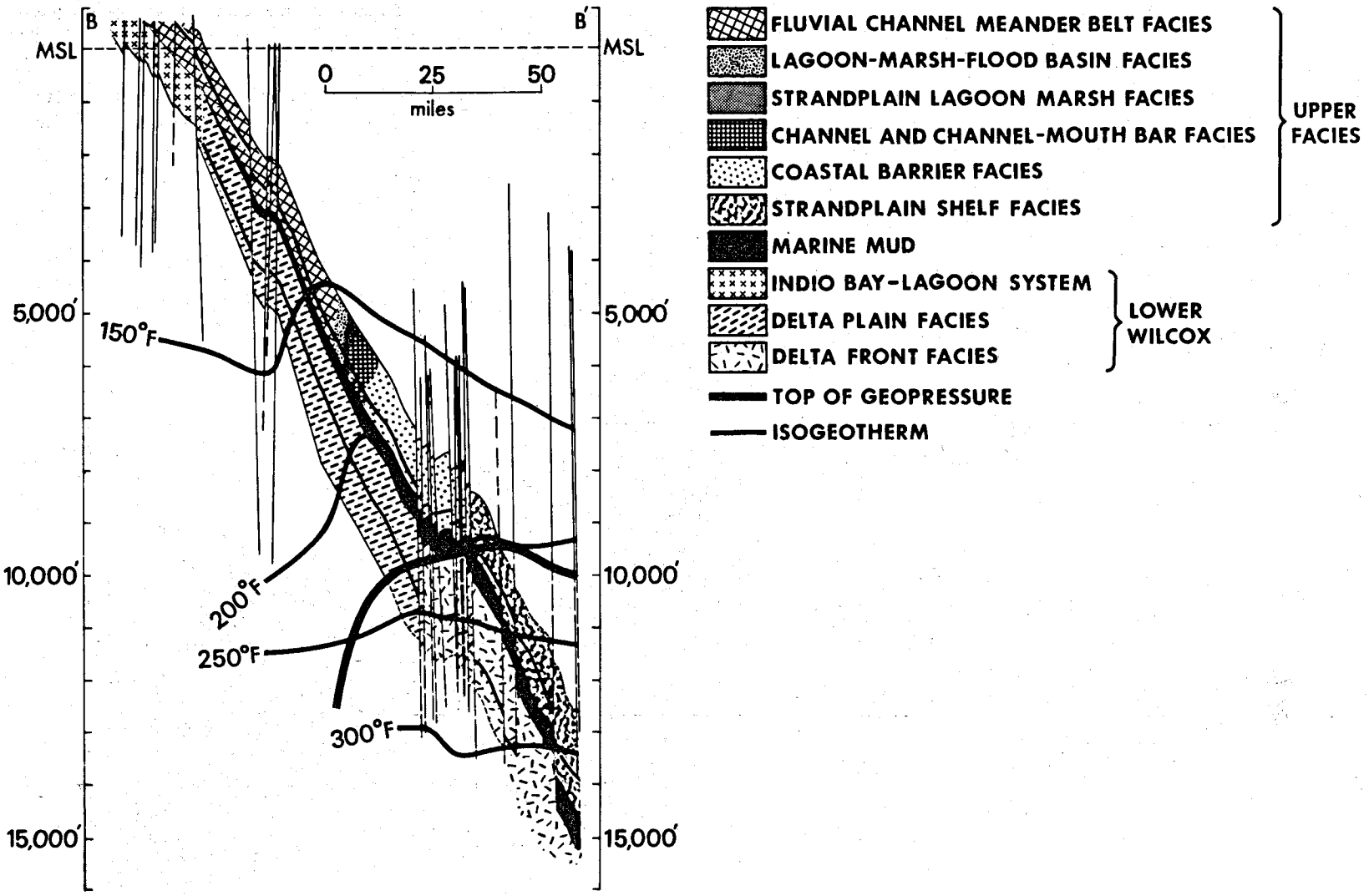

WATER RESOURCES DIVISION U.S.G.S.
GULF BASIN HYDROGEOLOGY

Figure 10. Geologic section across Texas Coastal plain along line *B–B'* on figure 8, showing sediment facies of the Wilcox group, major faults, the top of the geopressure zone, and four isotherms.

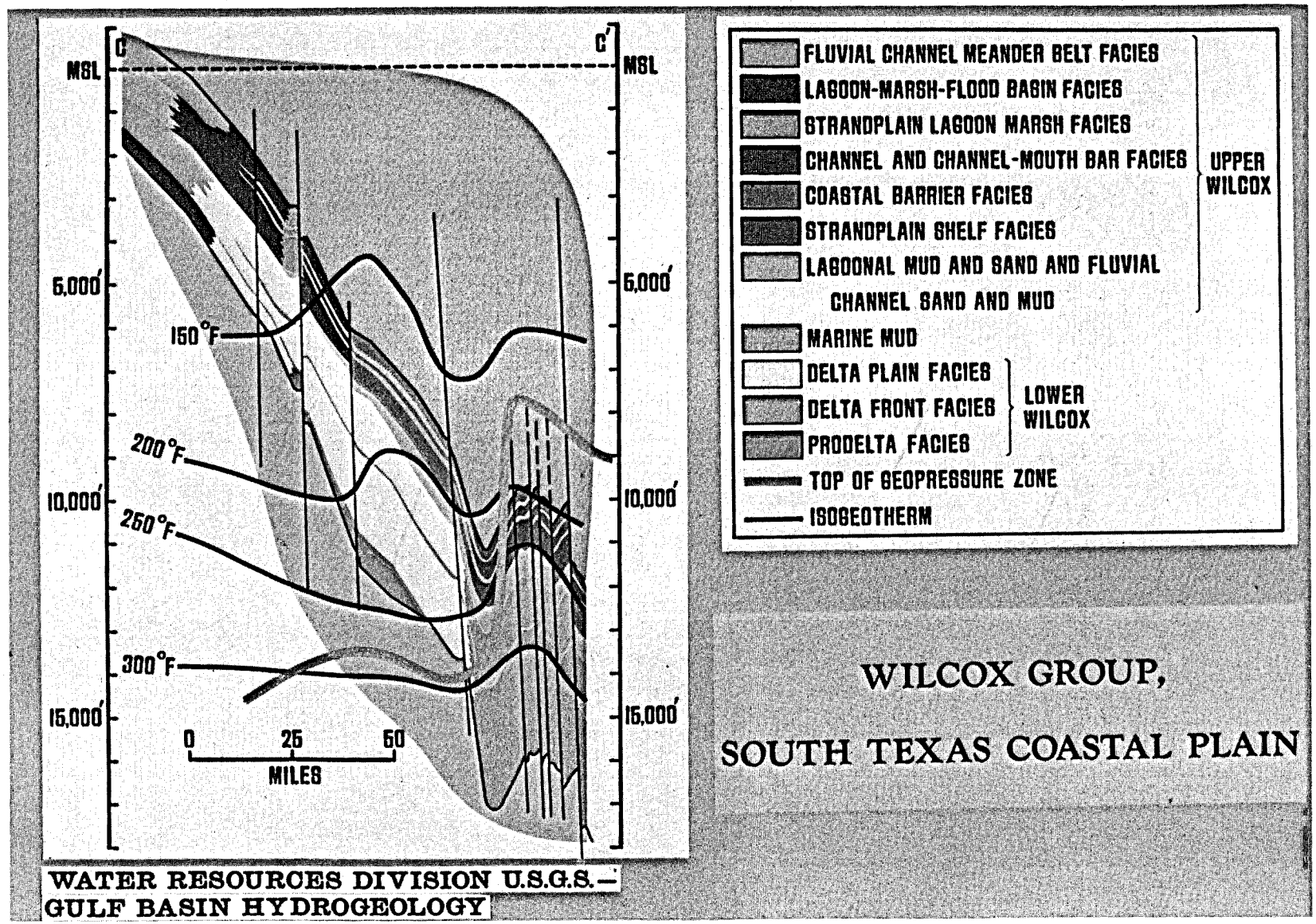

Figure 11. Geologic section across Texas Coastal Plain along line *C–C'* on figure 8, showing sediment facies of the Wilcox group, major faults, the top of the geopressure zone, and four isotherms.

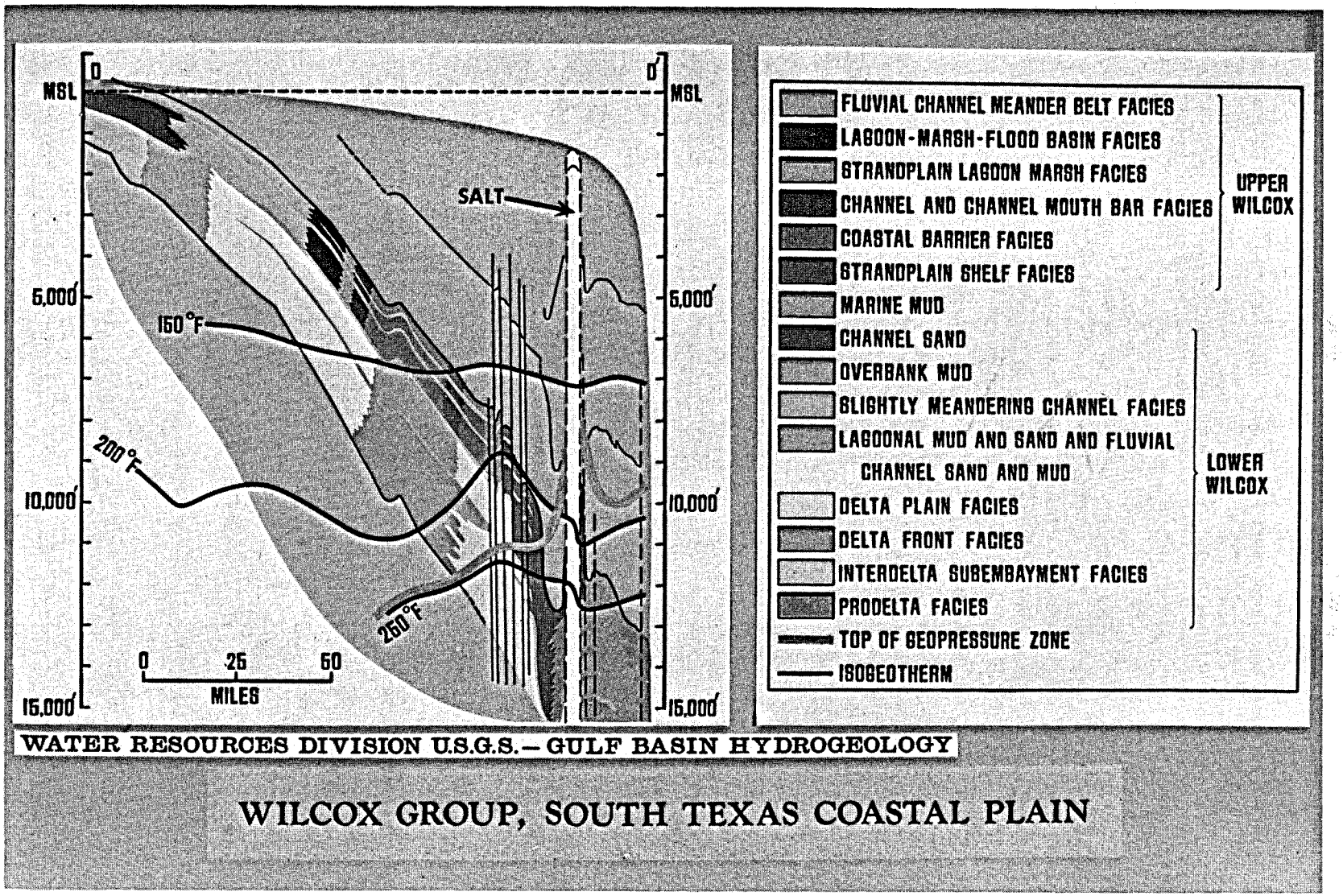

Figure 12. Geologic section across Texas Coastal Plain along line *D–D'* on figure 8, showing sediment facies of the Wilcox group, major faults, the top of the geopressure zone, and three isotherms.

flowage, but little Wilcox growth faulting is evident. Again, the principal zone of deformation lies immediately gulfward from the massive lower Wilcox delta deposits; the delta front facies is folded and faulted and the apparent dip is flattened.

In the section shown in figure 12, which is trending almost due south from the East Texas basin toward the east end of Galveston Bay, the structural effects of a salt dome are shown. Downwarp landward is probably related to subsidence of the rim syncline, and a narrow belt of faults inland from the dome is associated with facies changes in both the lower and upper Wilcox. Displacements of 1,000 feet or more on single faults produced a great increase in thickness of the upper Wilcox strandplain and shelf deposits. The lower

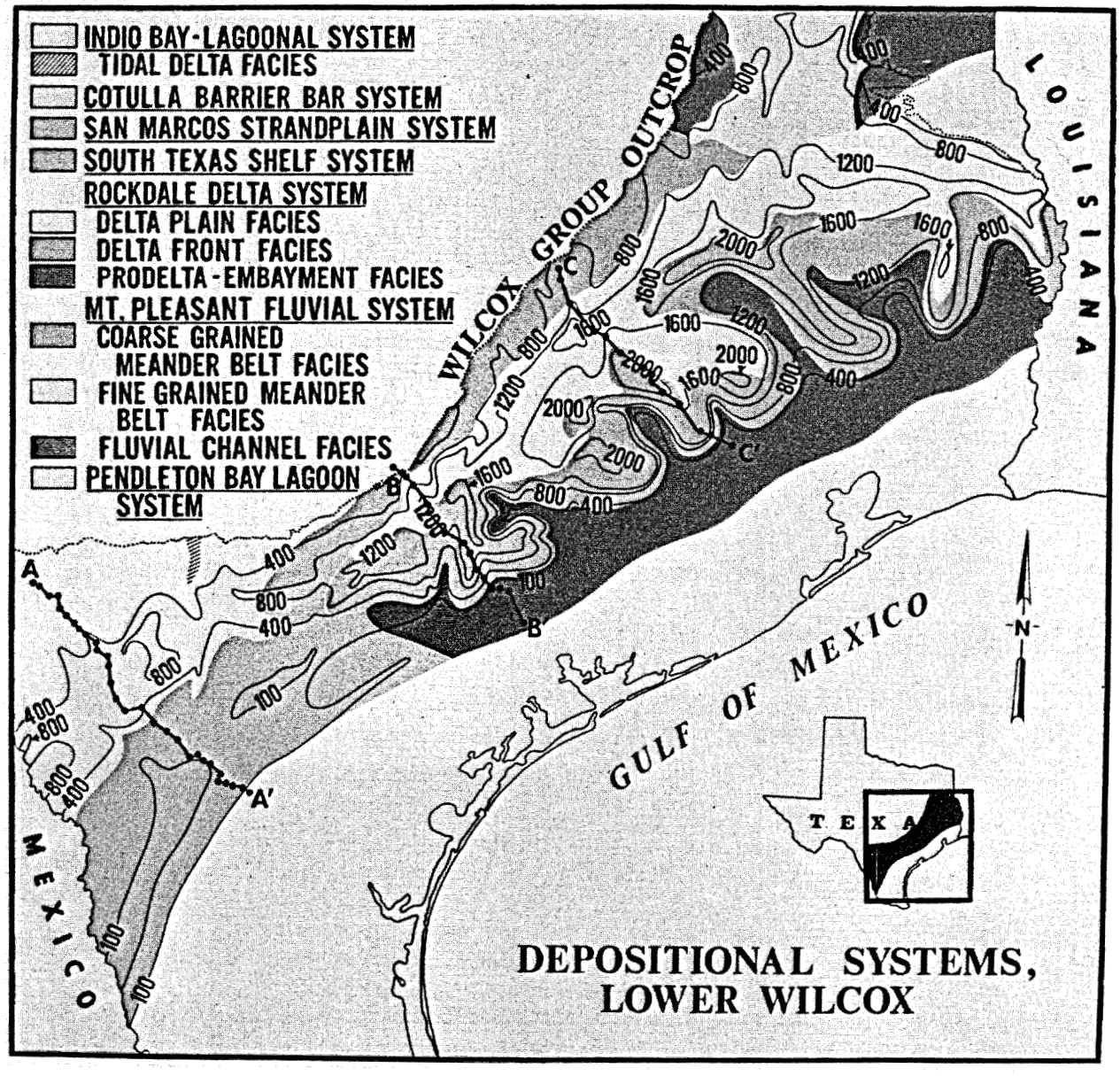

Figure 13. Depositional systems, sediment facies, and cumulative thickness of sand beds in the lower Wilcox deposits in Texas (After Fisher & McGowen, 1967, Texas Bureau of Economic Geology).

Wilcox delta plain deposits are almost 1/2 kilometre (1,600 ft) thick and occur at depths greater than 2½ km (8,000 ft) on this section.

The Rockdale delta is a major system that was the dominant factor in determining the distribution and thickness of sediments in the lower Wilcox of Texas. The several minor deltas in the upper Wilcox were extensively reworked by coastal processes. Growth faulting was restricted to the very gulfward margin of Wilcox deposits, probably because the area of deposition was underlain by a stable Cretaceous limestone shelf. Younger Tertiary delta systems "leapfrogged" the Wilcox and deposited sandy sediments upon marine clay, finding no such support.

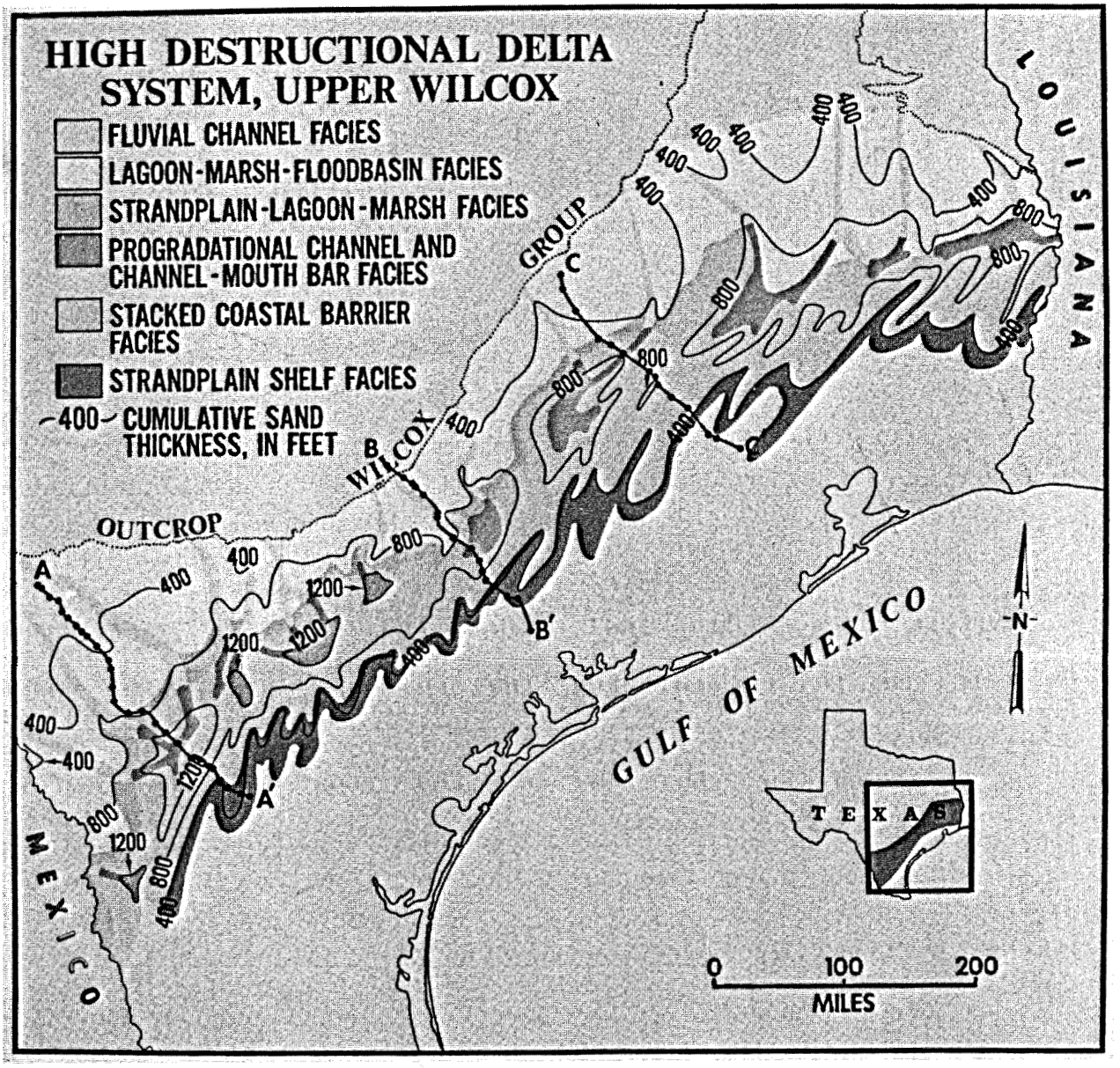

Figure 14. Sediment facies and cumulative thickness of sand beds in the upper Wilcox deposits in Texas (After Fisher & McGowen, 1967, Texas Bureau of Economic Geology).

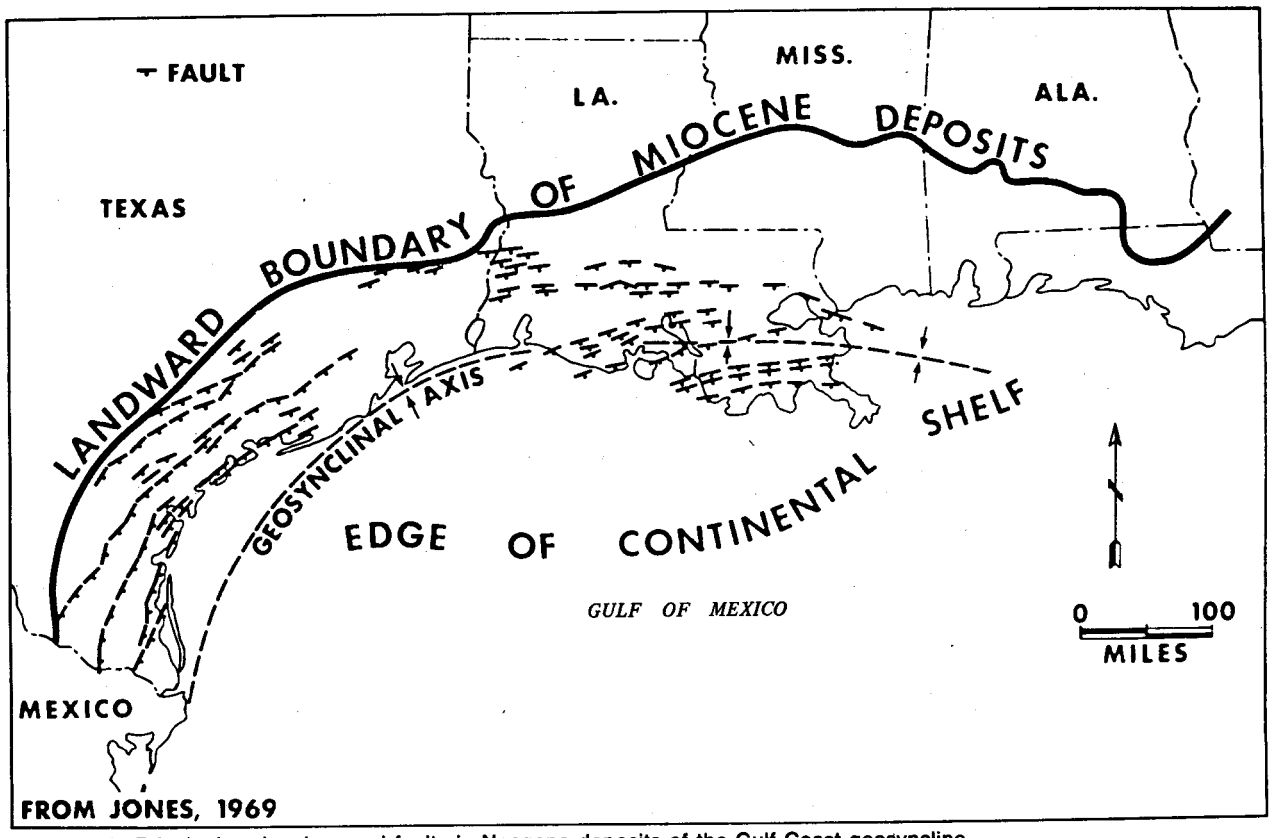

Figure 15. Principal regional normal faults in Neogene deposits of the Gulf Coast geosyncline.

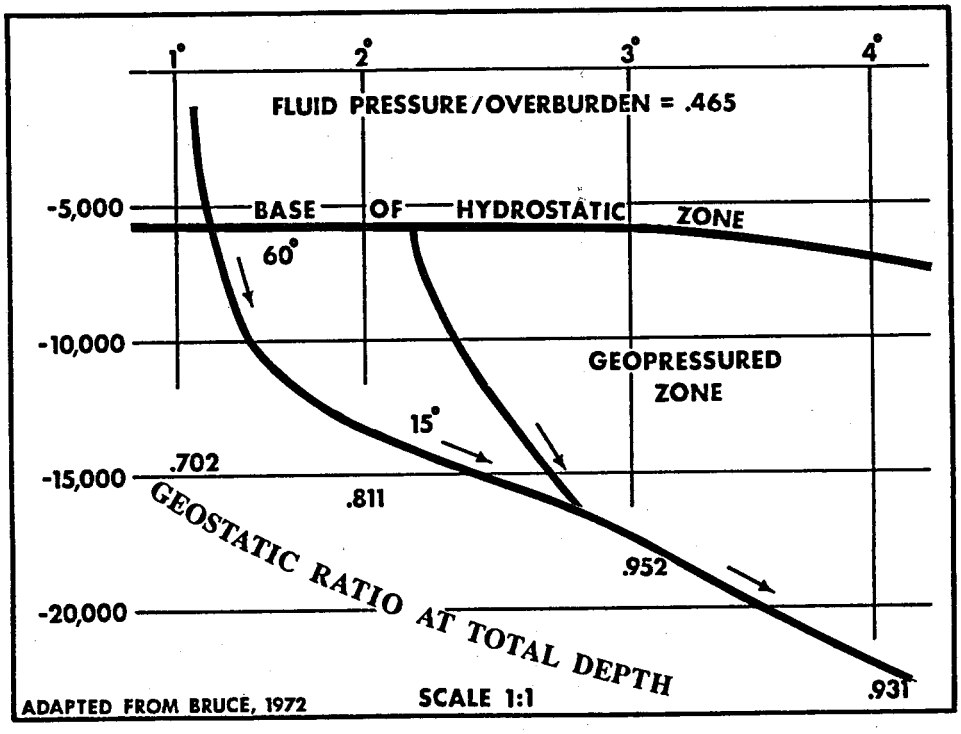

Figure 16. Relation of dip angie of contemporaneous faults to pressure gradient in geopressured shale, South Texas Coastal Plain.

The principal regional normal faults in Neogene deposits of the northern Gulf basin are shown in figure 15. Although these faults appear as discontinuous belts, thery are, in fact, continuous for many tens or even hundreds of kilometres. In profile, the fault planes are concave upward and gulfward (fig. 16). During rapid burial, increasing fluid pressure in the fine-grained deposits reduced their resistance to shearing stress and faulting occurred. Downward propagation of the fault plane was as shown in figure 16—the dip flattening with increasing pressure gradient (Bruce, 1973). The dip angle is high where fluid pressure is low and may be as great as 60° at the top of the geopressure zone; but at depths where the pressure reflects a gradient of about 184 g/cm^2/m (0.80 psi/ft), the dip is only about 15°. Resulting curvature of fault planes is shown on a grand scale in the regional dip section through the Rio Grande embayment in Texas in figure 17.

The profound effect of growth faulting on the geometry of sand-bed aquifer systems is evident in figure 17, which shows the abrupt thickening of correlative section on the gulfward (down-thrown) side of growth faults, the gulfward thinning of sand beds in the fault blocks, the rotation of down-thrown blocks into the fault planes, and the progressive reversal of dip. In this setting, barrier bar development is greatly enhanced, and this is extremely important in the structural evolution of Neogene deposits in the Texas part of the Gulf Coast geosyncline. Several buried equivalents of Padre Island have been found in the subsurface, one of these extends for 160 km (100 miles) or more parallel to the coast, and its sand deposits have a cumulative thickness greater than 1 km (3,200 ft) gulfward from a regional growth fault of the Frio-Vicksburg flexure (Boyd and Dyer, 1964).

Salt and shale diapirism alter and complicate the patterns of growth-faulted deposits, not only by upthrust and piercement, but also by producing heat-related changes in the load-bearing strength of the shale. A previously undocumented phenomenon, here termed hydrothermal tectonism, is keyed to the thermal diagenesis of montmorillonite (Burst, 1969). This process converts competent clay beds into a slurry wherever their temperature reaches or exceeds 100°C (212°F). Hydrothermal tectonism, as here defined, includes all aspects of subsidence, downwarp, normal faulting, and diapirism in sediments resulting from heating and the thermal diagenesis of clay minerals and the consequent release of bound and crystalline water, as well as deformation of deposits resulting from hot-water influx. The volume of water released by clay mineral conversion is equal to about half the volume of the clay mineral altered (Powers, 1967) and may be 10 to 15 percent of the compacted bulk volume of the rock (Burst, 1969).

Temperature-induced loss of load-bearing strength in shale—the most abundant rock type at depth in the Gulf Coast geosyncline (fig. 7)—and the expulsion of enormous volumes of water from shale made possible by this change, are believed to be the controlling factors in the movement on growth faults. Volumetric reduction at depth, accomplished by upward escape of the hot, high-pressure water via fault planes, makes possible rapid, large-scale regional subsidence of fault blocks—delicately balanced with the increasing sediment load. Superheated waters released to the hydropressure zone aquifers heat adjacent clay beds, causing progressive thermal diagenesis of montmorillonite in them and releasing water and triggering new shearing stresses.

Growth faulting, the principal aspect of hydrothermal tectonism in the Gulf Coast geosyncline, goes hand in hand with the hydrodynamic and geothermal

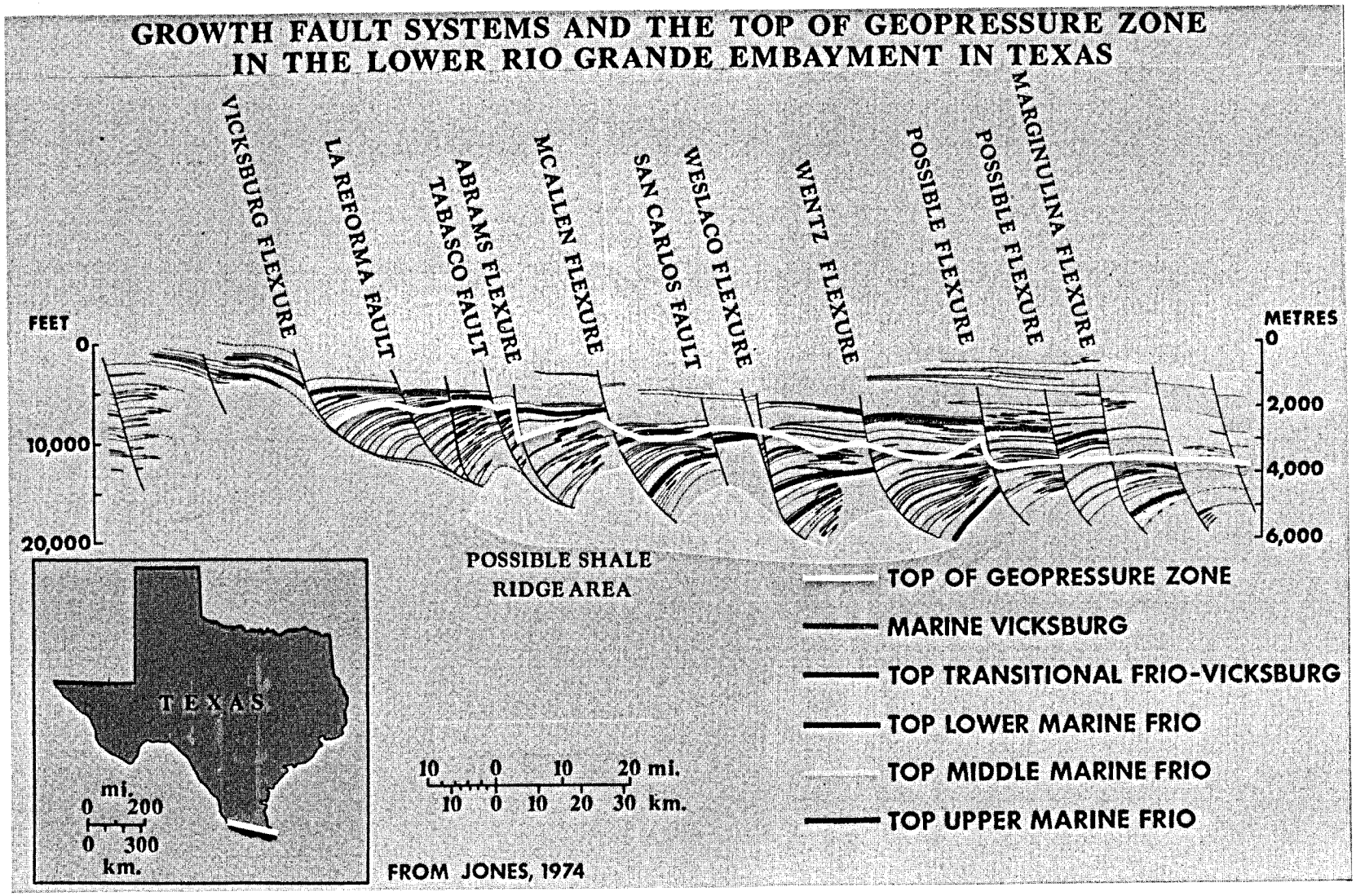

Figure 17. Generalized geologic dip section through the Rio Grande embayment of Texas, showing flattening of dip and die-out of contemporaneous faults at depth, reversal of dip of beds in the fault blocks, and the top of the geopressure zone.

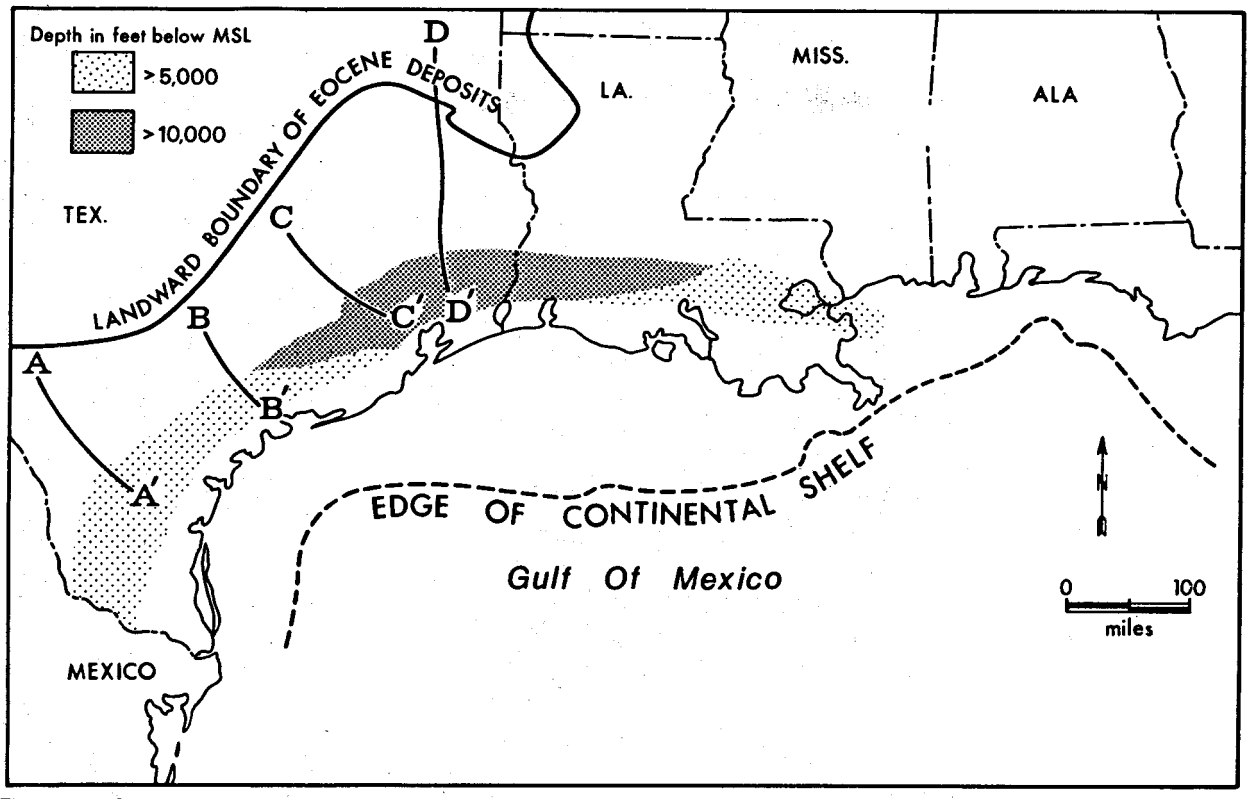

Figure 18. Geopressured zone in Eocene deposits, northern Gulf of Mexico basin (Modified from Jones, 1974).

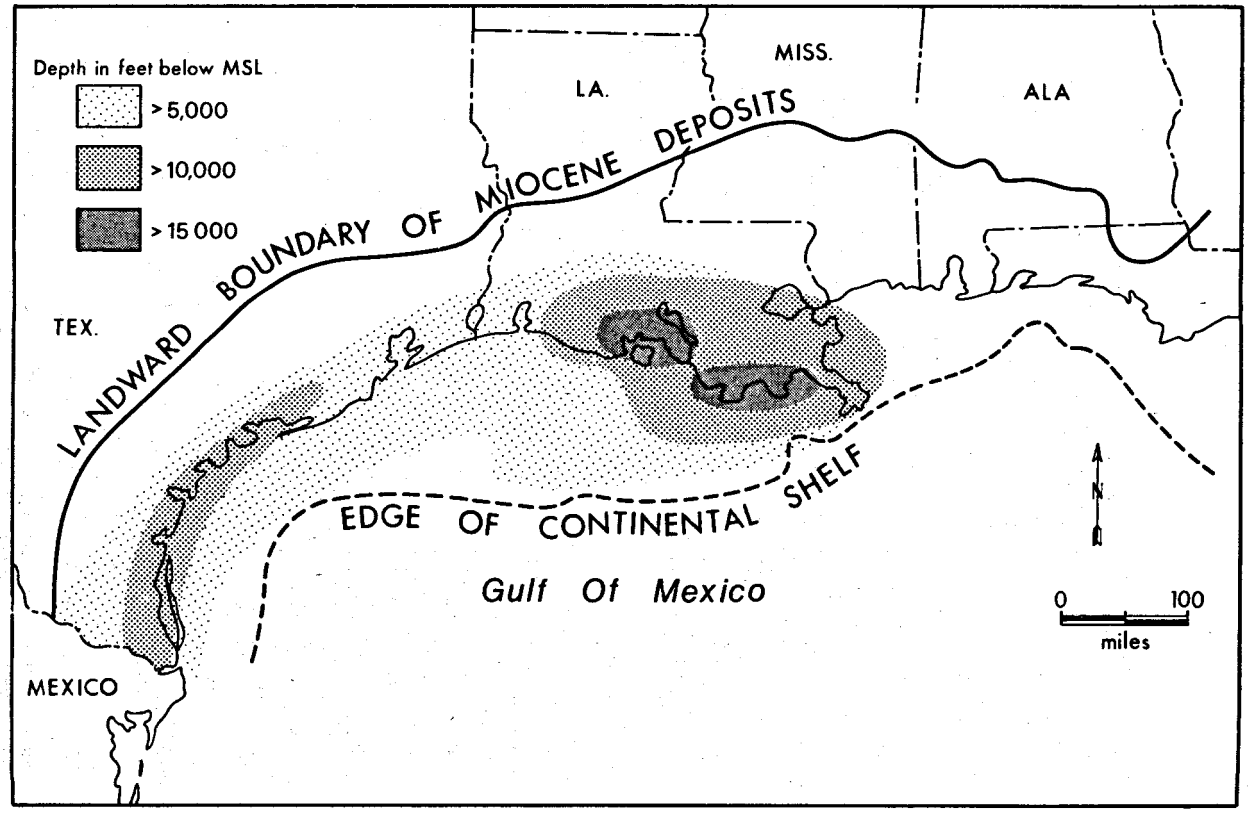

Figure 19. Geopressured zone in Neogene deposits, northern Gulf of Mexico basin (Modified from Jones, 1974).

regimes. The fault serves as an automatic valve at the top of the geopressure zone—when fluid pressure exceeds lithostatic load, the fault plane opens, water escapes, and subsidence of the fault block occurs. With this fluid loss, the pressure drops and the valve closes. It remains closed until fluid pressure again exceeds lithostatic, when the process is repeated.

HYDRODYNAMIC REGIME

The hydrodynamic regime of Cenozoic deposits in the northern Gulf of Mexico basin is a coupled function of two regional hydrodynamic systems: an underlying system in which fluid pressure reflects part of all of the weight of the rock overburden and an overlying system in which fluid pressure reflects only the weight of the superincumbent water column and the back pressure of outflowing water (Dickinson, 1953; Jones, 1969; Stuart, 1970). Dimensionally, the underlying system (the geopressure zone) is by far the largest; it underlies an area of at least 375,000 km^2 (150,000 mi^2) and extends downward some 15 km (50,000 ft) to the base of Cenozoic deposits in the Gulf Coast geosyncline. (See figs. 7, 18, and 19.) Leakage from the geopressure zone dominates all but the uppermost part of the hydropressure zone because the head of water in the geopressure zone is commonly an order of magnitude greater, and all water that escapes from the geopressure zone must pass through the hydropressure zone to reach the land surface or open water bodies.

In deposits of the hydropressure zone, a systematic loss of porosity occurs with increasing depth of burial. The loss of porosity in sand beds with depth is

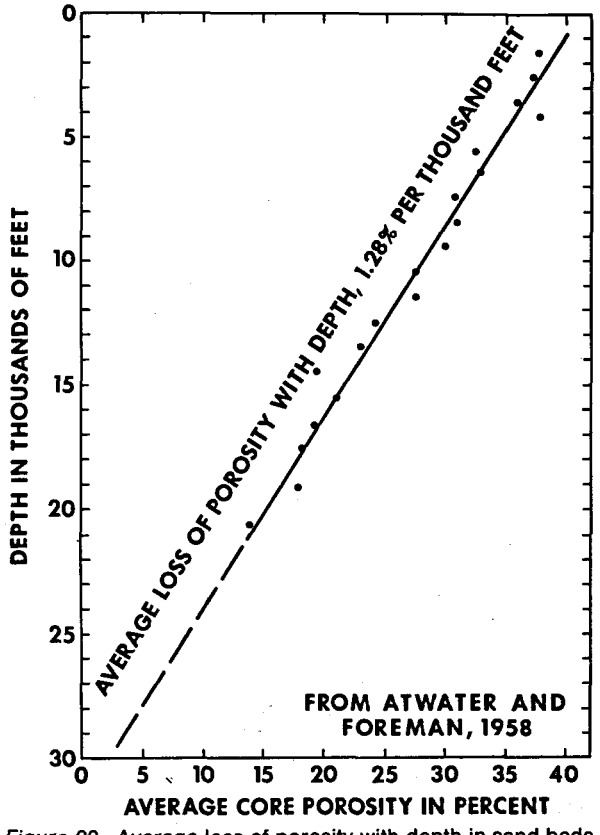

Figure 20. Average loss of porosity with depth in sand beds of the hydropressure zone, based on 17,367 samples from south Louisiana wells.

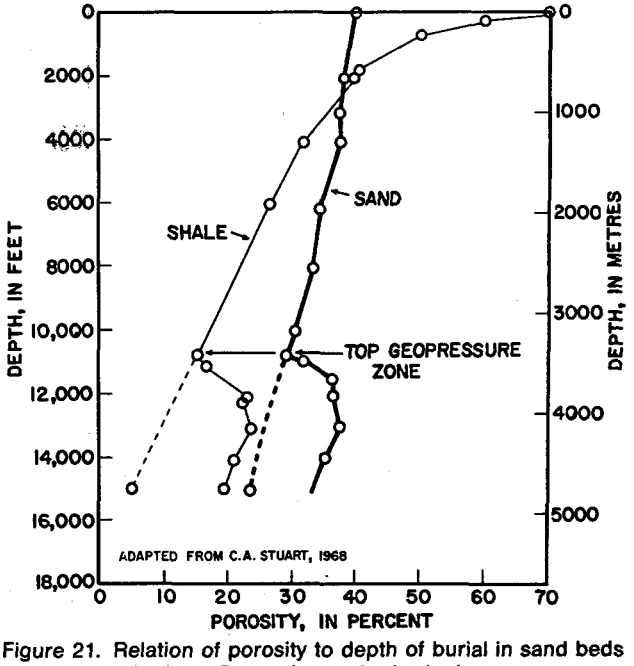

Figure 21. Relation of porosity to depth of burial in sand beds and in shale beds of Cenozoic age in the hydropressure zone and in the geopressure zone in the Gulf basin.

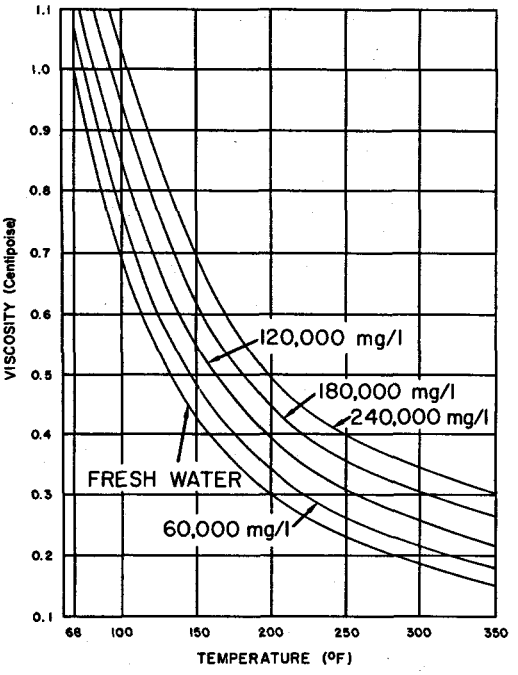

Figure 22. Relation between the viscosity, temperature, and dissolved-solids content of water (from Pirson, 1963).

approximately linear, at a rate of about 4.4 percent per km (1.28 percent per 100 ft) in southern Louisiana, over a depth range of 6 km (1/2 km to 6½ km) (1,600 ft to 20,800 ft). (See fig. 20.)

The loss of porosity in clay beds with deepening burial in the hydropressure zone is nonlinear, but it is systematic and predictable in a selected area over a given depth range. (See fig. 21.) Loss of porosity with depth indicates progressive compaction, which requires continuing expulsion of water and continuing discharge of this water upward through overlying deposits.

The gradient in head required to cause fluid discharge at any given rate increases as an exponential function of burial depth because the hydraulic permeability of the deposits decreases as an exponential function of the porosity, and the total length of the flow path increases as some such function of depth of burial. The drainage rate accordingly is drastically reduced with increasing depth of burial and, except where non-Newtonian flow is appreciable, increasing depth in the Gulf basin is always accompanied by increasing interstitial fluid pressure.

The loss of hydraulic permeability in sediments with increasing depth of burial is offset to some degree by decrease in the viscosity of pore waters with rising temperature. For example, water having a dissolved-solids content of 120,000 mg/l has a viscosity of 0.8 centipoise at 38°C (100°F); at 150°C (302°F), the viscosity is only 0.25 centipoise. In this temperature range, the viscosity of fresh water is reduced form about 0.7 centipoise to about 0.17 centipoise. (See fig. 22.) Waters of the geopressure zone decrease in salinity with depth, and dissolved solids in the range of 5,000 to 20,000 mg/l may be common. The effective permeability of deposits containing low-salinity water may thus be increased by factors of 3 to 5.

An abrupt reversal of the depth-porosity trend occurs at the top of the geopressure zone (fig. 21); the porosity sharply increases with depth in both sand and shale, and the porosity may be up to 10 percent greater than that at equivalent depth in the hydropressure zone. This porosity increase must accompany a sizable permeability increase, but there are no data to support this conclusion.

The porosity change with depth below the top of the geopressure zone is a function of changing pore pressure of interstitial fluids, and departures from the extrapolated depth-porosity trend of the hydropressure zone can be interpreted in terms of pore pressure in the geopressure zone. This is especially true in shale beds. An empirical relation between the porosity and electrical resistivity of shale serves as the basis for a highly useful technique for estimating formation fluid pressure from the electric log. This technique is described in detail by Hottman and Johnson (1965) and Wallace (1965). Figure

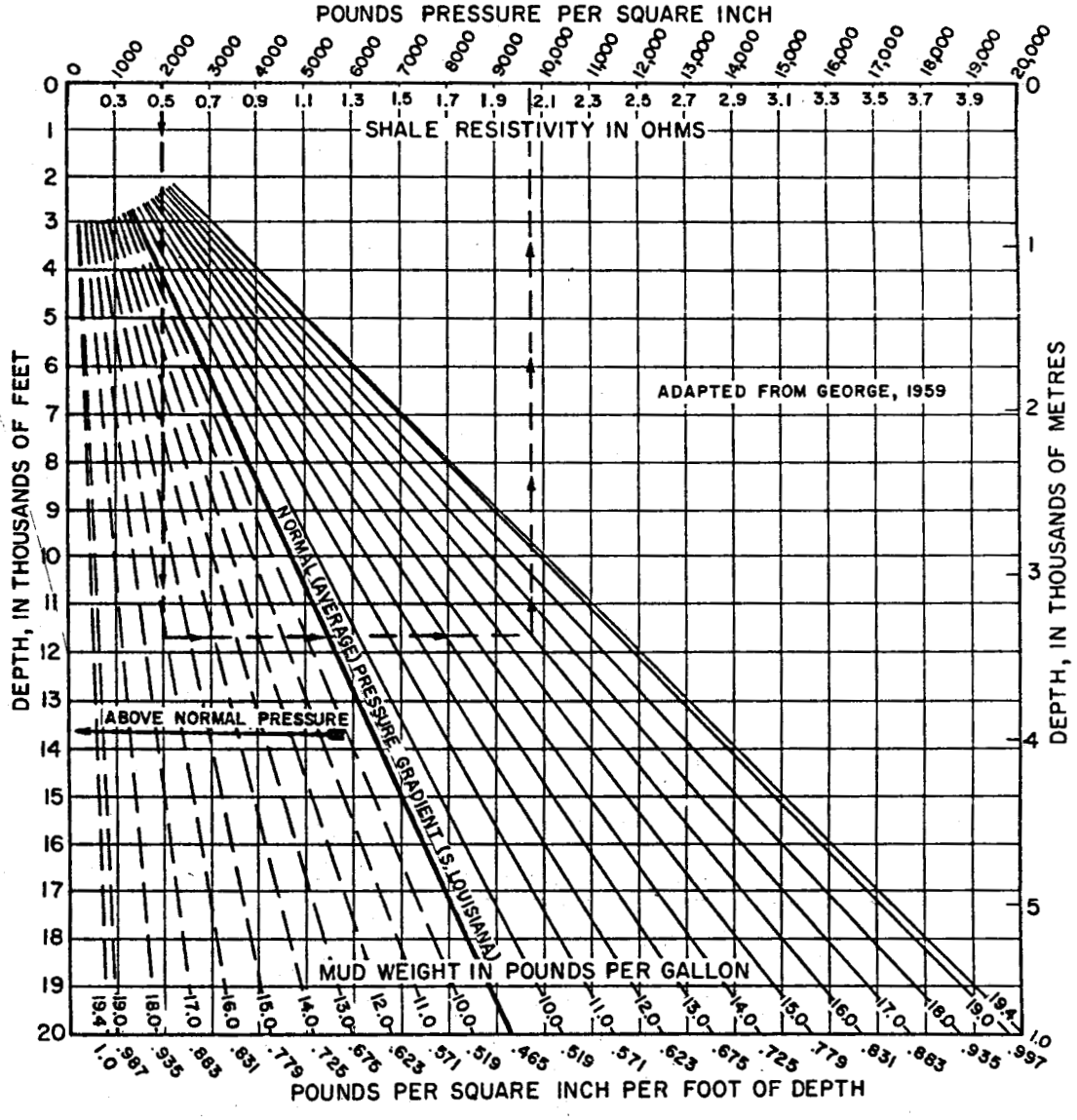

Figure 23. Chart for estimating formation fluid pressure from resistivity logs in south Louisiana.

23 is a chart developed by Rush George (1959) for estimating fluid pressure from resistivity. Coupled with mud weight data, this technique is used effectively to map the top of the geopressure zone (fig. 24) and to analyze the hydrodynamics of deposits within the zone.

Pressure gradients in the hydropressure zone, in the zone of transition from hydropressure to geopressure, and in the geopressure zone are shown in figure 25. The Gulf Coast normal pressure gradient is about 107 g/cm^2/m (0.465 psi/ft), which is the pressure gradient in a column of salty water containing about 80,000 mg/l total solids (Dickinson, 1958). In figure 25, the pressure differential between depths of 3.8 km (12,160 ft) and 4.7 km (15,000 ft) is 552 kg/cm^2 (7,850 psi), and the pressure gradient between them is 613.3 g/cm^2/m (2.76 psi/ft). The closed-in wellhead pressure of a well tapping the deposits at a depth of 4.7 km (15,000 ft), filled with salty water (80,000 mg/l), would be 422 kg/cm^2 (6,000 psi).

A great many oil-test wells were lost when they reached the geopressure zone, considered impenetrable until the middle 1950's. According to Stuart (1970), "Most wells in which an attempt was made to drill to deep objectives in the geopressure environment were either junked or became too expensive to drill to the target objective." Contractors escaped responsibility for hole completion by requiring contract provisions relieving them of the obligation if they encountered such things as "hot saltwater flows, oil flows, gas flows, gas-cut mud, heaving shale, sheath, lost circulation, no drilling progress, stuck pipe, or blowout."

Technology that enables the drilling and completion of wells to tap geopressured zone reservoirs includes (1) methods of pressure prediction, which describe conditions below the drill bit, and (2) methods of drilling safely and economically in known geopressure environments. Methods of pressure prediction are based upon knowledge and understanding of the conditions in geopressured deposits; they are therefore highly instructive in terms of geology and hydrology. The following are five common methods of pressure prediction shown in figure 26.

1. Acoustic velocity in sediments increases as porosity decreases; the top of the geopressure zone seal, a shale bed, is generally cemented, and a slight velocity increase occurs at this depth. Immediately below this cemented zone, high pressure is associated with an abrupt increase in porosity, and acoustic velocity drops abruptly. Methods are now available by which acoustic velocity can be interpreted in terms of sediment pore-fluid pressure (Pennebaker, 1969).

2. The upward movement of the waters of compaction is the principal factor in the heat flow in deep sedimentary basins (Bogomolov, 1967). Restriction of upward water flow in the geopressure zone results in retardation of heat flow, overheating of deposits, and geothermal gradients two to three times as great as in the overlying hydropressure zone. Lewis and Rose (1969) state, furthermore, that "an overpressure zone does constitute a thermal barrier because it is undercompacted; the greater the water content, the greater the insulating value of the zone." Conductive heat flow and minor water losses from the overheated geopressure zone warms the lower part of the hydropressure zone, and the temperature of mud returning while drilling this zone may be used to detect an underlying geopressure zone. The effectiveness of this geopressure indicator is shown in figures 27 through 30.

3. The rate of penetration of the drill bit is reduced by the cemented zone in the geopressure seal (shale bed) mentioned above but abruptly increases immediately below it as the hole enters undercompacted shale in the transition

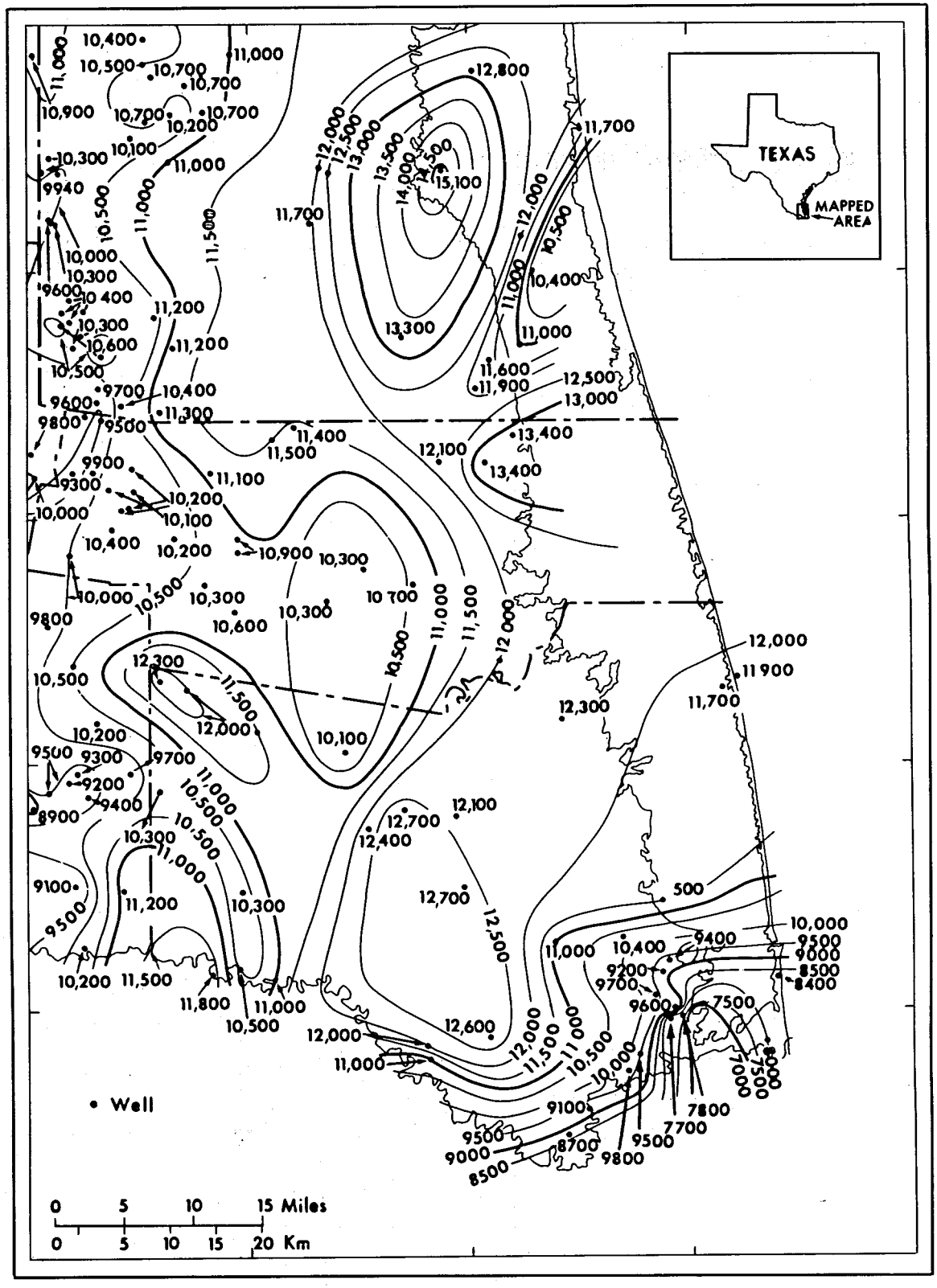

Figure 24. Map of the geopressured zone in the southeastern Texas Coastal Plain, showing the depth below which the pressure gradient equals or exceeds 162 g/cm^2/m (0.7 psi/ft).

zone from hydropressure to geopressure. This is an indicator that no driller can fail to notice.

4. Shale porosity changes suggested by changes in the penetration rate can be checked by measurements of the density of shale cuttings from the shaker, which separates drill cuttings from the mud returning to the pit.

5. Electric logs made in other wells in the vicinity can be used to define the fluid-pressure profile, and these serve the driller as a guide. The electrical resistivity of shale increases with density in an orderly way, and empirical correlation of density with porosity enables the log analyst to interpret departures from the depth-resistivity trend in the hydropressure zone in terms of fluid pressure in the geopressure zone.

Advances in drilling mud technology have played a major part in the exploration and economic development of oil and gas reservoirs in the geopressure zone (Dresser Industries, 1972). Additives increase mud weight, reduce its viscosity, change its dielectric and chemical properites, and greatly increase its thermal stability.

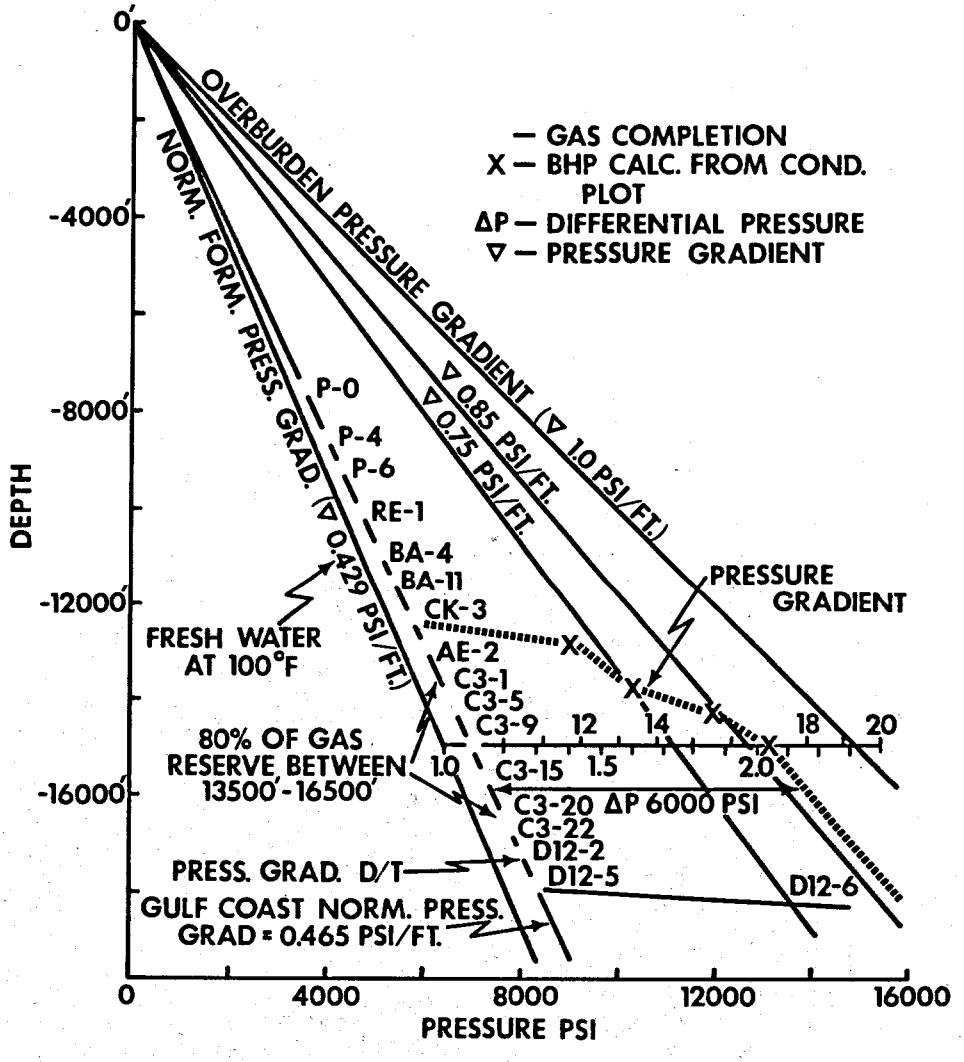

Figure 25. Changes in pressure gradients with depth in deposits penetrated by an offshore Louisiana well (from Meyers, 1968).

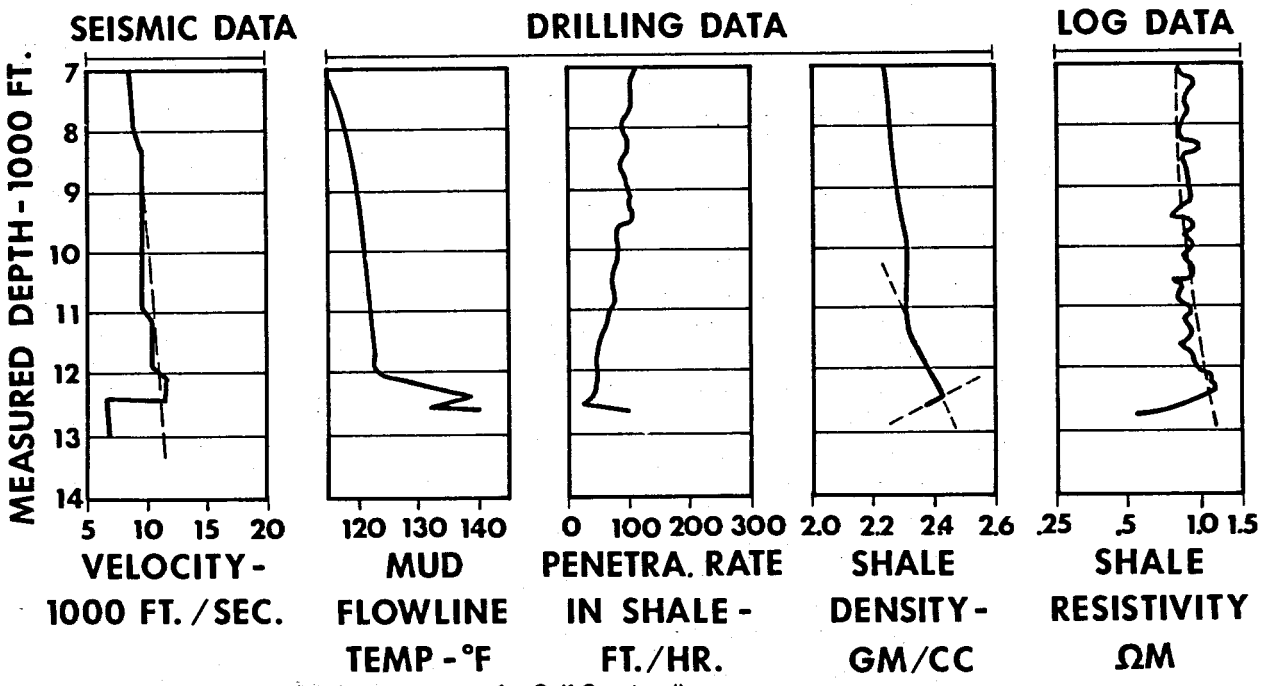

Figure 26. Five pressure-prediction parameters for Gulf Coast wells.

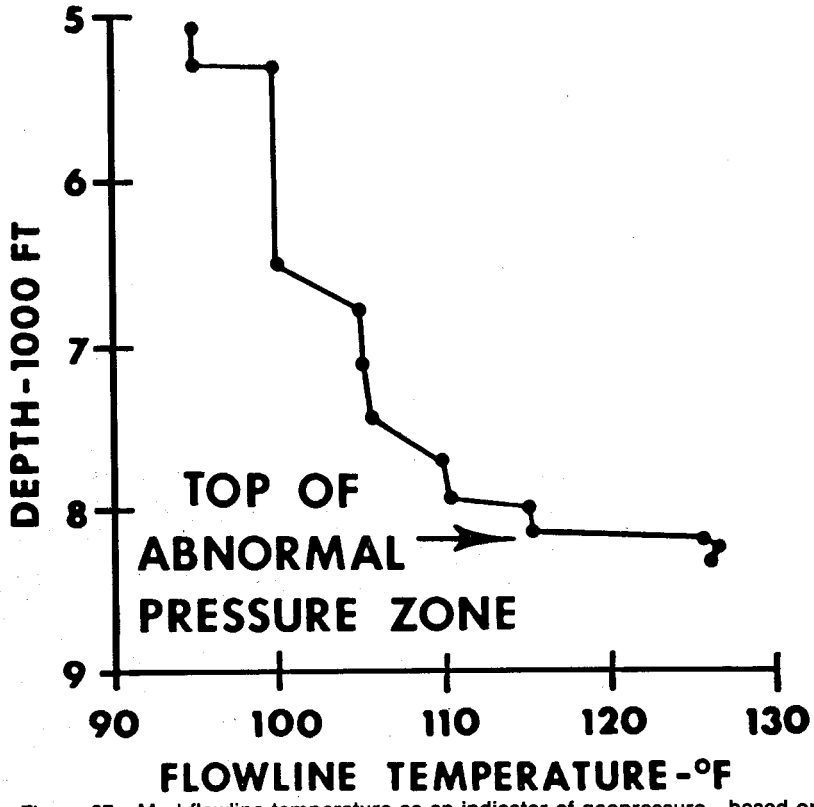

Figure 27. Mud flowline temperature as an indicator of geopressure, based on data from a Gulf Coast well.

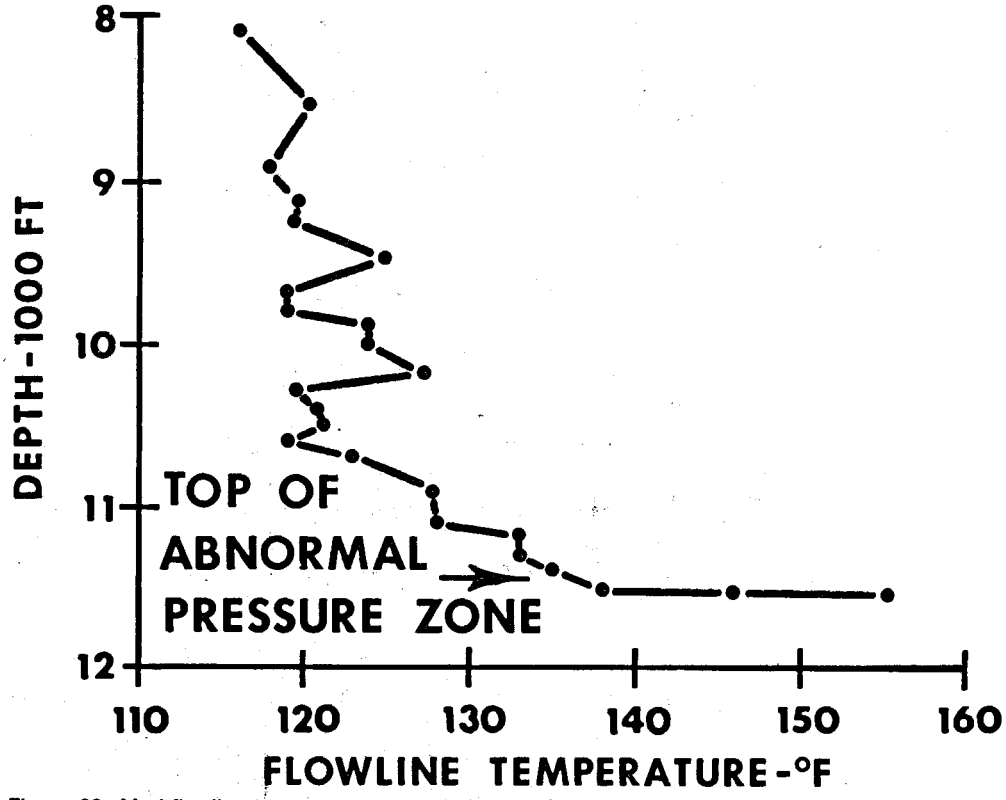

Figure 28. Mud flowline temperature as an indicator of geopressure, based on data from a South Texas well.

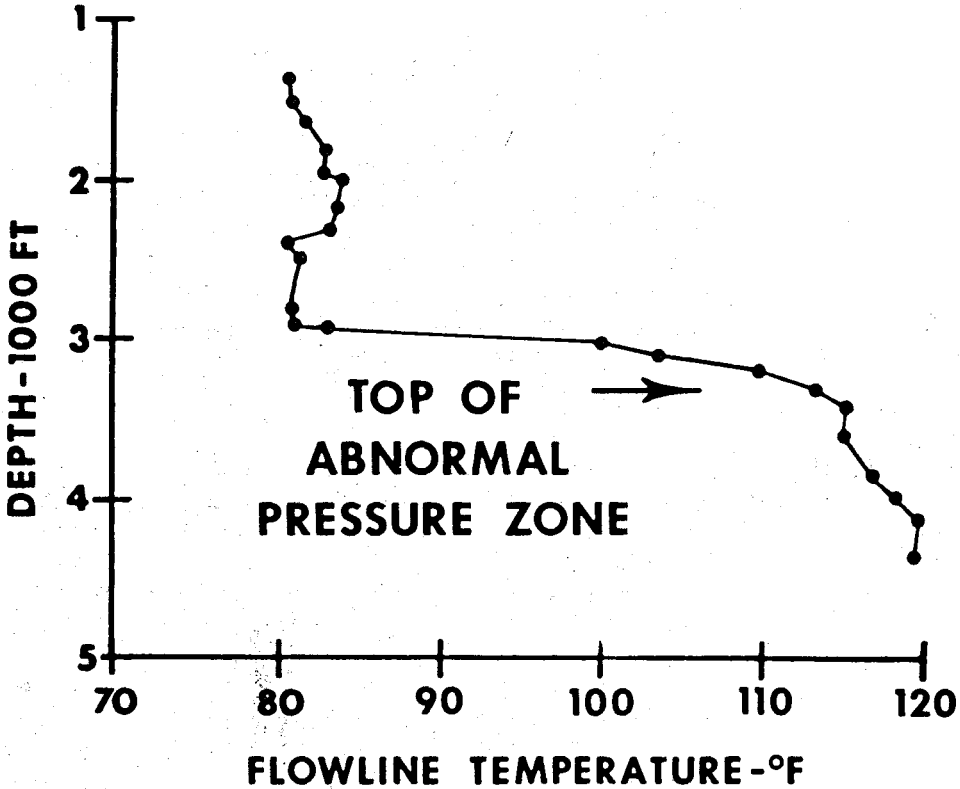

Figure 29. Mud flowline temperature as an indicator of geopressure, based on data from a North Sea well.

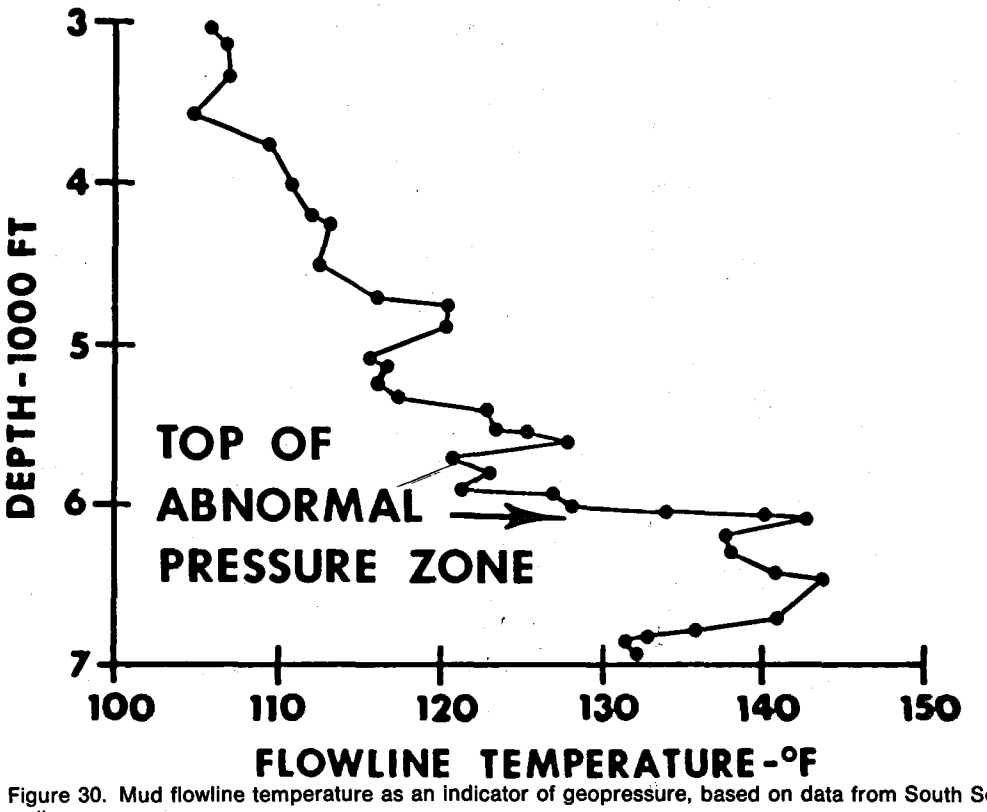

Figure 30. Mud flowline temperature as an indicator of geopressure, based on data from South Sea well.

The head of water at any depth in the hydropressure zone reflects both the average density of the outflowing water. The density of free pore water is primarily a function of its dissolved-solids content (salinity) and its temperature. (See fig. 31.) Although the salinity of free pore waters in sedimentary basins generally increases with depth, at a rate of "about 50 grams per litre per thousand feet" (160,000 mg/l per km) (Dickey, 1966), this is not true in the Cenozoic deposits of the Gulf basin. (See fig. 32.) Differences in water salinity with depth in the Wilcox and Frio shown in figure 32 result in maximum water density differences no greater than 0.05 g/cc (0.02 psi/ft of depth). In comparison with other hydrodynamic forces in these systems, water salinity differential is minor, if not negligible.

HYDROTHERMAL REGIME

It is asserted by Bogomolov (1967) that "water carries out the major role in the redistribution and subtraction of heat [in the geothermal field]; the thermophysical properties of rocks are mainly determined by the liquid phase . . ." The thermal conductivity of water is only about one-fifth that of the mineral grains of sand and clay in the northern Gulf of Mexico basin, and the specific heat of water is about five times as great as that of the mineral grains. The porosity of Cenozoic deposits above a depth of 6 km (20,000 ft) averages about 28 percent for sand and about 20 percent for clay. In this depth interval every grain of sand and every clay mineral platelet are almost entirely enveloped by water. If this water has macroscopic movement, be it ever so slow, heat flow through the deposits is essentially a function of the rate of this mass transfer.

And conversely, if the water is held almost motionless by molecular forces, heat flow is reduced far below that which would occur if the deposits had no porosity at all.

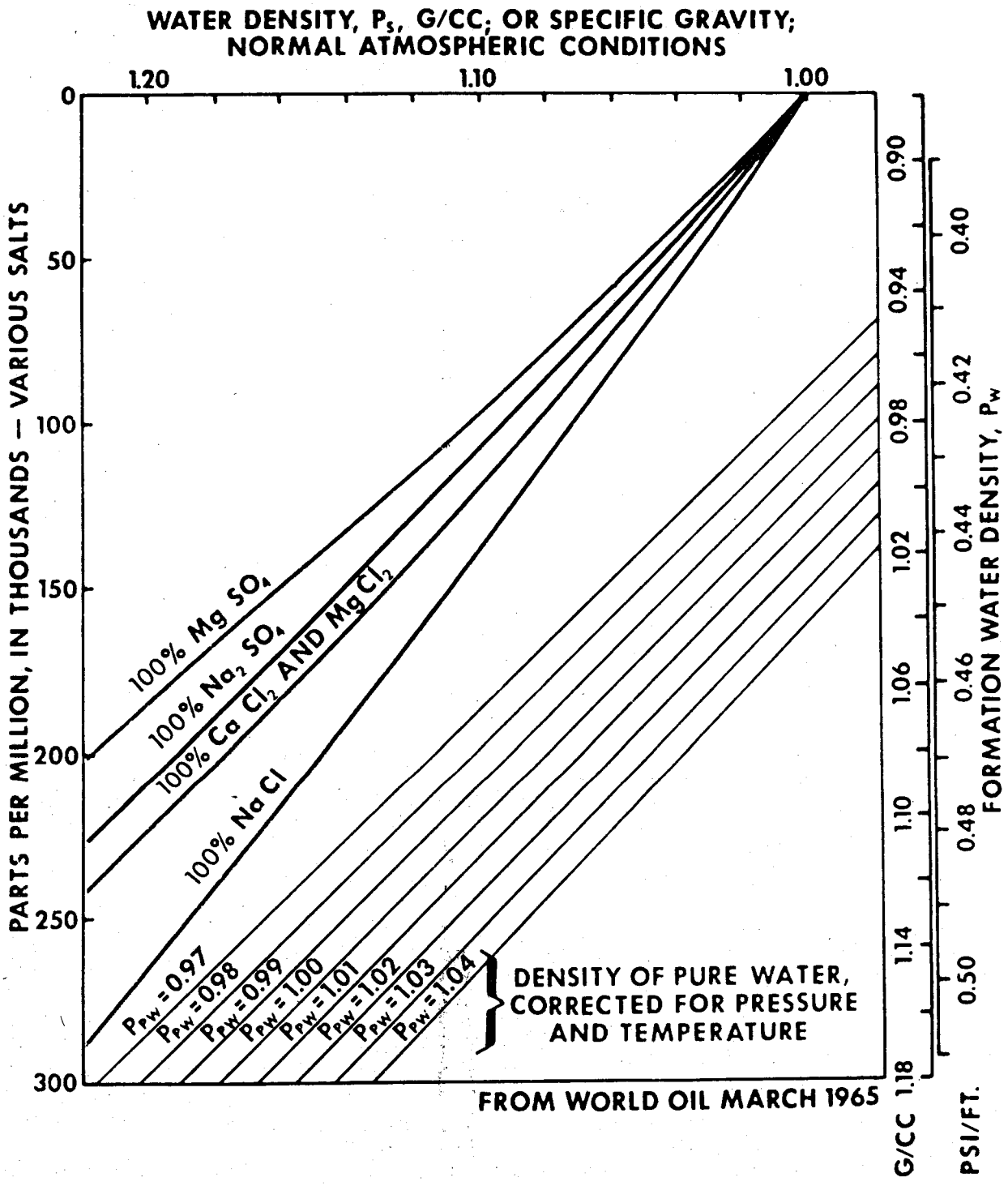

Figure 31. Relation of water density to salinity and types of dissolved solids.

If there were no upward flow of water out of the Gulf basin deposits—that is, if the compaction process were arrested indefinitely—the geothermal flux might be determined by relatively few measurements. For any given depth interval, it would only be necessary to measure the average geothermal gradient, the percentage of sand and of shale in the interval, and the water-filled porosity of each sediment type. The thermal conductivity of sand increases with its porosity (Zierfuss and Van der Vliet, 1956), owing to "the occurrence of convective heat transport in the wider pores." However, Lapwood's studies (1948)

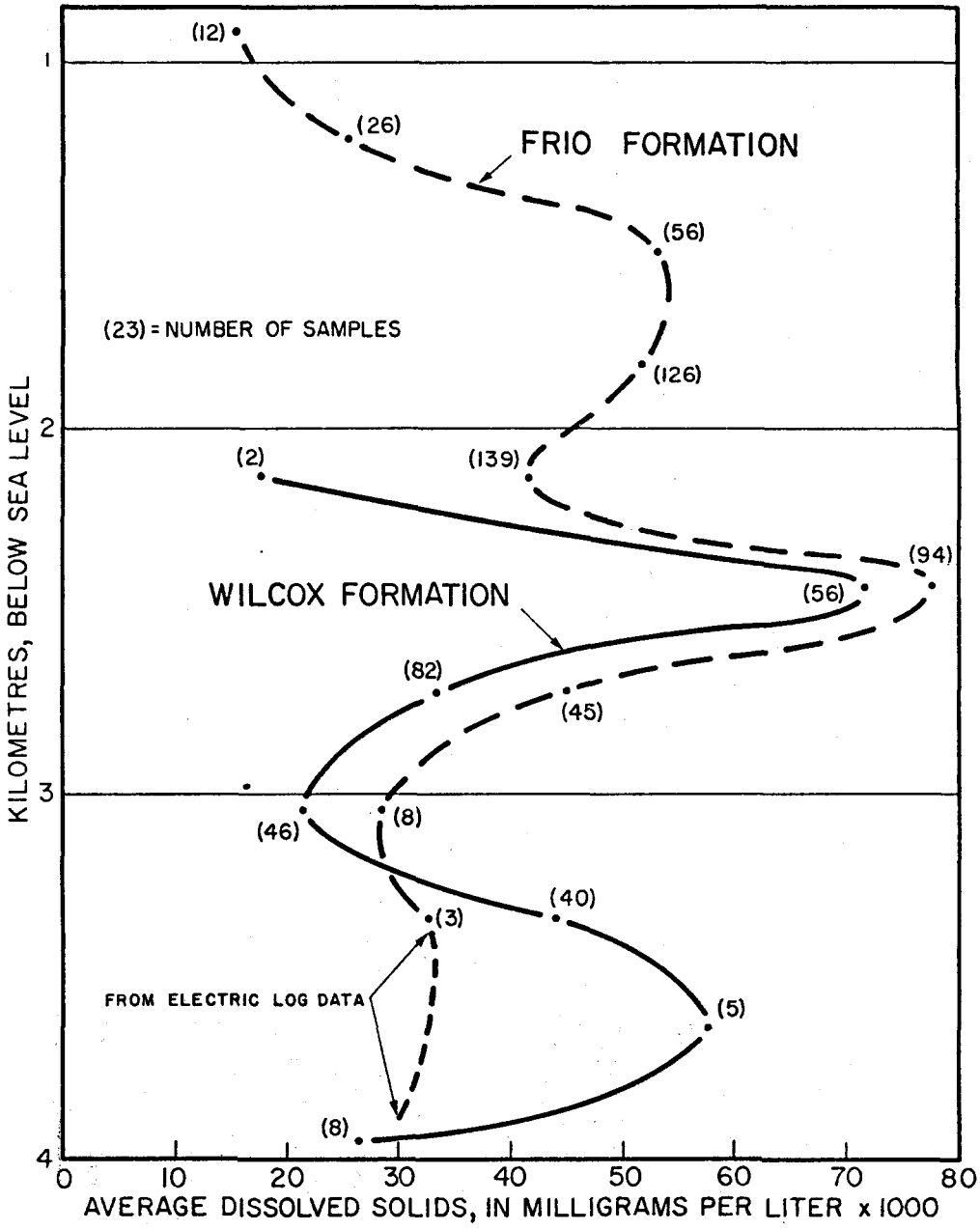

Figure 32. Salinity change with depth and geologic formation in South Texas Coastal Plain, based upon the average salinity of waters from aquifers in depth intervals of 330 m (1,000 ft).

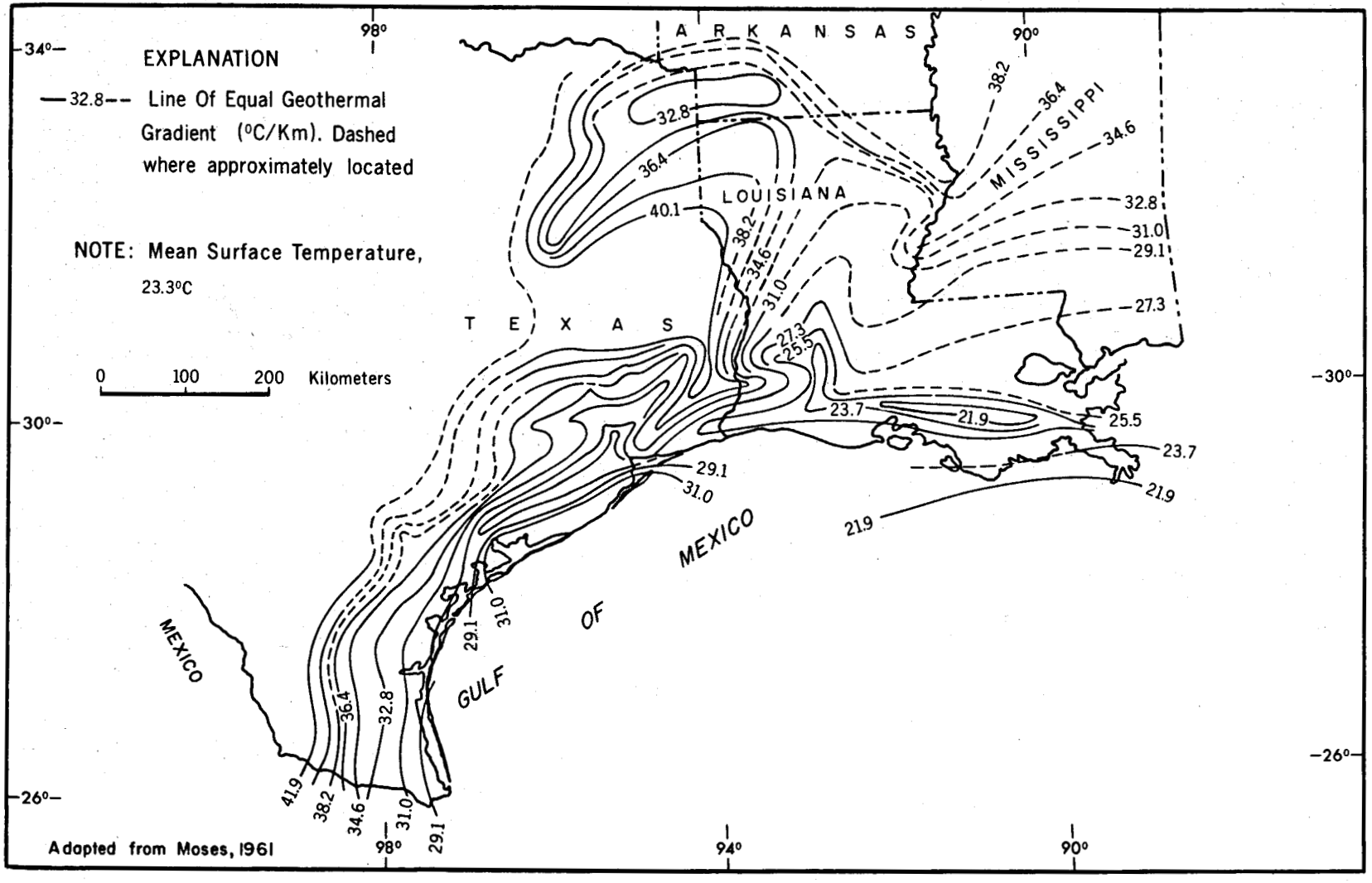

Figure 33. Geothermal gradients in the hydropressure zone in the northern Gulf of Mexico basin.

revealed that, in a horizontal layer uniformly heated from below, convective flow does not occur until the temperature difference across the layer exceeds some minimum value. The thermal conductivity of shale (clay) varies inversely with its water content (Langseth, 1965). Precise measurements of the thermal conductivity of sand and clay, corrected for bed thickness and porosity variation might enable calculation of representative rates of heat flow in the basin. But water movement on a grand scale is in progress, and observed geothermal gradients are essentially functions of the rate at which such movement occurs.

It has been known for many years that temperature increase is approximately linear with depth in the hydropressure zone of the Gulf basin. The rate of increase with depth differs from locality to locality, and these differences are shown on the geothermal gradient map of Moses (1961), figure 33. Based on bottom-hole temperature measurements in oil-test wells before extensive exploration of the geopressure zone had begun, this map describes very well the geotemperature conditions in the hydropressure zone. In general, the gradients shown vary inversely with the thickness of Cenozoic deposits in the basin.

The average geothermal gradient in deposits of the hydropressure zone ranges from about 20°C/km to 40°C/km over a depth range of 1 to 2 km. In the transition zone between hydropressure and geopressure, very sharp increases in the geothermal gradient occur, in some places exceeding 100°C/km (Jones, 1970). Within the geopressure zone, the gradient is commonly two to three times greater than that in the overlying hydropressure zone. (See figs. 34 through 38.)

Most published temperature data available for wells in the Gulf basin are not corrected to equilibrium conditions and are therefore conservative; the observed bottom-hole temperature is always lower than rock temperature at

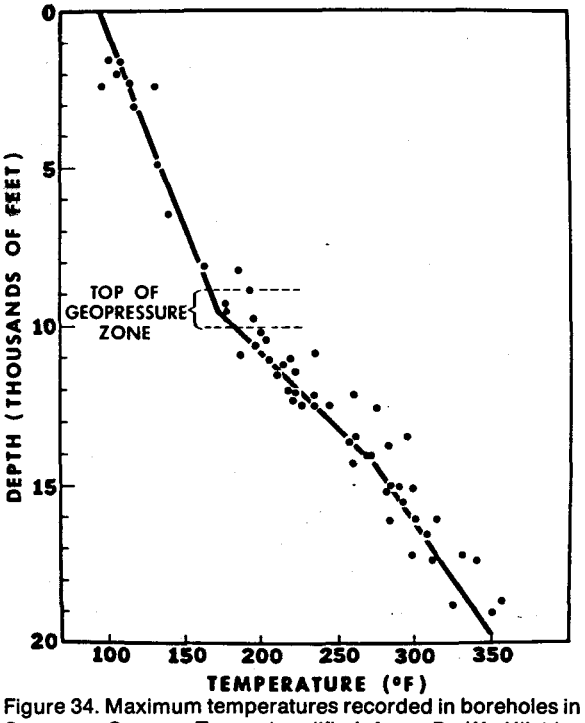

Figure 34. Maximum temperatures recorded in boreholes in Cameron County, Texas (modified from D. W. Hilchie, 1968).

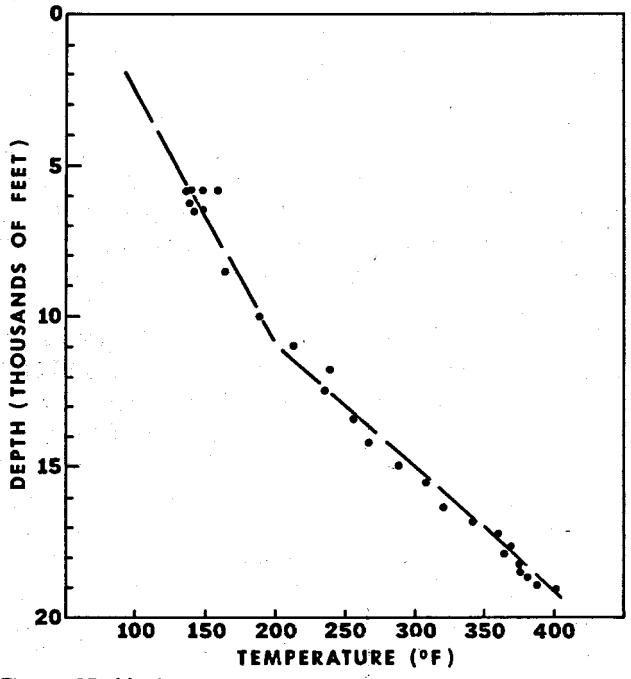

Figure 35. Maximum temperatures recorded in boreholes in Jackson County, Texas (modified from D. W. Hilchie, 1968).

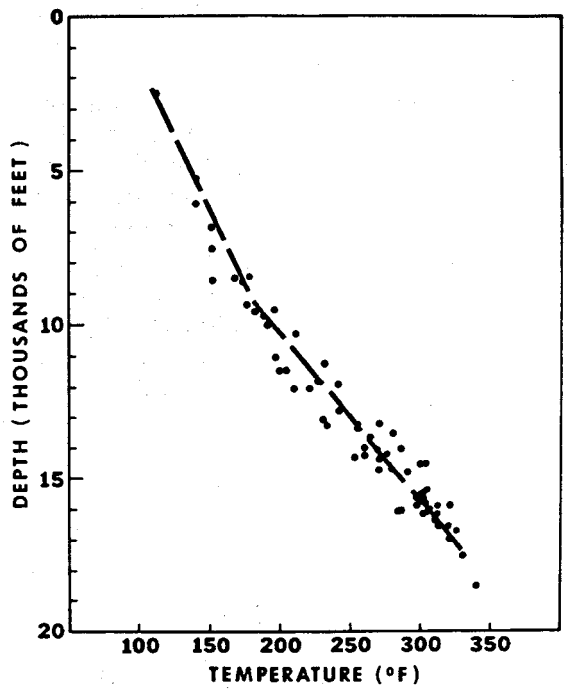

Figure 36. Maximum temperatures recorded in boreholes in Matagorda County, Texas (modified from D. W. Hilchie, 1968).

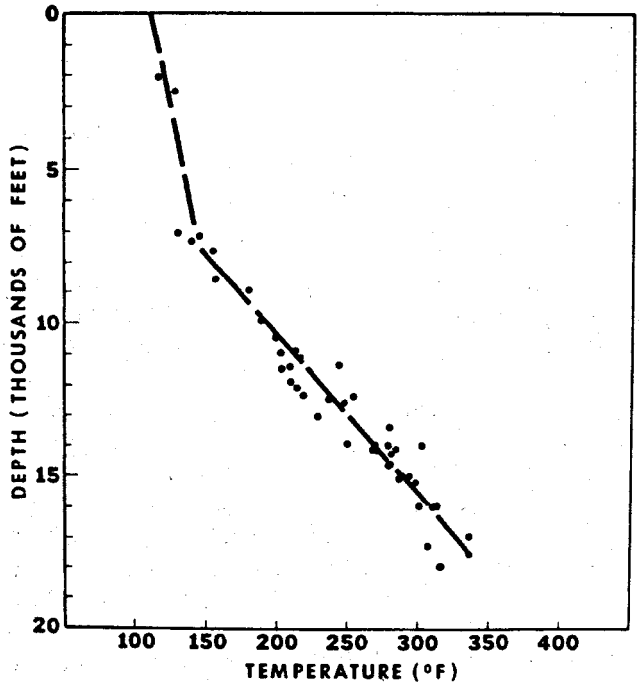

Figure 37. Maximum temperatures recorded in boreholes in Brazoria County, Texas (modified from D. W. Hilchie, 1968).

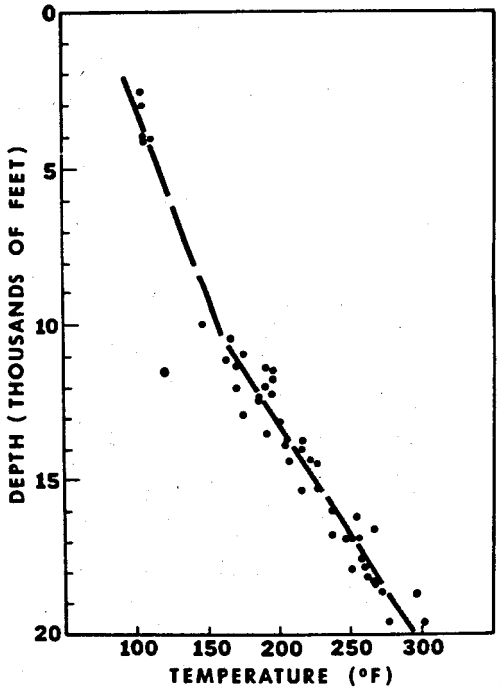

Figure 38. Maximum temperatures recorded in boreholes in Plaquemines Parish, Louisiana (modified from D. W. Hilchie, 1968).

equivalent depth. Nonequilibrium temperature data can be plotted against depth to obtain general information on the geotemperature regime in a selected locality. Figures 34 through 38 are based on nonequilibrium data for wells in several counties in the SouthTexas Gulf Coast and in one parish in the lower Mississippi delta in Louisiana.

In Cameron County, Texas, (fig. 34) data points are widely scattered, and a given temperature may occur over a depth range of several thousands of feet. The "dog-leg" in the gradient associated with the transition to geopressure at a depth of about 3 km (9,600 ft) is clearly evident, and it appears that the likelihood of temperatures exceeding 200°C (392°F) at depths less that 6 km (20,000 ft) is remote.

In Jackson County, Texas, (fig. 35) the depth-temperature data points lie upon a distinct line; the top of geopressure is at a depth of about 3.4 km (10,880 ft), and the temperature at a depth of 6 km (20,000 ft) is likely to exceed 215°C (419°F). In Matagorda and Brazoria Counties, Texas, (figs. 36 and 37) depth-temperature data points are scattered, and maximum temperature at depths of 6 km (20,000 ft) are not likely to exceed 200°C (392°F). In Plaquemines Parish, Louisiana, (fig. 38) the depth to the top of the geopressure zone is about 3.3 km (10,600 ft), and the temperature at a depth of 6 km (20,000 ft) is not likely to exceed 150°C (302°F).

The geothermal gradient dog-leg in the zone of transition to geopressure (figs. 34 through 38) makes generalized geothermal gradient maps useless and misleading, unless they are restricted to the hydropressure zone or to the geopressure zone. The only way to describe subsurface geotemperature conditions where geothermal gradients vary with depth is to map the depths of selected isothermal surfaces. These maps have great meaning because they describe not only the thermal environment at depth, but also the mass movement of water in the sediments.

Bottom-hole temperatures measured on successive logging runs in the same wells were used without correction to equilibruim temperature in the preparation of the isothermal map of the South Texas Coastal Plain, figure 39. Although conservative, it is a good representation of subsurface temperatures. Figure 40, a regional map of the northern Gulf of Mexico basin, shows depth of occurrence of the 120°C (250°F) isothermal surface and identifies those areas in which high-temperature water may be found at shallow depth. It also indicates the depth at which shale mineral diagenesis is well advanced, and where geopressure conditions may be expected.

A series of isothermal maps at temperatures at 66°C (150°F), 93°C (200°F), 120°C (250°F), and 149°C (300°F) were prepared early in this study of the geotemperature regime. These map temperatures were selected because of their relation to the hydrology of the deposits. The 66°C isothermal surface is always in and near the base of the hydropressure zone. The 93°C isotherm is always within and near the top of the geopressure zone *except* where water is leaking through fault planes or through fault-produced avenues of escape. The 120°C isotherm is generally 300 to 500 metres or more below the top of the geopressure zone, and the 149°C isotherm is a kilometre or more below it. Relief on the 66°C isothermal surface is commonly 500 to 1,000 metres in a county-sized area and even greater on the 93°C isotherm—in some places exceeding 2 km. Relief is less—seldom greater than 300 to 500 metres—on the 120°C and 149°C isotherms.

Isothermal profiles on the geologic sections, figures 9 through 12, are closely related to sediment facies and geologic structure. The upwarp of the 66°C and

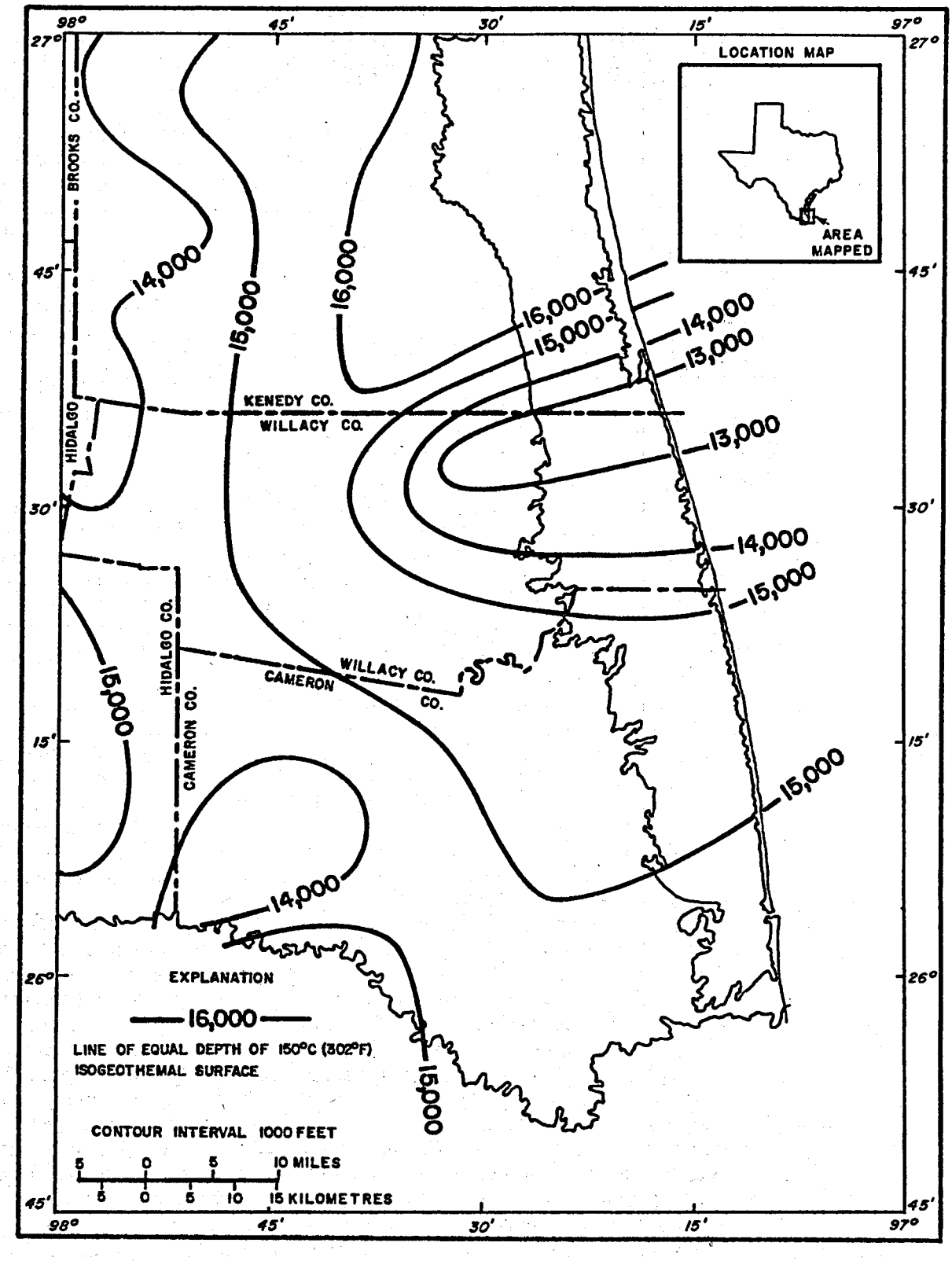

Figure 39. Depth of occurrence of the 150°C (302°F) isothermal surface in the South Texas Coastal Plain.

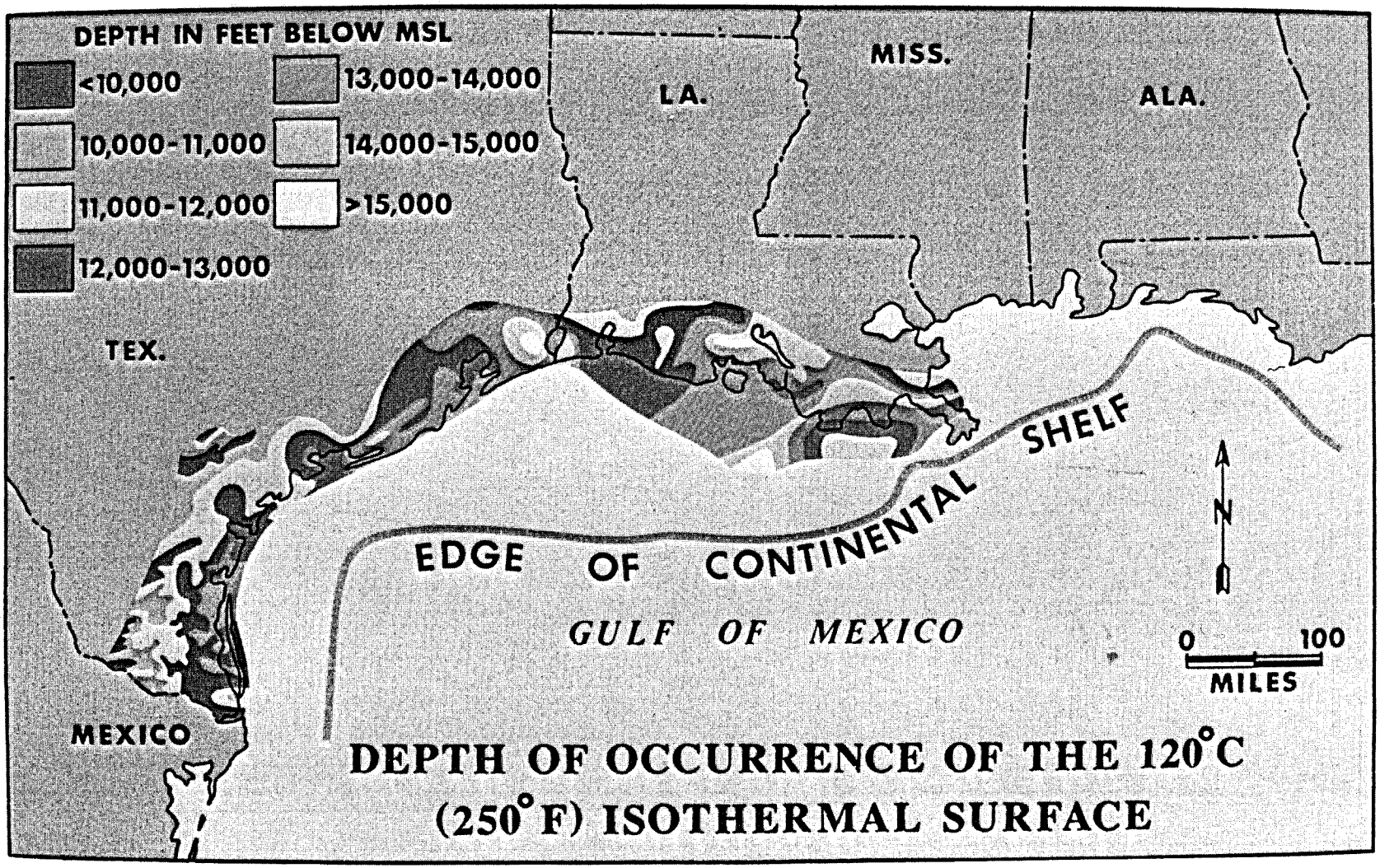

Figure 40. Depth of occurrence of the 120°C (250°F) isothermal surface beneath the Gulf Coastal Plain in Texas and Louisiana (modified from Jones, 1970).

93°C isotherms in the downdip deposits in figure 9 was caused by water leakage up fault planes. The upwarp of these two isotherms at middle depths of the Wilcox group in figure 10 are the result of water movement updip in sandy deposits. In figure 11, upwarp of all isotherms is evidently related to water movement up fault planes in the geopressured zone. Upwarp of the 66°C and 93°C isotherms appears to be related to water movement updip in lower Wilcox delta plain deposits and possibly in sandy deposits of the overlying Claiborne group. The upwarps of isotherms in figure 12 appear to be fault-leakage effects. Downwarps at the salt dome suggest that heat redistribution by highly conductive salt is restricted to rather narrow depth range. The salt column does not appear to extend to great depth, where it would receive an appreciable heat inflow.

The isothermal profiles shown in figures 9 through 12 indicate that the geotemperature regime of the hydropressure zone in these deposits is transitory, and is mainly a function of the rate of water escape from the geopressure zone. This conclusion is supported by the results of recent studies by Pusey (1973) who has measured the maximum temperature to which these deposits

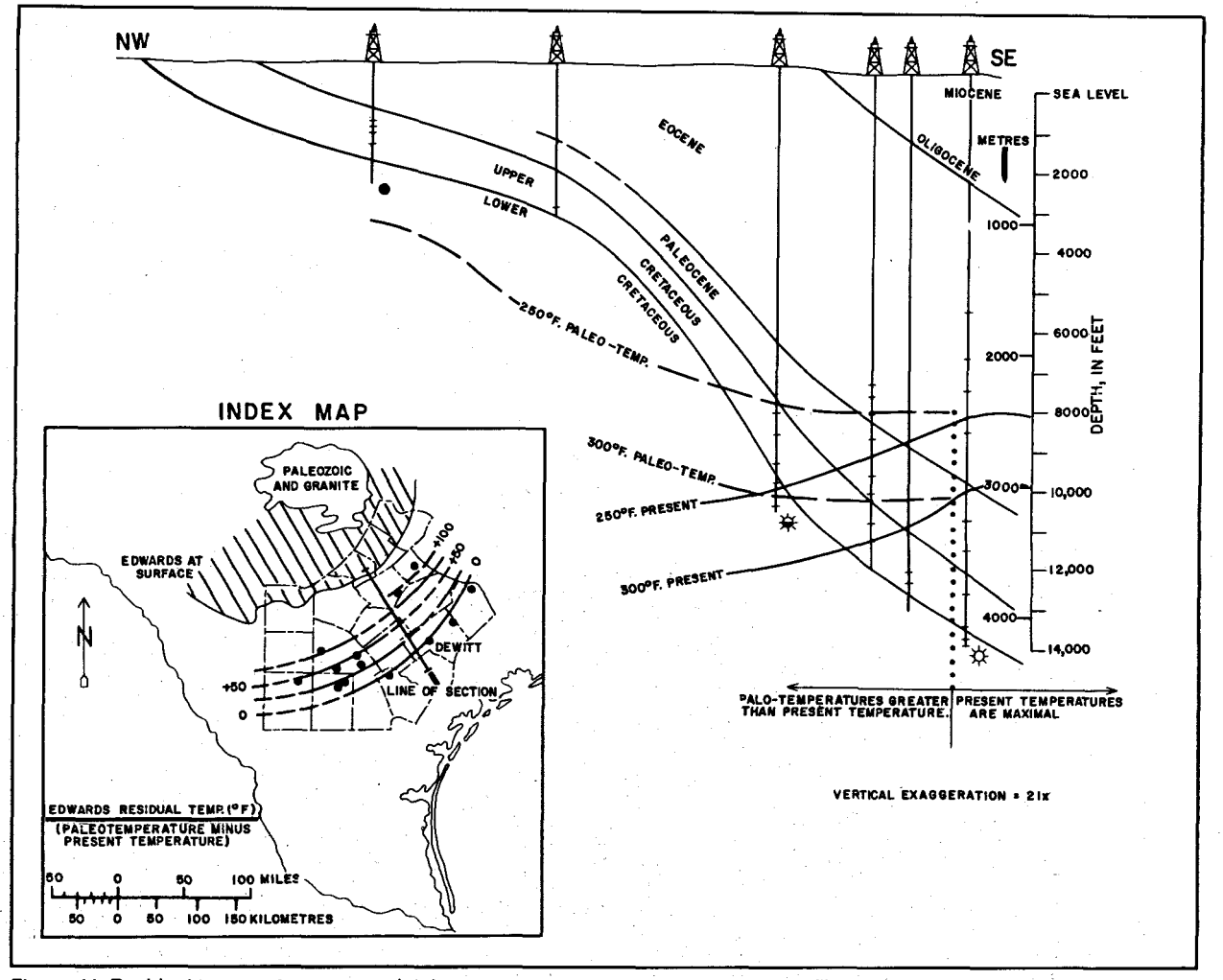

Figure 41. Residual temperature map and paleotemperature-present temperature profiles on a dip section along the south flank of San Marcos Arch, Texas Coastal Plain.

have been exposed. Using the electron spin resonance of kerogen extracted from well samples ranging in age from lower Cretaceous to lower Eocene, Pusey has mapped the 120°C (250°F) and 149°C (300°F) paleotemperature isotherms along the dip section shown in figure 41. Also shown in this section is the present depths of these two isotherms. Lower Cretaceous deposits at a depth of about 3.3 km (10,500 ft) are now more than 28°C (50°F) cooler than they once were. Gulfward the paleoisotherms and present-day isotherms converge, and farther gulfward the deposits are now as warm as they have ever been.

The convergence of modern and paleoisotherms gulfward on the profile in figure 41 suggests that hot water escaping from the geopressure zone causes a isothermal wave, the crest of which moves gulfward in geologic time. This gulfward-moving isothermal wave is accompanied by a gulfward-moving pressure wave; the top of the geopressure zone rises gulfward and sinks landward in geologic time, as suggested in figure 7.

Perhaps the most profound effect of the geotemperature regime on the hydrology of the basin is the massive flush of water resulting from clay mineral

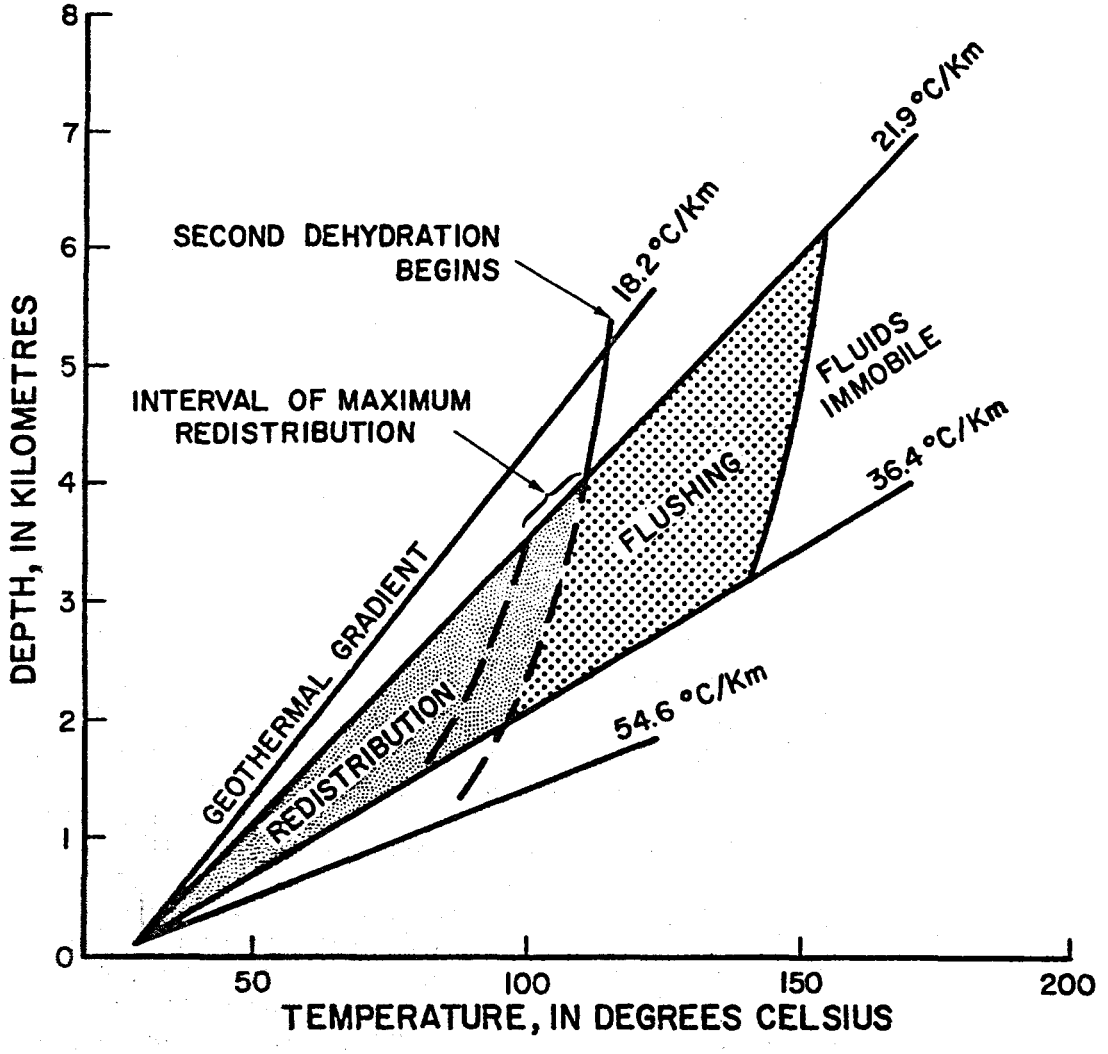

Figure 42. Shale-water redistribution model for the northern Gulf of Mexico basin (from Burst, 1969).

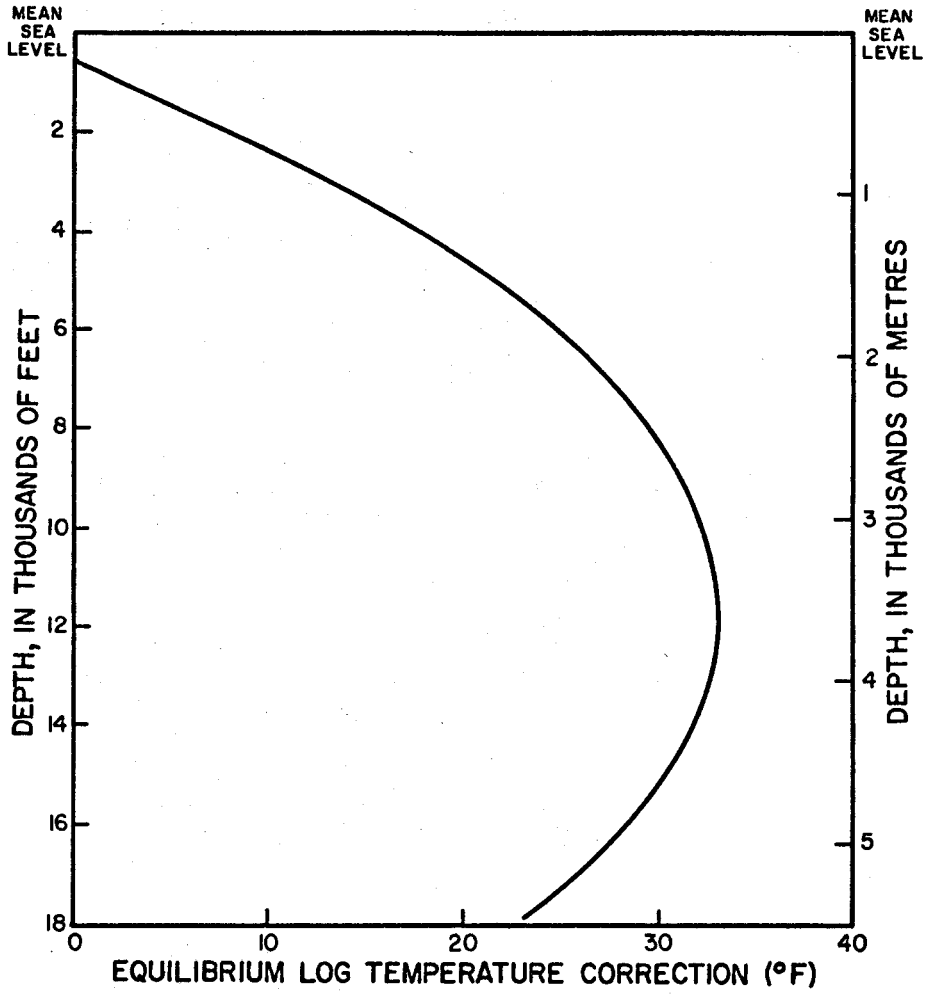

Figure 43. Curve for adjusting nonequilibrium bottom-hole temperatures to approximate equilibrium temperatures.

diagenesis. The depth at which this flush occurs in any locality is defined by the geothermal gradient; the volume of water released may equal 10 to 15 percent of the bulk volume of the rock. As the flush begins at temperatures of about 100°C and continues through temperatures of about 150°C, the depth range of the flush can be described by a diagram such as that in figure 42. The geothermal gradients are not linear in the zone of transition from hydropressure to geopressure, and true gradients with appropriate dog-legs should be graphed for any locality. The flush is capable of producing geopressure, and it probably sustains geopressure in geologic time by replacing leakage losses.

Data on equilibrium temperature at depth for 366 Gulf Coast wells were used in the Geothermal Survey of North America (Kehle, 1971) to derive an empirical correction curve by which a nonequilibrium bottom-hole temperature from the well-log reading can be converted to approximate equilibrium temperature. This curve (fig. 43) shows maximum correction at depths of about 12,000 feet. The equation of this curve has been used to adjust all bottom-hole temperature data used for isothermal mapping by the U.S. Geological Survey in its study of the Rio Grande embayment area in Texas.

HYDROCHEMICAL REGIME

The expulsion of water from shale with porosities less than about 45 percent apparently is restricted by hyperfiltration. The flow of salt solutions through such clays in the laboratory generates appreciable osmotic pressure opposing the flow. McKelvey, of the Gulf Research and Development Co. (written communication, 1966) reports that:

> In general, the generated osmotic pressures are within 95 percent of the calculated theoretical pressures; i.e., a one normal sodium chloride solution versus fresh water yields an osmotic pressure of 690 psi. Since experimental errors tend to reduce measured values, it is probably safe to assume that, under our laboratory conditions, the clay acts like a perfect semipermeable membrane.

White (1965) states that:

> The evidence is now convincing that fine-grained sediments behave as semipermeable membranes, permitting selective escape of water and concentrating dissolved components in remaining pore fluids.

The selective retention of ionized dissolved solids within clay beds from which water is expelled by compaction (with increasing depth of burial and overburden load) produces an osmotic pressure gradient resisting compaction as water squeezed into adjacent sand beds is freshened. The salinities of water in sandstone cores (table 1) were taken at different distances from the clay boundary of a sand bed penetrated by a Gulf Coast well drilled with an oil-base mud. Hyperfiltration of water from the bounding clay bed is clearly evident.

The clay-bed seal of the geopressure zone separates two hydrodynamic systems. A very large gradient in head is present between the underlying geopressured zone and the overlying hydropressure zone. These conditions are shown in figure 44, in which no leakage up the fault plane has occurred. A field example of the hypothetical salinity distribution in figure 44 is shown in figure 45, for a well in Cameron County, Texas. The actual salinity differential across the clay-bed seal penetrated by well CAM-183 is 45,000 mg/l, and the

TABLE 1

Core Data for a Nueces County, Texas, Oil Test Well, Showing Decrease in Formation Water Salinity at Sand Bed Boundaries

Sample	Depth Feet	Permeability, Millidarcys	Porosity %	Residual Saturation % by volume Oil	Residual Saturation % by volume Gas	Residual Saturation % pore space Oil	Residual Saturation % pore space Gas	Total Chloride, ppm	Probable Production
16	11070—71	18.0	21.9	0.9	5.9	4.1	68.8	15,500	condensate
17	11071—72	29.0	20.9	5.3	5.7	25.4	47.2	27,000	condensate
18	11072—73	1.0	13.7	1.6	4.4	11.7	56.1	25,800	condensate
19	11073—74	1.5	18.2	2.5	6.5	13.7	50.6	27,800	condensate
20	11074—75	7.8	21.2	1.5	6.9	7.1	60.3	22,500	condensate
21	11075½—76	1.9	19.3	2.5	7.0	13.0	50.7	24,800	condensate
22	11076—77	21.0	21.3	4.5	6.4	21.1	48.9	25,100	condensate
23	11077—78	2.2	19.9	3.4	6.5	17.1	50.3	27,500	condensate
24	11078—78¼	1.1	13.3	0.0	4.5	0.0	66.1	21,800	condensate
25	11079—80	8.2	23.7	3.3	6.4	13.9	59.2	25,700	condensate
26	11080¼—81	0.0	11.7	0.0	5.2	0.0	55.4	24,400	
27	11081—81½	0.9	15.7	1.6	5.8	10.2	52.7	26,200	condensate
28	11082—82½	15.0	23.8	2.5	5.5	10.5	66.4	16,500	condensate

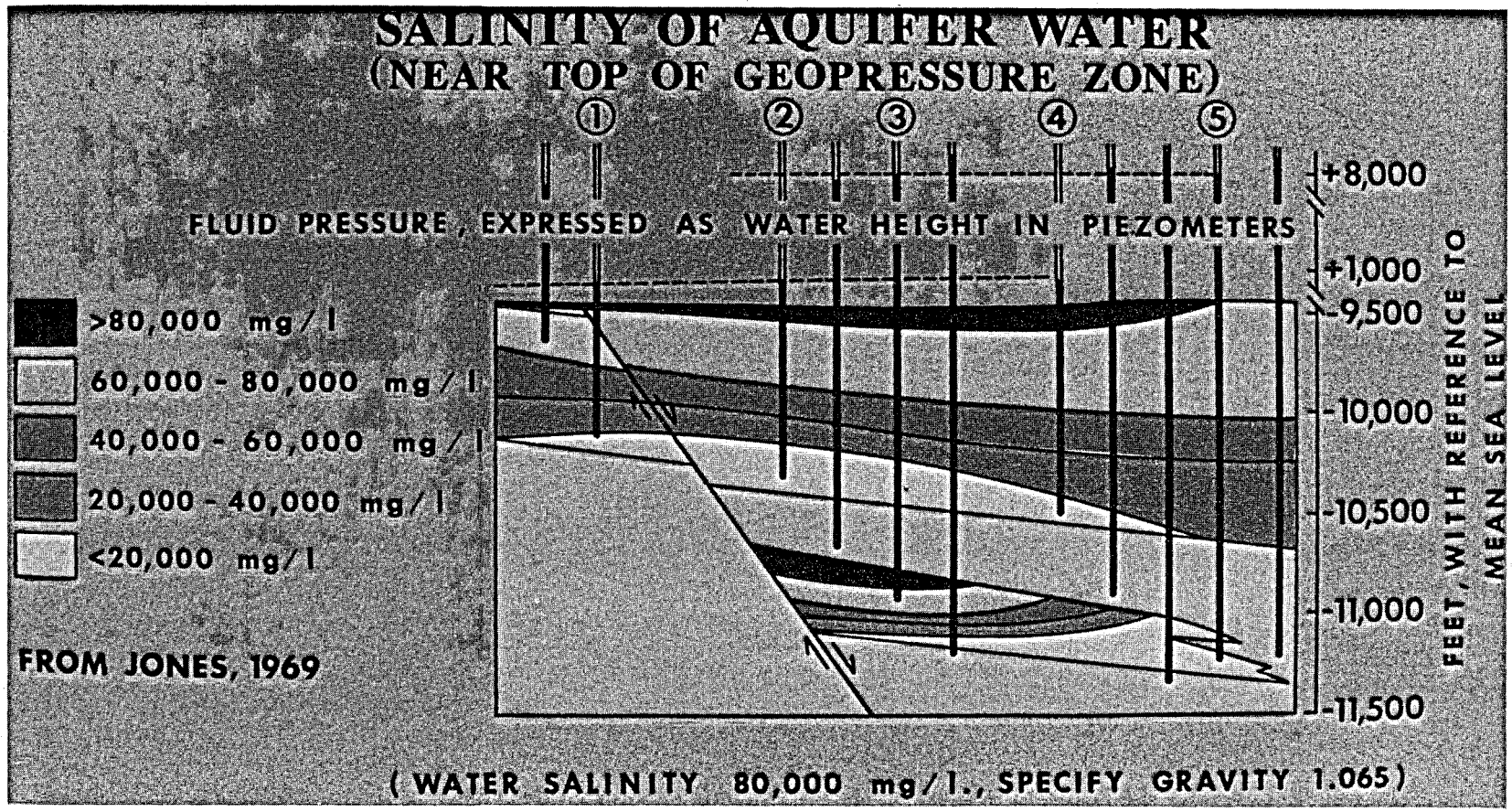

Figure 44. Idealized aquifer water salinity distribution near the top of the geopressure zone and the base of the hydropressure zone.

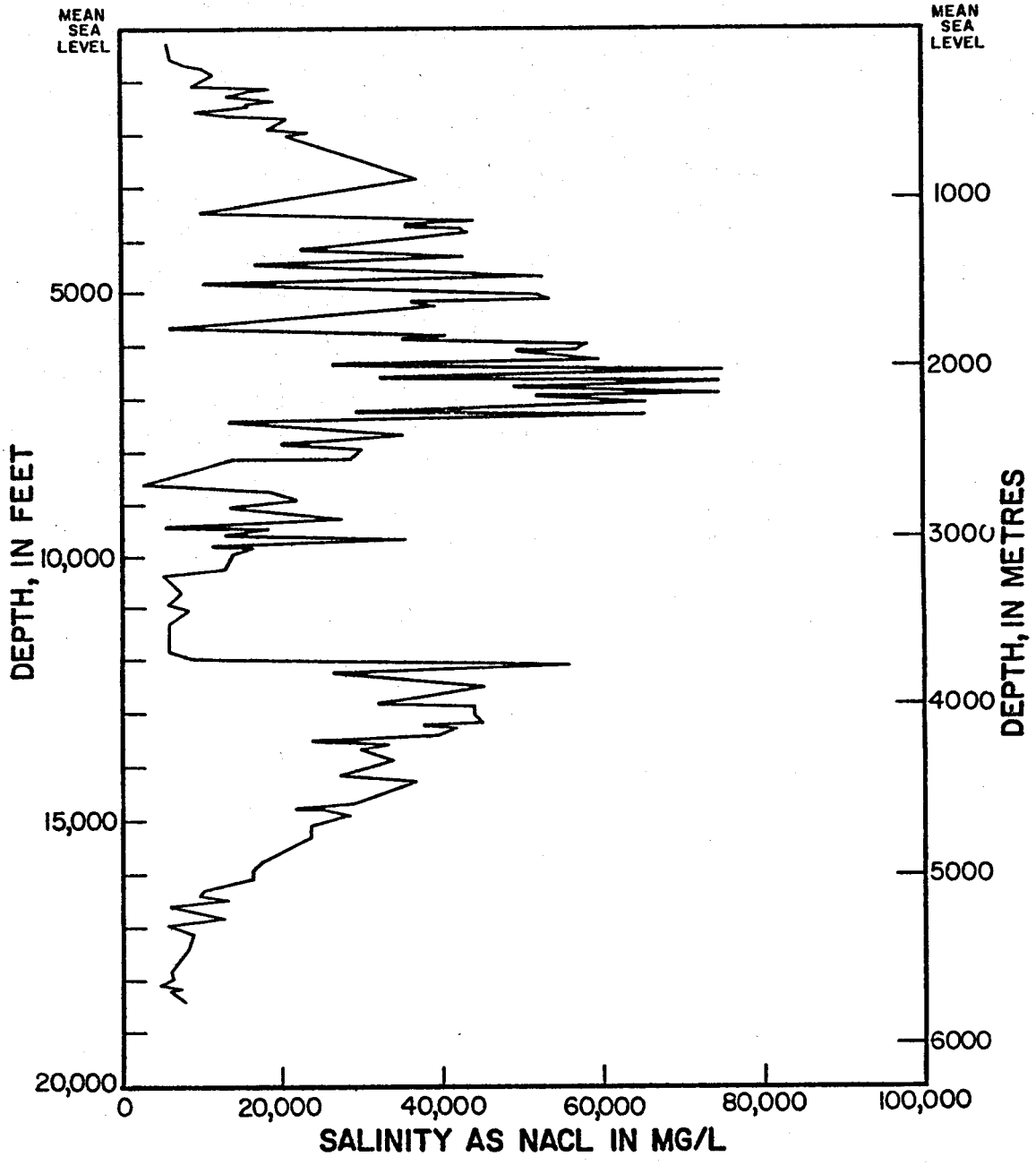

Figure 45. Depth-salinity profile for sand-bed aquifers penetrated by a well in Cameron County, Texas.

maximum osmotic pressure differential possible under these conditions is about 28.1 kg/cm^2 or about 400 psi. (See fig. 46.) The effectiveness of the clay-bed seal of the geopressure zone as a hyperfiltration membrane is indicated, and a mechanism for concentrating dissolved solids in Gulf basin ground waters to observed salinities is suggested, if not demonstrated, by these figures.

A reasonable inference from the phenomena and principles discussed above is that the resistance of a clay bed to compaction (i.e., its load-bearing strength) depends upon the salinity contrast between the clay-pore water and water in the adjacent sand beds. Any change in the salinity of water in a sand bed, such as changes produced by regional mass movement of ground water, could, according to this thesis, result in delayed or accelerated compaction of adjacent clay beds—depending upon the resulting pore-water salinity contrast.

In general, the escape of high-salinity water from the geopressure zone up fault planes has greatly increased the salinity of water in the basal sands of the hydropressure zone. The common pattern of the depth-salinity profile is that shown in figures 47 and 48. This process has completely flushed the geopressure zone of high-salinity water in broad areas, making possible the mapping of depth below which the salinity of formation water is less than 10,000 mg/l. An example is shown in figure 49. The data upon which these maps and profiles of formation-water salinity are based are derived mainly by use of spontaneous potential measurements on the electric logs. These potentials are analysed in terms of the dissolved solids in the formation water, expressed as mg/l of sodium chloride. Computed data graphed in figures 45 and 47 are listed in table 2.

The large-scale release of fresh water from clay beds into sand beds of the geopressure zone resulting from clay mineral diagenesis at elevated

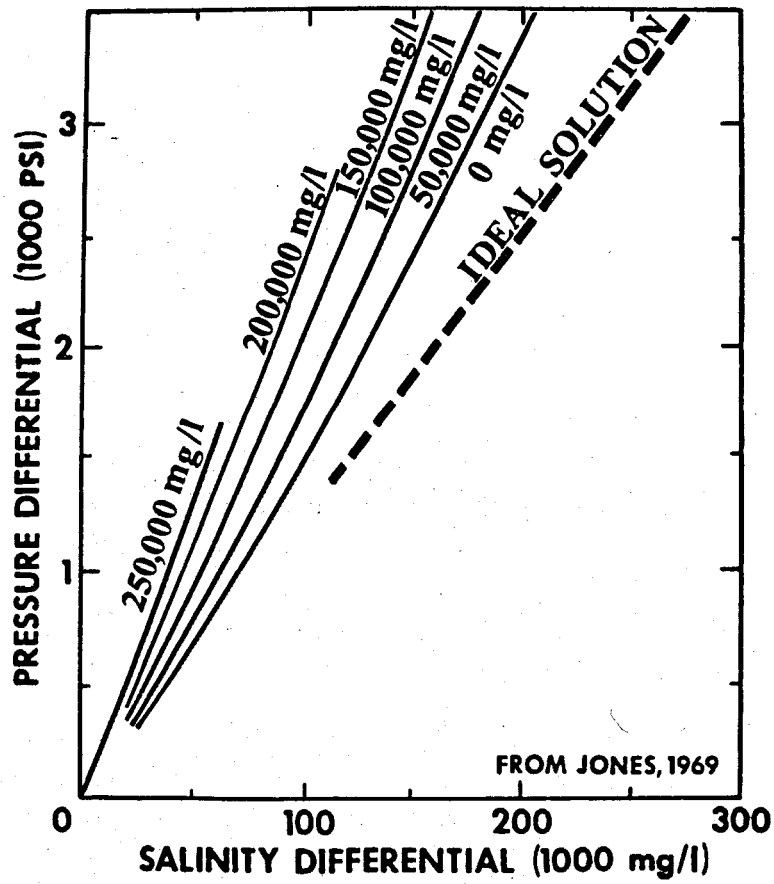

Figure 46. Theoretical osmotic pressure across a clay membrane.

TABLE 2

Salinity of Formation Waters
in Sand Beds Penetrated by Wells
in Hidalgo and Cameron Counties,
Texas, Graphed in Figures 45 and 47.

Hidalgo County, Well No. 57, Countywide Temperature, 83°F, Countywide Depth, 443 ft below MSL

Interval No.	Depth below MSL	Thick-ness	Mud Weight	Temp.	ppm NaCl	Log Run	Type of Fluid	SP	Log Depth
1	−2494 to −2514	20	10.4	114	40223	1	QBC6	−24	2565 to 2585
2	−2574 to −2634	60	10.4	115	55649	1	QBC6	−36	2645 to 2705
3	−2939 to −3024	85	10.4	121	89530	1	QBC6	−55	3010 to 3095
4	−3064 to −3157	93	10.4	123	100756	1	QBC6	−61	3135 to 3228
5	−3484 to −3577	93	10.4	129	76648	1	QBC6	−49	3555 to 3648
6	−3639 to −3689	50	10.4	131	128454	1	QBC6	−73	3710 to 3760
7	−3764 to −3804	40	10.4	133	80395	1	QBC6	−52	3835 to 3875
8	−3949 to −3974	25	10.4	136	123303	1	QBC6	−71	4020 to 4045
9	−4059 to −4104	45	10.4	137	118295	1	QBC6	−69	4130 to 4175
10	−4174 to −4234	60	10.4	139	75666	1	QBC6	−49	4245 to 4305
11	−4254 to −4294	40	10.4	140	127045	1	QBC6	−73	4325 to 4365
12	−4799 to −4829	30	10.4	148	43688	1	QBC6	−27	4870 to 4900
13	−4901 to −4934	33	10.4	150	65590	1	QBC6	−43	4972 to 5005
14	−5154 to −5204	50	10.4	154	88266	1	QBC6	−57	5225 to 5275
15	−5311 to −5361	50	10.4	156	76002	1	QBC6	−50	5382 to 5432
16	−5447 to −5529	82	10.4	159	94201	1	QBC6	−60	5518 to 5600
17	−5627 to −5684	57	10.4	161	102769	1	QBC6	−64	5698 to 5755
18	−6204 to −6229	25	10.4	169	59100	1	QBC6	−39	6275 to 6300
19	−6254 to −6274	20	10.4	170	62336	1	QBC6	−41	6325 to 6345
20	−6724 to −6774	50	10.4	177	76302	1	QBC6	−50	6795 to 6845
21	−7644 to −7681	37	10.4	191	63426	1	QBC6	−41	7715 to 7752
22	−7764 to −7844	80	10.4	193	65270	1	QBC6	−42	7835 to 7915
23	−8004 to −8029	25	10.4	196	67137	1	QBC6	−43	8075 to 8100
24	−8244 to −8274	30	10.4	200	50850	1	QBC6	−32	8315 to 8345
25	−8544 to −8584	40	10.4	205	47155	1	QBC6	−29	8615 to 8655
26	−8699 to −8784	85	10.4	207	88956	1	QBC6	−57	8770 to 8855
27	−8829 to −8874	45	10.4	209	77645	1	QBC6	−51	8900 to 8945
28	−9034 to −9074	40	10.4	212	55528	1	QBC6	−36	9105 to 9145
29	−9219 to −9264	45	10.4	215	28603	1	QBC6	−13	9290 to 9335
30	−9324 to −9364	40	10.4	216	29533	1	QBC6	−14	9395 to 9435
31	−9899 to −9949	50	10.4	225	16028	1	QBC6	5	9970 to 10020
32	−10999 to −11029	30	14.0	248	28767	2	CQBX	2	11070 to 11100
33	−11719 to −11739	20	14.0	264	24636	2	CQBX	7	11790 to 11810
34	−12054 to −12064	10	14.0	272	25564	2	CQBX	6	12125 to 12135
35	−12509 to −12539	30	14.0	283	29400	2	CQBX	2	12580 to 12610
36	−13809 to −13824	15	15.1	309	19441	3	CQBX	10	13880 to 13895
37	−14254 to −14264	10	15.1	317	21513	3	CQBX	7	14325 to 14335
38	−14739 to −14764	25	15.1	326	22310	3	CQBX	6	14810 to 14835
39	−15259 to −15299	40	15.1	334	33922	4	C6QB	6	15330 to 15370
40	−15919 to −15949	30	15.1	343	33102	4	C6QB	7	15990 to 16020
41	−16054 to −16064	10	15.1	345	29434	4	C6QB	11	16125 to 16135
42	−16164 to −16319	155	15.1	347	27314	4	C6QB	14	16235 to 16390

TABLE 2, *continued*

Cameron County, Well No. 183, Countywide Temperature, 78°F, Countywide Depth, 121 ft below MSL

Interval No.	Depth below MSL		Thick-ness	Mud Weight	Temp.	ppm NaCl	Log Run	Type of Fluid	SP	Log Depth	
1	−273 to	−299	26	9.1	80	5604	1	NATU	−9	334 to	360
2	−332 to	−359	27	9.1	81	5596	1	NATU	−9	393 to	420
3	−492 to	−545	53	9.1	84	5988	1	NATU	−11	553 to	606
4	−559 to	−591	32	9.1	84	6317	1	NATU	−12	620 to	652
5	−686 to	−719	33	9.1	86	8046	1	NATU	−17	747 to	780
6	−729 to	−807	78	9.1	87	9874	1	NATU	−21	790 to	868
7	−866 to	−889	23	9.1	89	11404	1	NATU	−24	927 to	950
8	−1090 to	−1110	20	9.1	92	8875	1	NATU	−19	1151 to	1171
9	−1126 to	−1149	23	9.1	92	18566	1	NATU	−37	1187 to	1210
10	−1159 to	−1191	32	9.1	93	16370	1	NATU	−34	1220 to	1252
11	−1282 to	−1309	27	9.1	94	13501	1	NATU	−29	1343 to	1370
12	−1336 to	−1361	25	9.1	95	18527	1	NATU	−37	1397 to	1422
13	−1379 to	−1402	23	9.1	96	19265	1	NATU	−38	1440 to	1463
14	−1406 to	−1444	38	9.1	96	15750	1	NATU	−33	1467 to	1505
15	−1467 to	−1499	32	9.1	97	15743	1	NATU	−33	1528 to	1560
16	−1501 to	−1569	68	9.1	98	13907	1	NATU	−30	1562 to	1630
17	−1587 to	−1627	40	9.1	99	9076	1	NATU	−20	1648 to	1688
18	−1695 to	−1743	48	9.1	100	20909	1	NATU	−40	1756 to	1804
19	−1911 to	−1922	11	9.1	103	18388	1	NATU	−37	1972 to	1983
20	−1954 to	−2012	58	9.1	104	23512	1	NATU	−43	2015 to	2073
21	−2024 to	−2069	45	9.1	105	20843	1	NATU	−40	2085 to	2130
22	−2839 to	−2869	30	9.1	116	37194	1	NATU	−56	2900 to	2930
23	−2908 to	−2926	18	9.1	117	34765	1	NATU	−54	2969 to	2987
24	−3484 to	−3507	23	12.4	126	10090	2	UCAL	−22	3545 to	3568
25	−3529 to	−3559	30	12.4	127	38622	2	UCAL	−47	3590 to	3620
26	−3566 to	−3580	14	12.4	128	30929	2	UCAL	−49	3627 to	3641
27	−3624 to	−3639	15	12.4	129	43911	2	UCAL	−60	3685 to	3700
28	−3709 to	−3739	30	12.4	130	35906	2	UCAL	−53	3770 to	3800
29	−3756 to	−3776	20	12.4	131	35879	2	UCAL	−53	3817 to	3837
30	−3782 to	−3808	26	12.4	131	42513	2	UCAL	−59	3843 to	3869
31	−3854 to	−3869	15	12.4	132	43576	2	UCAL	−60	3915 to	3930
32	−3992 to	−4021	29	12.4	135	37873	2	UCAL	−55	4053 to	4082
33	−4189 to	−4209	20	12.4	138	22831	2	UCAL	−41	4250 to	4270
34	−4264 to	−4299	35	12.4	139	39565	2	UCAL	−57	4325 to	4360
35	−4306 to	−4319	13	12.4	140	42892	2	UCAL	−60	4367 to	4380
36	−4478 to	−4490	12	12.4	143	17092	2	UCAL	−33	4539 to	4551
37	−4588 to	−4638	50	12.4	145	45651	2	UCAL	−63	4649 to	4699
38	−4670 to	−4686	16	12.4	146	52719	2	UCAL	−69	4731 to	4747
39	−4839 to	−4849	10	12.4	149	10476	2	UCAL	−22	4900 to	4910
40	−4889 to	−4907	18	12.4	150	16499	2	UCAL	−32	4950 to	4968
41	−4931 to	−4952	21	12.4	150	32780	2	UCAL	−51	4992 to	5013
42	−5017 to	−5048	31	12.4	152	52139	2	UCAL	−69	5078 to	5109
43	−5071 to	−5121	50	12.4	153	53605	2	UCAL	−70	5132 to	5182
44	−5157 to	−5170	13	12.4	154	36732	2	UCAL	−55	5218 to	5231
45	−5230 to	−5260	30	12.4	155	39365	2	UCAL	−58	5291 to	5321

TABLE 2, *continued*

Cameron County, Well No. 183, Countywide Temperature, 78°F, Countywide Depth, 121 ft below MSL

Interval No.	Depth below MSL	Thickness	Mud Weight	Temp.	ppm NaCl	Log Run	Type of Fluid	SP	Log Depth
46	−5680 to −5696	16	12.4	163	6261	2	UCAL	−12	5741 to 5757
47	−5789 to −5811	22	12.4	165	40740	2	UCAL	−60	5850 to 5872
48	−5880 to −5898	18	12.4	166	35730	2	UCAL	−55	5941 to 5959
49	−5922 to −5969	47	12.4	167	58487	2	UCAL	−74	5983 to 6030
50	−6041 to −6066	25	12.4	169	57100	2	UCAL	−73	6102 to 6127
51	−6069 to −6087	18	12.4	169	49756	2	UCAL	−68	6130 to 6148
52	−6249 to −6295	46	12.4	172	59513	2	UCAL	−75	6310 to 6356
53	−6309 to −6334	25	12.4	173	40189	2	UCAL	−60	6370 to 6395
54	−6346 to −6366	20	12.4	174	26727	2	UCAL	−47	6407 to 6427
55	−6389 to −6509	120	12.4	175	75050	2	UCAL	−85	6450 to 6570
56	−6600 to −6617	17	12.4	178	32626	2	UCAL	−53	6661 to 6678
57	−6642 to −6690	48	12.4	179	74907	2	UCAL	−85	6703 to 6751
58	−6742 to −6784	42	12.4	181	49472	2	UCAL	−68	6803 to 6845
59	−6817 to −6839	22	12.4	182	70499	2	UCAL	−82	6878 to 6900
60	−6867 to −6909	42	12.4	183	74780	2	UCAL	−85	6928 to 6970
61	−6913 to −6956	43	12.4	184	52260	2	UCAL	−70	6974 to 7017
62	−6973 to −7096	123	12.4	185	65669	2	UCAL	−79	7034 to 7157
63	−7227 to −7254	27	12.4	189	29506	2	UCAL	−51	7288 to 7315
64	−7269 to −7319	50	12.4	190	65500	2	UCAL	−79	7330 to 7380
65	−7431 to −7442	11	12.4	192	13749	2	UCAL	−29	7492 to 7503
66	−7674 to −7718	44	12.4	196	35333	2	UCAL	−56	7735 to 7779
67	−7839 to −7859	20	12.4	199	20494	2	UCAL	−40	7900 to 7920
68	−7954 to −7970	16	12.4	201	30216	2	UCAL	−52	8015 to 8031
69	−8101 to −8121	20	12.4	203	28942	2	UCAL	−51	8162 to 8182
70	−8134 to −8176	42	12.4	204	14238	2	UCAL	−30	8195 to 8237
71	−8595 to −8651	56	12.4	212	3075	2	UCAL	2	8656 to 8712
72	−8731 to −8759	28	12.4	214	18643	2	UCAL	−38	8792 to 8820
73	−8909 to −8928	19	12.4	217	22269	2	UCAL	−44	8970 to 8989
74	−9027 to −9039	12	12.4	218	13943	2	UCAL	−30	9088 to 9100
75	−9253 to −9293	40	12.4	222	27765	2	UCAL	−51	9314 to 9354
76	−9304 to −9349	45	12.4	223	25497	2	UCAL	−49	9365 to 9410
77	−9416 to −9431	15	12.4	225	5795	2	UCAL	−10	9477 to 9492
78	−9439 to −9479	40	12.4	226	18690	2	UCAL	−39	9500 to 9540
79	−9551 to −9579	28	12.4	227	13263	2	UCAL	−29	9612 to 9640
80	−9609 to −9681	72	12.4	229	35827	2	UCAL	−59	9670 to 9742
81	−9769 to −9784	15	12.4	231	11563	2	UCAL	−26	9830 to 9845
82	−9793 to −9829	36	12.4	231	16755	2	UCAL	−36	9854 to 9890
83	−9910 to −9937	27	12.4	233	14140	2	UCAL	−31	9971 to 9998
84	−10196 to −10209	13	12.4	238	13044	2	UCAL	−29	10257 to 10270
85	−10346 to −10357	11	12.4	240	5397	2	UCAL	−8	10407 to 10418
86	−10629 to −10657	28	12.4	245	7449	2	UCAL	−16	10690 to 10718
87	−10704 to −10803	99	12.4	247	6807	2	UCAL	−14	10765 to 10864
88	−10866 to −10879	13	12.4	249	5802	2	UCAL	−10	10927 to 10940
89	−10994 to −11009	15	12.4	251	8444	2	UCAL	−19	11055 to 11070
90	−11239 to −11289	50	12.4	256	5963	2	UCAL	−11	11300 to 11350
91	−11765 to −11781	16	12.4	264	5771	2	UCAL	−10	11826 to 11842
92	−11924 to −11949	25	12.4	267	8788	2	UCAL	−20	11985 to 12010

TABLE 2, *continued*

Cameron County, Well No. 183, Countywide Temperature, 78°F, Countywide Depth, 121 ft below MSL

Interval No.	Depth below MSL	Thick-ness	Mud Weight	Temp.	ppm NaCl	Log Run	Type of Fluid	SP	Log Depth
93	−12024 to −12041	17	15.4	268	56062	3	UCAL	−40	12085 to 12102
94	−12120 to −12153	33	15.4	269	45616	3	UCAL	−30	12181 to 12214
95	−12174 to −12196	22	15.4	270	26814	3	UCAL	−11	12235 to 12257
96	−12429 to −12449	20	15.4	272	45526	3	UCAL	−30	12490 to 12510
97	−12559 to −12639	80	15.4	274	39153	3	UCAL	−24	12620 to 12700
98	−12754 to −12766	12	15.4	276	32593	3	UCAL	−17	12815 to 12827
99	−12799 to −12829	30	15.4	277	44398	3	UCAL	−29	12860 to 12890
100	−12939 to −12979	40	15.4	278	44358	3	UCAL	−29	13000 to 13040
101	−13109 to −13129	20	15.4	280	45335	3	UCAL	−30	13170 to 13190
102	−13169 to −13194	25	15.4	281	38163	3	UCAL	−23	13230 to 13255
103	−13215 to −13249	34	15.4	281	42136	3	UCAL	−27	13276 to 13310
104	−13317 to −13399	82	15.4	283	39865	3	UCAL	−25	13378 to 13460
105	−13467 to −13477	10	15.4	284	24446	3	UCAL	−8	13528 to 13538
106	−13526 to −13543	17	15.4	285	33474	3	UCAL	−18	13587 to 13604
107	−13605 to −13635	30	15.4	285	30357	3	UCAL	−15	13666 to 13696
108	−13792 to −13869	77	15.4	288	34386	3	UCAL	−19	13853 to 13930
109	−14064 to −14192	128	15.4	291	27802	3	UCAL	−12	14125 to 14253
110	−14229 to −14255	26	15.4	292	37082	3	UCAL	−22	14290 to 14316
111	−14594 to −14699	105	15.4	297	29405	3	UCAL	−14	14655 to 14760
112	−14735 to −14755	20	15.4	298	22142	3	UCAL	−4	14796 to 14816
113	−14762 to −14794	32	15.4	298	25135	3	UCAL	−9	14823 to 14855
114	−14869 to −14907	38	15.4	299	28606	3	UCAL	−13	14930 to 14968
115	−15056 to −15101	45	15.4	302	24012	3	UCAL	−7	15117 to 15162
116	−15254 to −15284	30	15.4	304	24026	3	UCAL	−7	15315 to 15345
117	−15372 to −15429	57	15.4	305	22252	3	UCAL	−4	15433 to 15490
118	−15709 to −15809	100	15.4	309	17655	3	UCAL	4	15770 to 15870
119	−15869 to −15959	90	15.4	311	16545	3	UCAL	6	15930 to 16020
120	−16064 to −16119	55	15.4	313	16602	3	UCAL	6	16125 to 16180
121	−16257 to −16319	62	15.4	315	10741	3	UCAL	18	16318 to 16380
122	−16332 to −16362	30	15.4	315	10294	3	UCAL	19	16393 to 16423
123	−16389 to −16407	18	15.4	316	9905	3	UCAL	20	16450 to 16468
124	−16464 to −16536	72	15.4	317	13427	3	UCAL	12	16525 to 16597
125	−16593 to −16639	46	15.4	318	6270	3	UCAL	33	16654 to 16700
126	−16779 to −16819	40	15.4	320	10794	3	UCAL	18	16840 to 16880
127	−16829 to −16849	20	15.4	321	13037	3	UCAL	13	16890 to 16910
128	−16951 to −16989	38	16.4	322	6002	4	UCAL	13	17012 to 17050
129	−17114 to −17150	36	16.4	324	9052	4	UCAL	2	17175 to 17211
130	−17404 to −17426	22	16.4	328	8465	4	UCAL	4	17465 to 17487
131	−17549 to −17604	55	16.4	330	7594	4	UCAL	7	17610 to 17665
132	−17721 to −17734	13	16.4	332	6766	4	UCAL	10	17782 to 17795
133	−17794 to −17841	47	16.4	333	6265	4	UCAL	12	17855 to 17902
134	−17909 to −18046	137	16.4	335	6497	4	UCAL	11	17970 to 18107
135	−18084 to −18114	30	16.4	337	5081	4	UCAL	17	18145 to 18175
136	−18139 to −18151	12	16.4	337	6757	4	UCAL	10	18200 to 18212
137	−18179 to −18199	20	16.4	338	7578	4	UCAL	7	18240 to 18260
138	−18216 to −18229	13	16.4	338	6493	4	UCAL	11	18277 to 18290
139	−18359 to −18404	45	16.4	340	7844	4	UCAL	6	18420 to 18465

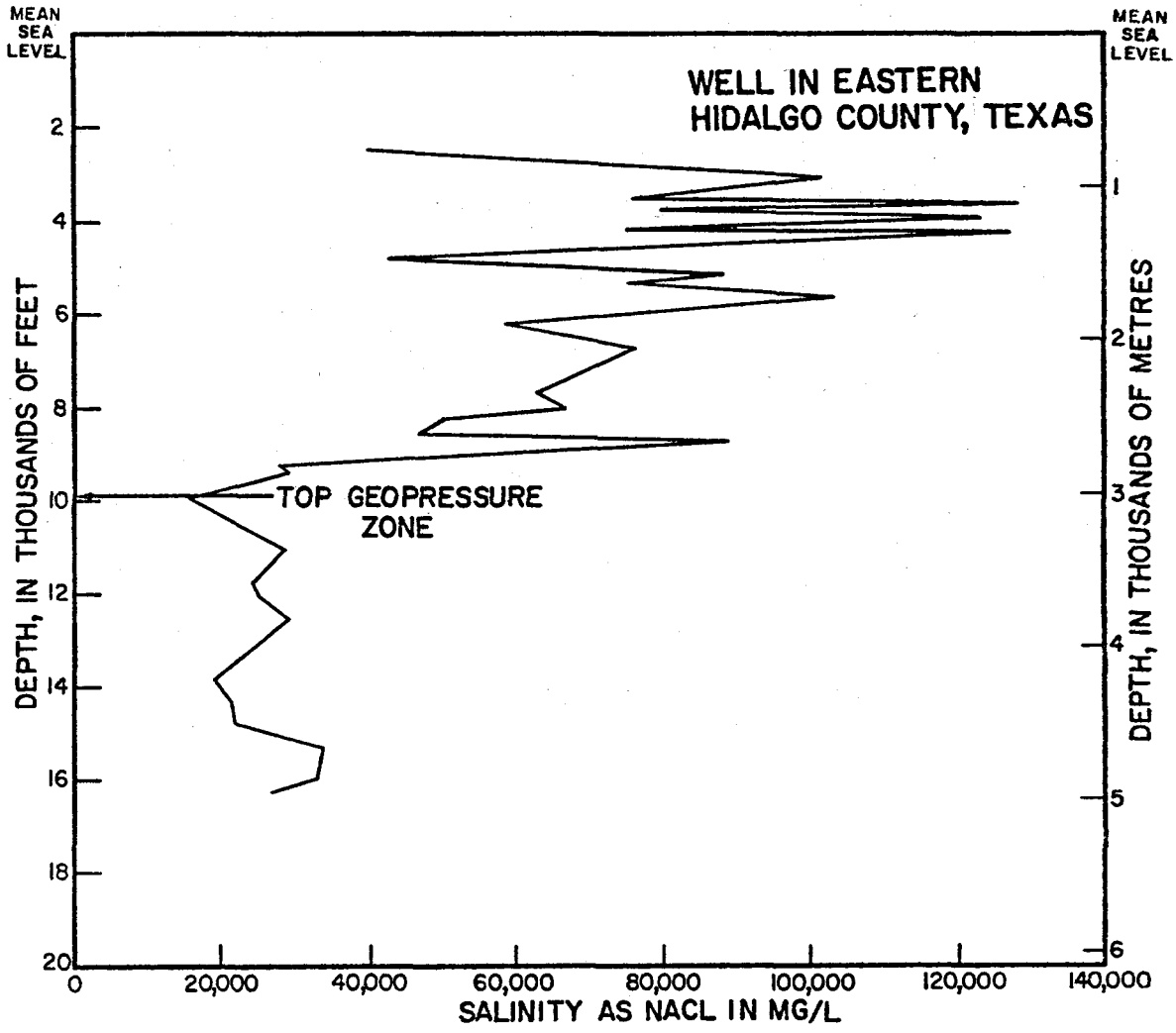

Figure 47. Graph of the salinity of formation waters with reference to depth in a well in eastern Hidalgo County, Texas.

temperature (Burst, 1969) reduces the load-bearing strength of clay by converting bound and crystalline water to fresh pore water that is able to drain from the clay bed without hyperfiltration-induced resistance. As the deposits in the basin are heated from below, the isotherms gradually rise through them. The 100°C isotherm triggers the thermal diagenesis of montmorillonite and liberates fresh water that rises as a wave, or front, through the deposits in geologic time.

The upward flush of fresh water drives the salty "connate" water already in the sand-bed systems ahead of it. Although less dense than the overlying saline waters, the fresh water sweeps the saline waters upward and out of the basin because it is driven by forces equivalent to the weight of the overlying rocks. Salinity patterns in the Eocene Wilcox group shown in figures 50 through 53 are excellent examples of the effects of regional upward flush. In plan, salinity patterns reflect sediment facies distributions. Water having less than 6,000 mg/l occurs in marine deposits that are gulfward from water having more than 70,000 mg/l of dissolved solids, now occupying delta plain deposits of freshwater origin. Water having the greatest salinity occurs at intermediate depth in

each mapped unit; the highest salinity water in the lower Wilcox occurs in its upper part, and the highest salinity water in the upper Wilcox occurs in its upper part.

In figure 54 all paramenters having important effects on the movement and salinity of ground water in Cenozoic deposits of the Gulf Coast geosyncline are shown on a profile from Zavala County, Texas, through Kenedy County, Texas, to the coastline. This section shows principal faults and key stratigraphic markers, six isothermal profiles, two fluid-pressure profiles, and the salinity of formation waters in five dissolved-solids ranges.

Perhaps the most obvious feature on this section is the freshness of water in the older deposits (landward) and the high salinity of water in younger deposits, gulfward from the Vicksburg flexure. Increased salinity is associated with deepening occurrence of isotherms gulfward from a regional isothermal high beneath Duval County. Conversely, deepening isotherms landward from the Duval County high are associated with marked freshening of formation waters. These salinity and temperature trends are associated with a fluid pressure high beneath the gulfward part of Duval County, deepening steeply gulfward from a fault zone in northwestern Kleberg County, and deepening landward across the full thickness of the Wilcox group near the Webb-Duval County boundary.

One may infer from this profile that isotherms are depressed beneath younger deposits, probably because these deposits are cold and carry a great amount of water that escapes upward early in the compaction cycle and effectively dissipates heat from below. Easy escape of compaction water is suggested by gulfward-sloping pressure surfaces. High-salinity water in the sand beds of this mass of Neogene deposits is partly due to the upward escape of salty water from the geopressure zone beneath it and partly to the expulsion

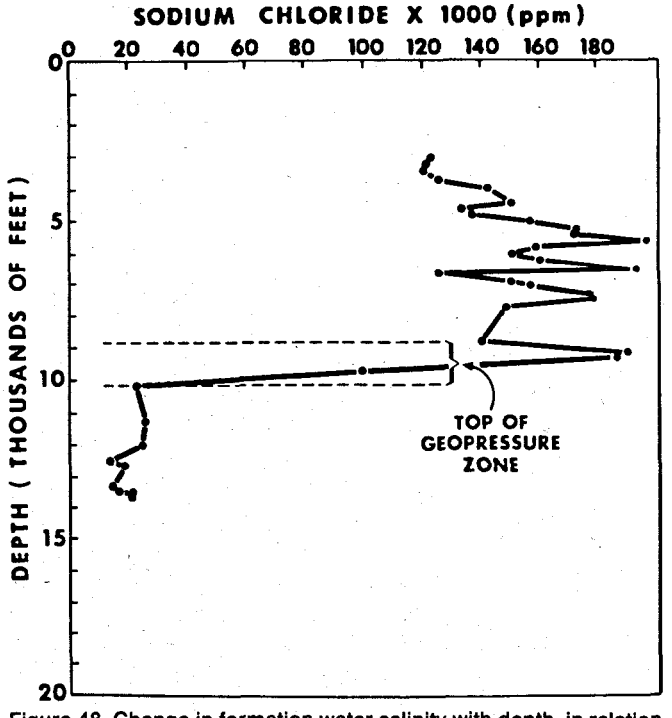

Figure 48. Change in formation water salinity with depth, in relation to the occurrence of the geopressure zone, Manchester Field, Calcasieu Parish, Louisiana (from Schmidt, 1971).

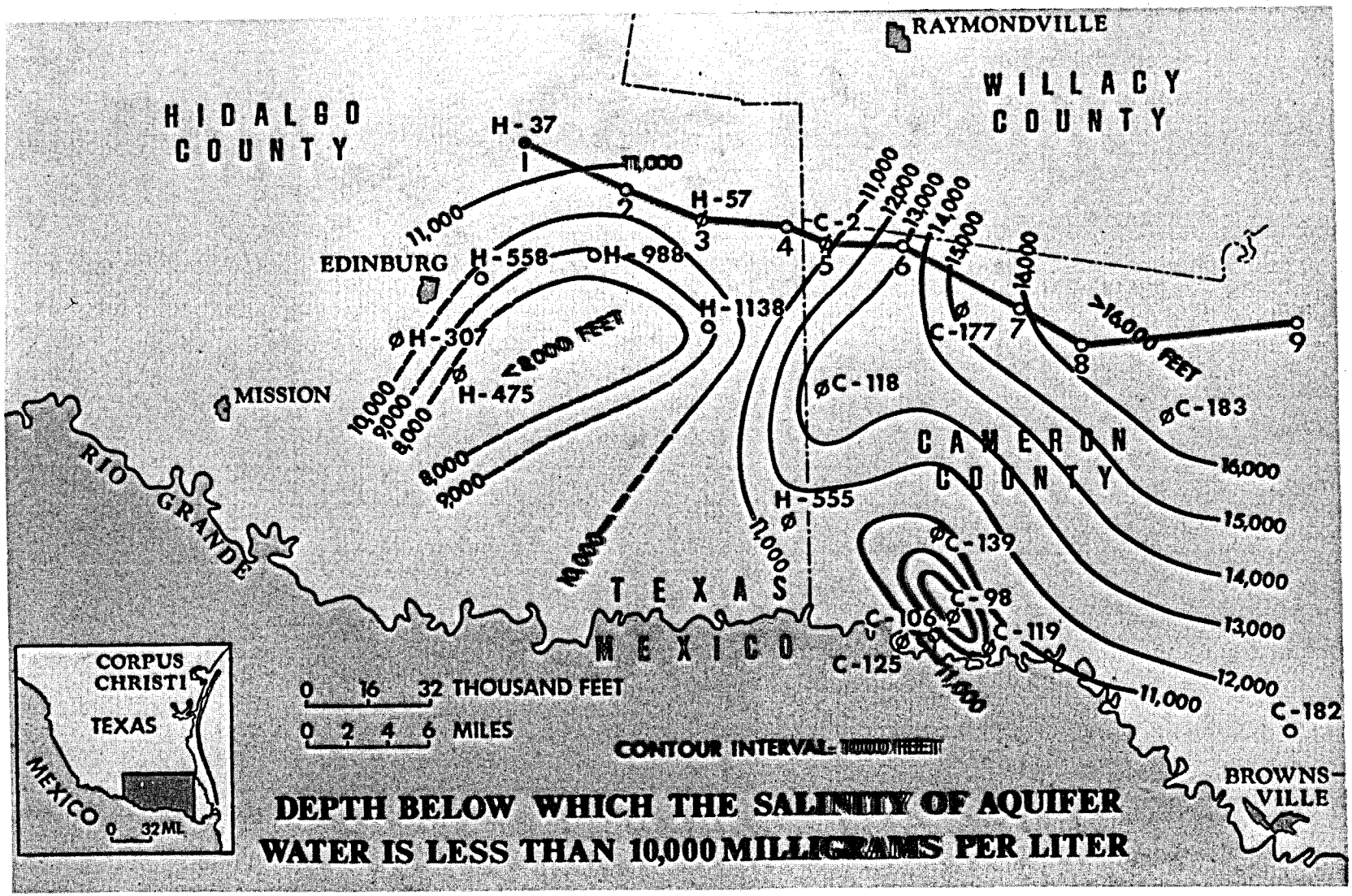

Figure 49. Map of an area in the lower Rio Grande embayment showing the depth below which the dissolved-solids content of formation water is less than 10,000 mg/l.

of saline water from the pores of clay beds in which conversion of calcium montmorillonite to sodium montmorillonite has occurred, with consequent loss of water molecules from pore waters as the newly formed sodium montmorillonite sorbed layer after layer of water on its mineral surfaces. This salinity concentration process begins during deposition, because the sorption capacity of the sodium montmorillonite thus created is some ten times greater than that of the calcium montmorillonite clay that is, and has been, carried to the Gulf of Mexico by streams that drain some two-thirds of the land area of the conterminous United States.

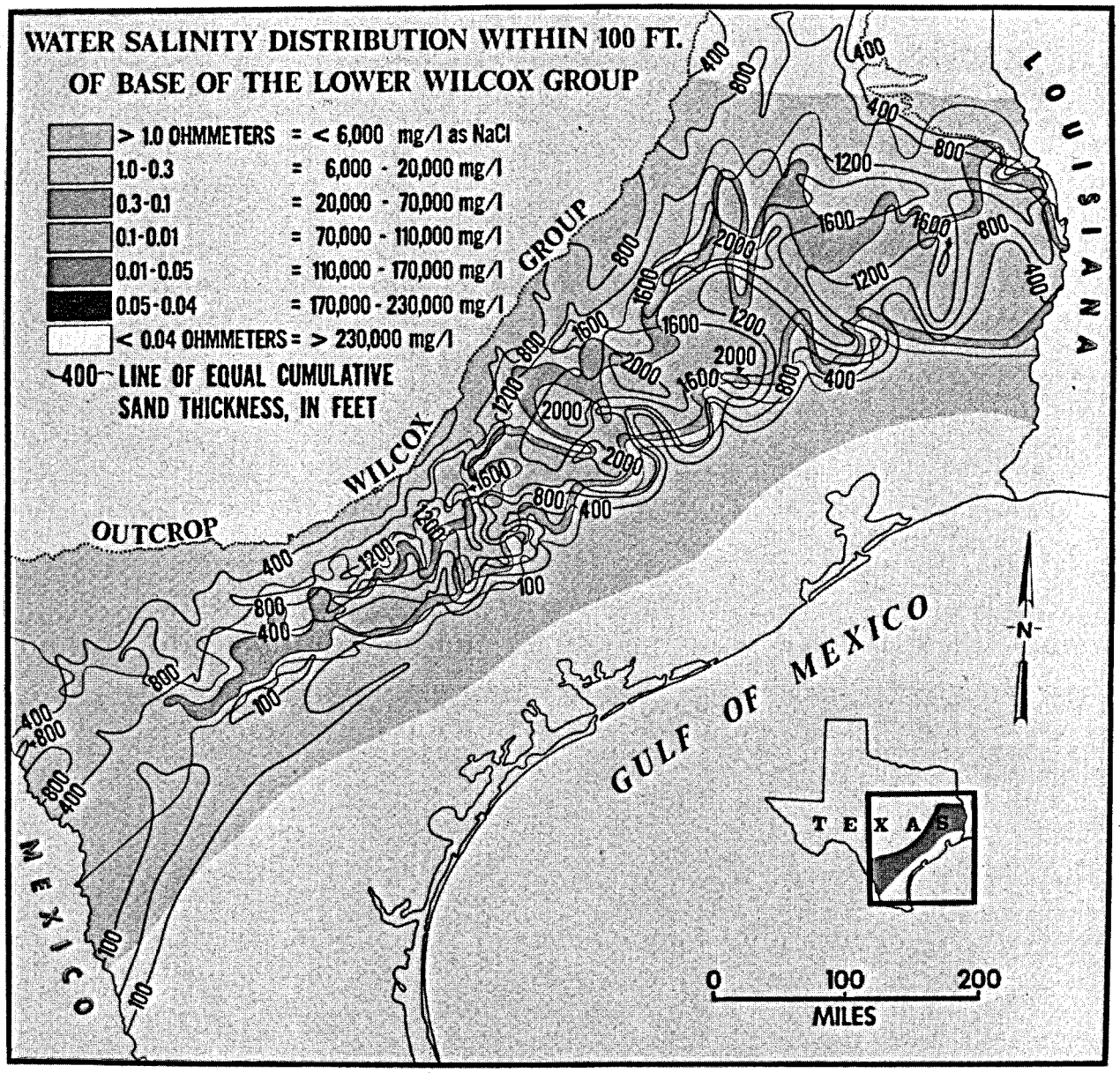

Figure 50. Cumulative thickness of sand beds in the lower Wilcox in Texas, and salinity of water in sand beds within about 30 metres (100 feet) of its base (sand thickness data from Texas Bureau of Economic Geology; salinity data from Mobil Oil Company).

Loss of salty water from the geopressure zone (up fault planes) has resulted in a widespread freshening of water in sand beds at great depth. On section *A–A'* (fig. 54), loss of salty water upward across the isothermal, isopressure high beneath Duval County has allowed many sands at depth to receive clay water and freshen. Water loss from the geopressure zone in this part of the section has also included much fresh water. Flushing of the hydropressure zone by fresh water from below is in progress.

Landward from the Duval County pressure-temperature high, the flush of fresh water from below has swept saline water from the Carrizo along the line of profile. It is fresh above a depth of about 1,800 metres (5,760 ft).

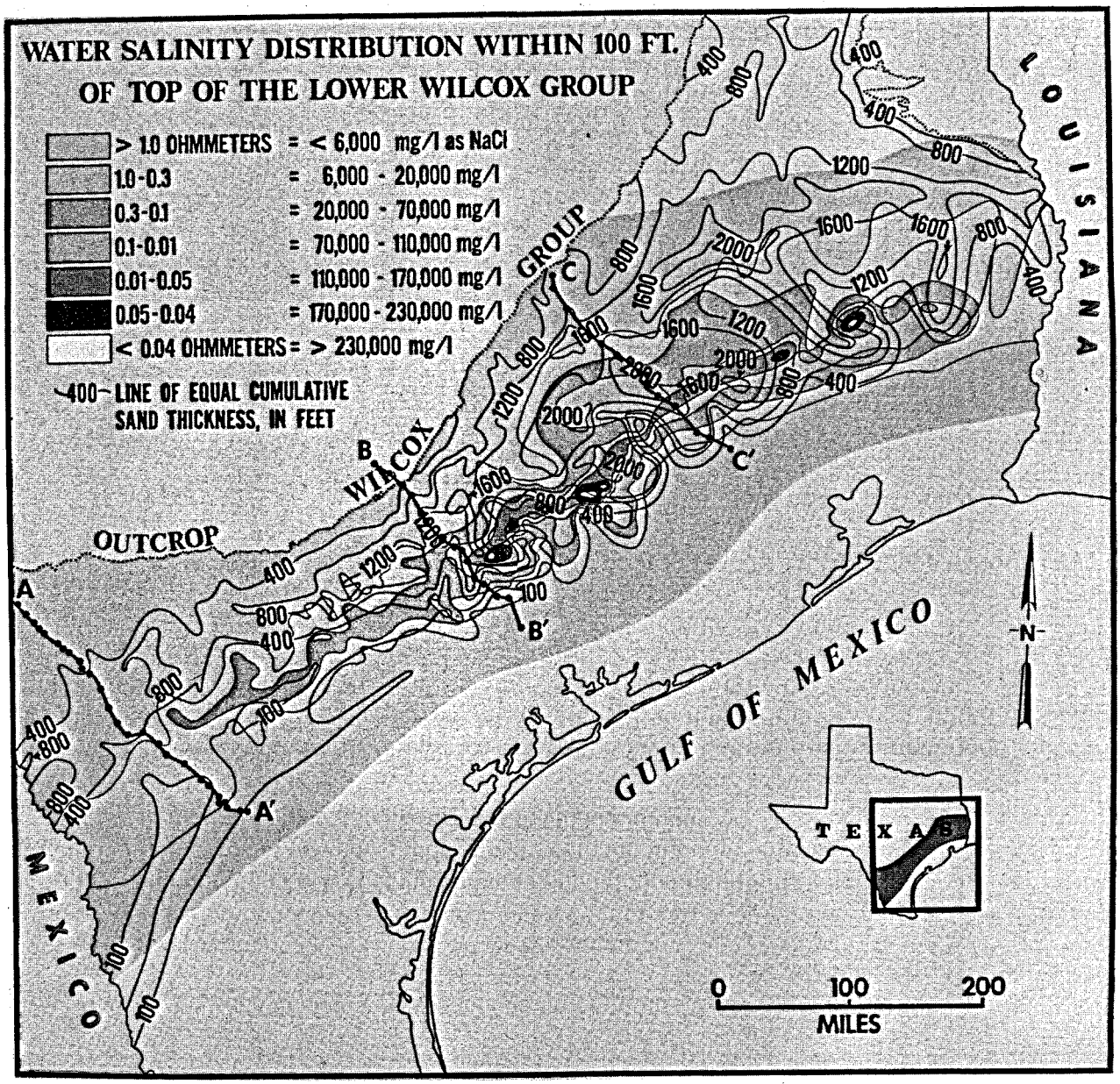

Figure 51. Cumulative thickness of sand beds in the lower Wilcox of Texas, and salinity of water in sand beds within about 30 metres (100 feet) of its top (sand thickness data from Texas Bureau of Economic Geology; salinity data from Mobil Oil Company).

On this profile there is general conformity of the 100°C isotherm with the depth interval between the isopressure surfaces representing fluid pressures equivalent to 0.6 and 0.7 times the weight of overlying sediments, indicating the transition zone between hydropressure and geopressure. Only where there is evidence of leakage up fault planes from the geopressure zone, as occurs immediately gulfward from the Webb-Duval County line, do these lines of profile cross at large angles. A second zone of leakage is apparent directly below the word "Duval" on this profile (fig. 54).

Upwarps of the 70°C isotherm in the hydropressure zone are associated with easy upward drainage in regional sand-bed aquifer systems. Formation-water

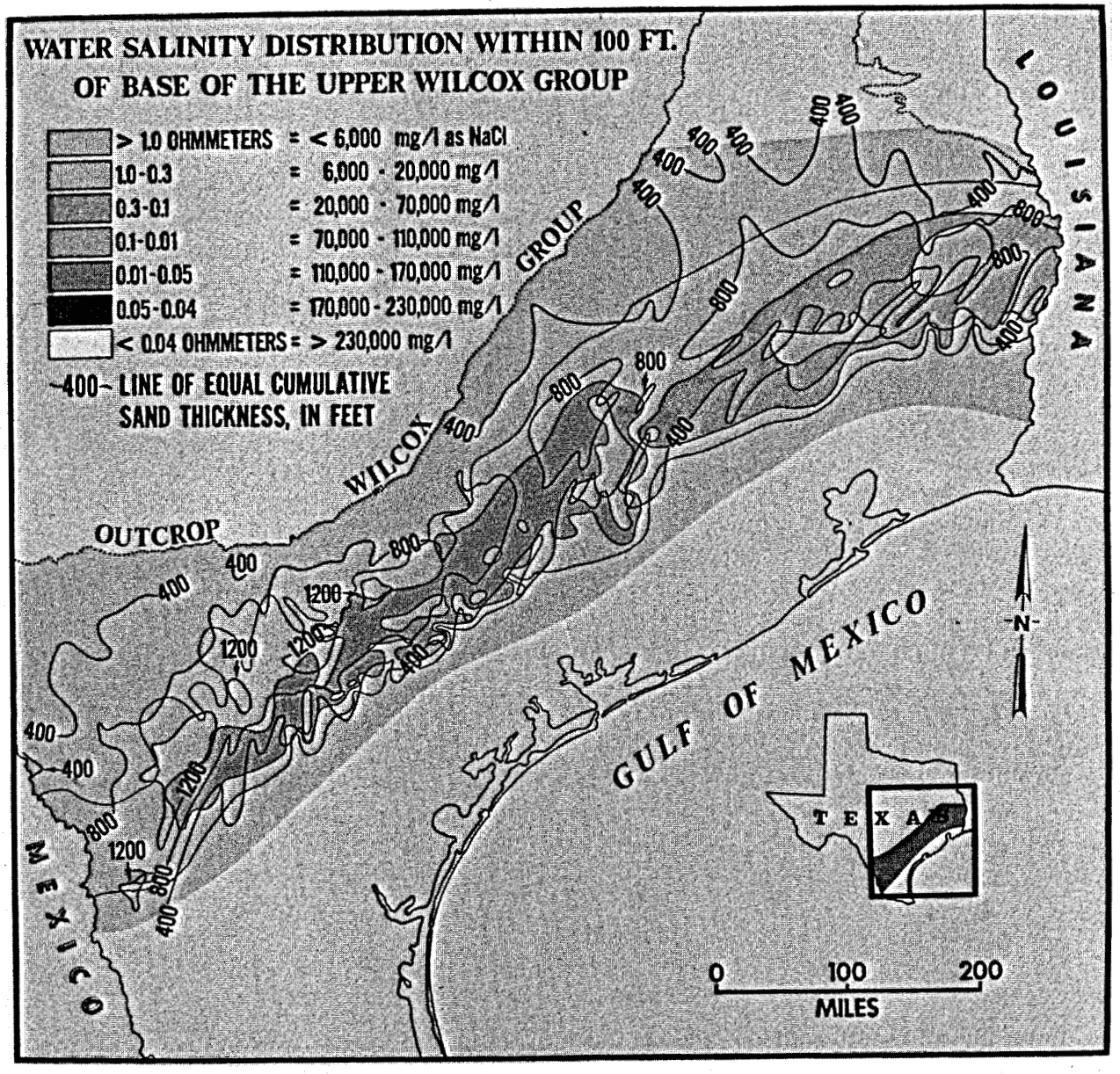

Figure 52. Cumulative thickness of sand beds in the upper Wilcox of Texas, and salinity of water in sand beds within about 30 metres (100 feet) of its base (sand thickness data from Texas Bureau of Economic Geology; salinity data from Mobil Oil Company).

salinity invariably reflects these mass movements, and temperature patterns are very useful for interpreting ground-water flow and water salinity distribution in geologically young basins.

The hydrochemical regime of the Gulf basin is thus coupled with both the hydrothermal regime and the hydrodynamic regime. Because these regimes are mutually interdependent, none can be analyzed effectively without study of the others because each provides diagnostic information regarding the others. Within the geologic framework of the basin, which in simplest terms describes the "plumbing" system, detailed information on temperature, fluid pressure (head), and water salinity define the hydrologic regime. And the hydrologic

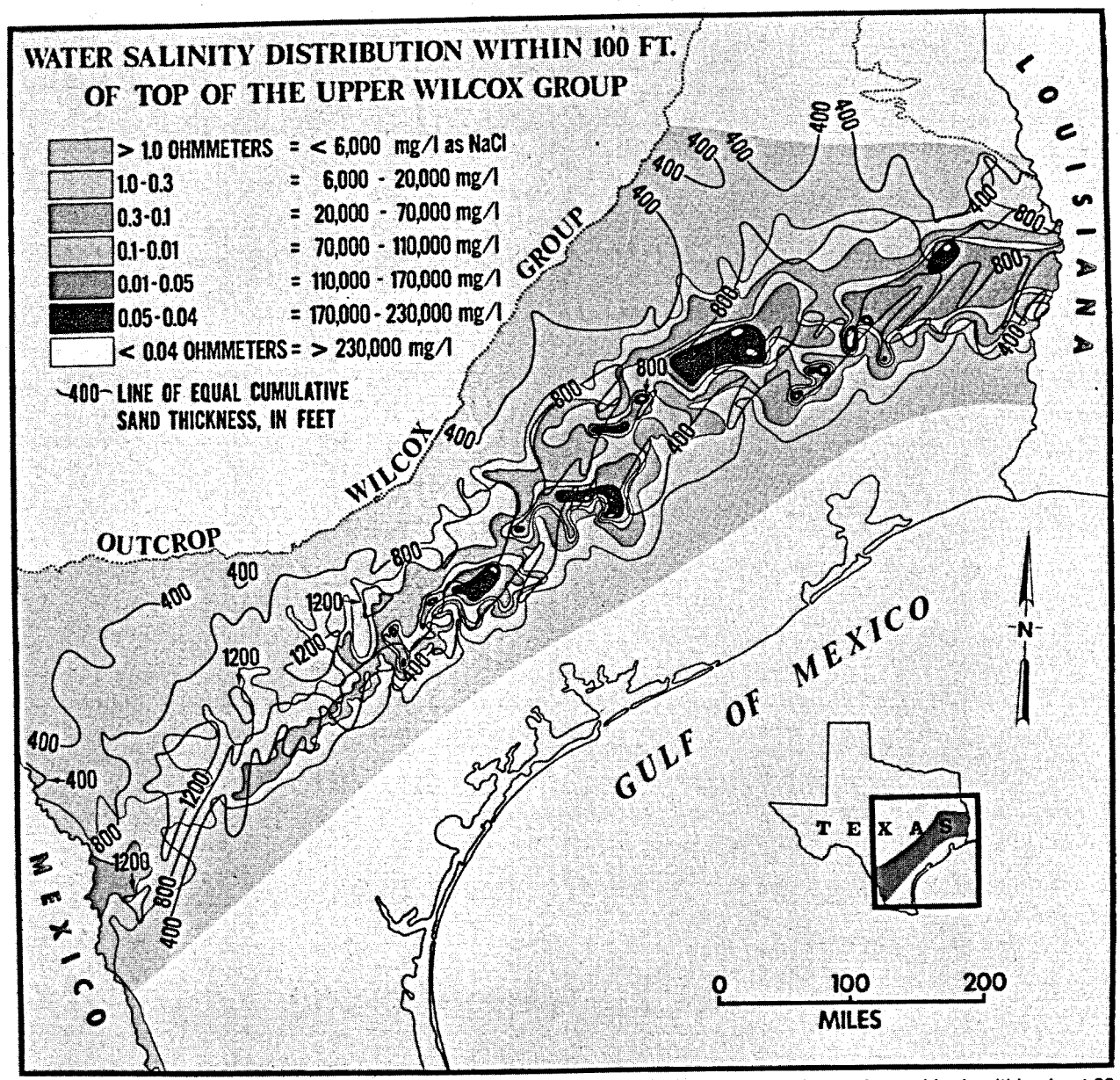

Figure 53. Cumulative thickness of sand beds in the upper Wilcox of Texas, and salinity of water in sand beds within about 30 metres (100 feet) of its top (sand thickness data from Texas Bureau of Economic Geology; salinity data from Mobil Oil Company).

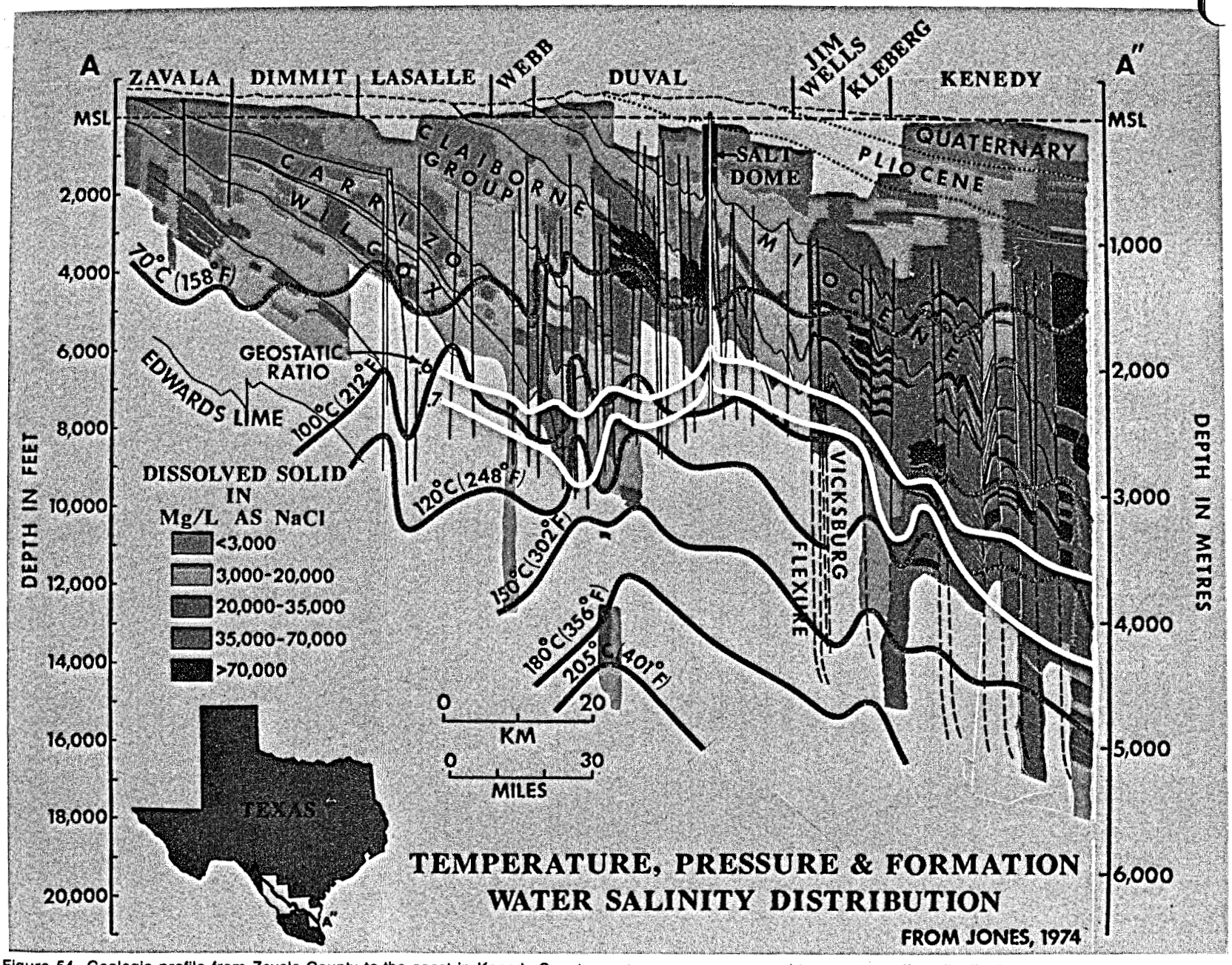

Figure 54. Geologic profile from Zavala County to the coast in Kenedy County, Texas, along the axis of the Rio Grande embayment, showing how geologic structure, geopressure, and temperature affect distribution of formation water salinity.

regime, with appropriate information on temperature, pressure, water salinity, and information on the type, distribution, and mineralogy of sediments, defines the principal elements of the hydrocarbon regime.

HYDROCARBON REGIME

Petroleum hydrocarbons are formed by the thermal metamorphism (maturation) of organic matter dispersed in marine shales. Insoluble kerogen is partially converted to water-soluble bitumens at a temperature controlled rate (LaPlante, 1974). Temperature increases with depth. The rate of hydrocarbon generation also increases with depth in the Gulf basin below a depth at which a "threshold" temperature is reached (Pusey, 1973). This process has been replicated in the laboratory in recent years, and a number of fundamental concepts regarding it have been formulated, largely as a result of intensive studies using improved equipment and techniques in analytical geochemistry (Philippi, 1965, 1968; Binder, 1965; Silverman, 1965; Welte, 1965; Hunt, 1968; Staplin, 1969; Tissot, et al, 1971; LaPlante, 1972, 1974; Cordell, 1972; Pusey, 1973; Price, 1973.)

The temperature at which hydrocarbon generation begins depends upon the type of organic matter present in the sediments, the sediment type and its mineralogy, and the time-temperature regime. In shales, sapropelic, organic-matter conversion may begin at about 60°C (140°F) and humic, organic-matter conversion may begin at about 93°C (200°F). The depth at which conversion begins is therefore dependent upon the geothermal gradient.

The way in which dispersed hydrocarbons generated in the source bed escape from low-permeability shale has been the subject of great interest for many years, and especially since 1965 (Burst, 1969; Perry and Hower, 1972; Price, 1973; Cordell, 1974; Philippi, 1974). Only recently was it learned that the aqueous solubility of hydrocarbon molecules in petroleum crude is sufficient, at temperatures, pressures, and water salinities known to occur in the geopressured zone, to account for the oil found in sedimentary basins (Price, 1973). (See figs. 55 and 56.) The "second-stage dehydration of montmorillonite" (Burst, 1969), also temperature controlled, provides the basis for

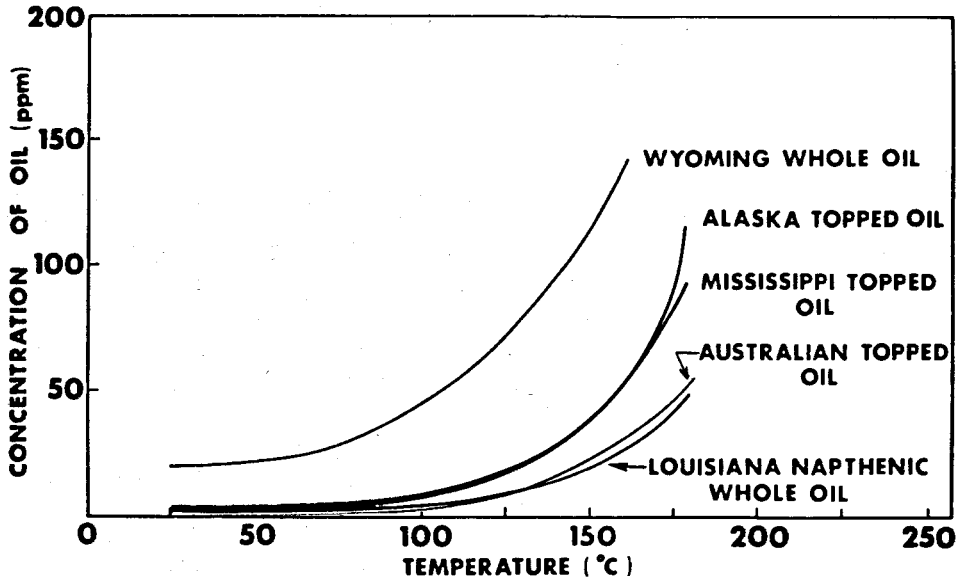

Figure 55. Solubility of oil in fresh water as a function of temperature (from Price, 1973).

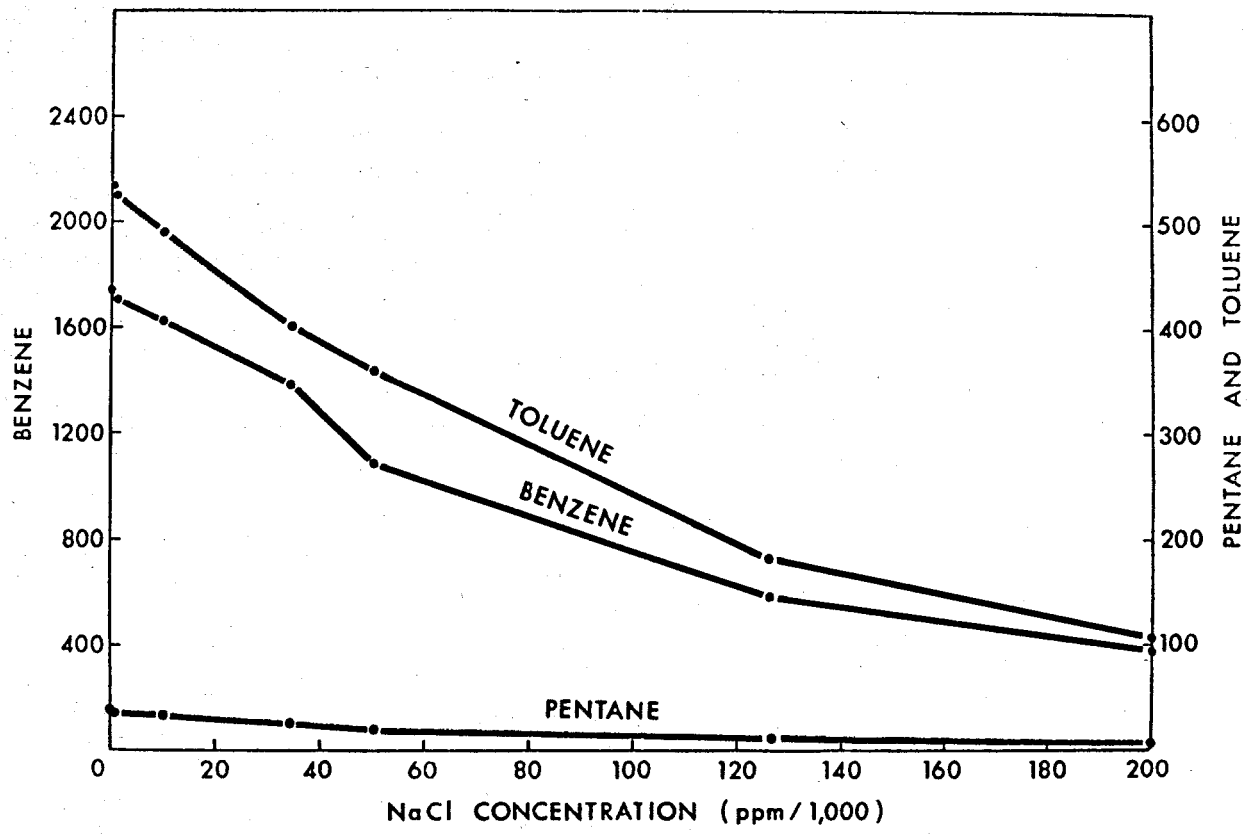

Figure 56. Solubility of benzene, toluene, and pentane in water at standard temperature (25°C) as a function of salinity; concentration expressed in parts per million (from Price, 1973).

an adequate and rational model for the primary migration of oil from shale-bed source to sand-bed reservoir.

The thermal diagenesis of montmorillonite, which makes up 60 to 80 percent of the clay in Cenozoic deposits of the Gulf basin, begins at temperatures above about 180°F (80°C) and is essentially complete at temperatures above 250°F (120°C). The chemical transformation of montmorillonite to illite and mixed-layer clay is endothermic and irreversible, releasing bound and intracrystalline water as fresh pore water in amounts up to half the volume of the mineral altered, or 10 to 15 percent of the compacted bulk volume of the fine-grained sediments (Burst, 1969). The zone of thermal diagenesis (collapse) of montmorillonite is, under hydrostatic conditions, "a relatively restricted, depth-dependent temperature zone in which the average dehydration temperature of the points measured is 221°F (105°C)," (Burst, 1969). This second-stage dehydration is retarded as pore pressure rises. The average dehydration temperatures may be as high as 250°F (120°C) at great depth and high geostatic ratio (Pusey, 1973).

Except where large-scale water losses from the geopressured zone have occurred locally, the 221°F (105°C) "average dehydration" isotherm is a short distance below the top of the geopressured zone, and fresh water, released as free pore water by the thermal diagenesis of montmorillonite, is under pressure ranging from 500 to 1,000 atmospheres depending upon the depth at which the seal of the geopressured zone occurs. Released pore water moves out of the

clay bed and toward the geopressured zone boundary, following the path of least resistance—generally a sand bed leading to fault planes that cut through the overlying shale-bed seal of the geopressured zone.

Dispersed hydrocarbon molecules generated in shale-source beds are probably taken into water solution soon after they are formed by the fresh water released from the very grains that enclose the newly formed bitumens. As the release of hot, fresh water from mineral grains to the interstitial pores continues, the fluid pressure rises, porosity and permeability are increased, the thermal conductivity is reduced, geothermal gradients steepen, and the

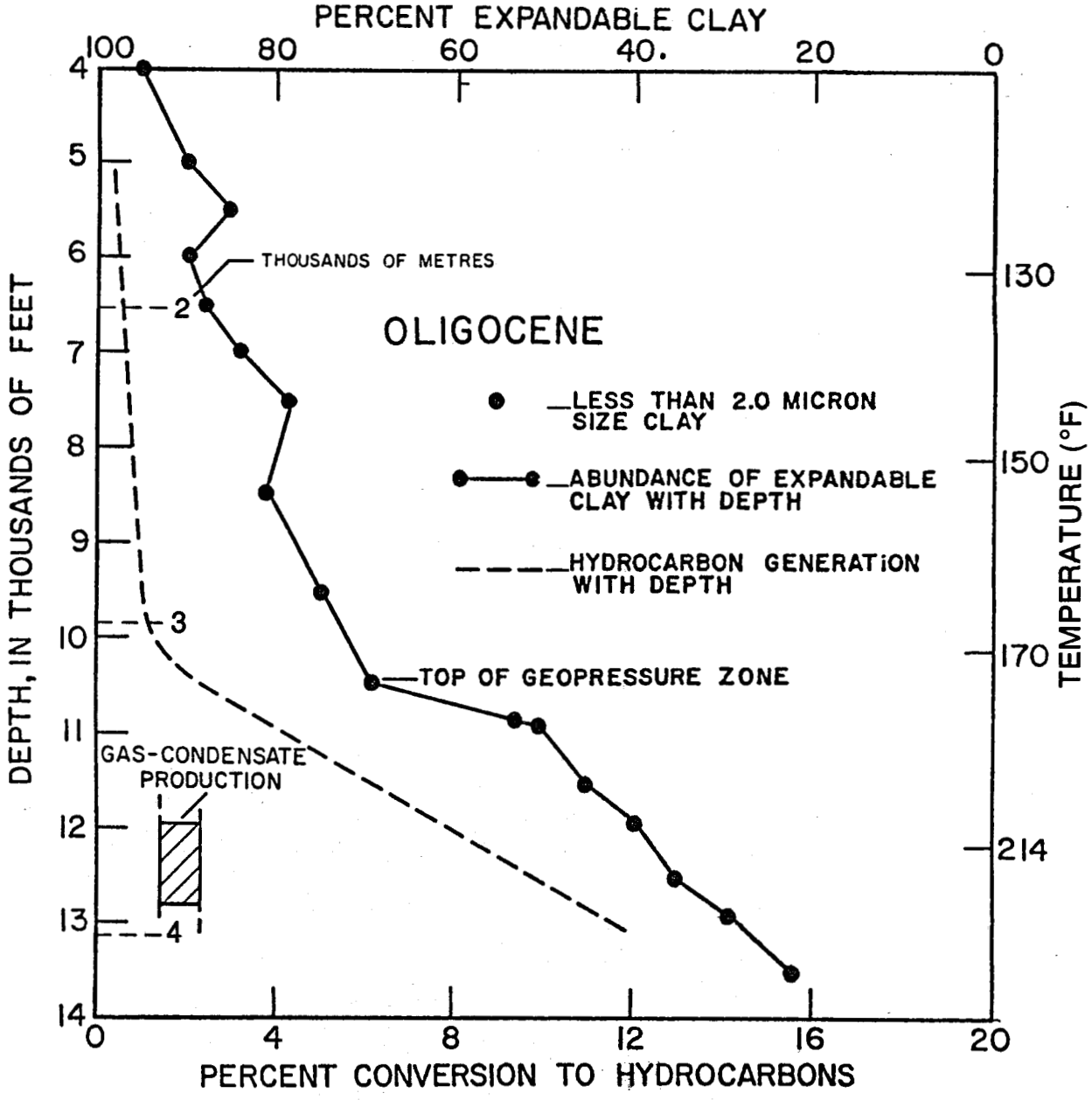

Figure 57. Relation between the rate of kerogen conversion to hydrocarbon, and the rate of clay mineral diagenesis as a function of increasing depth and temperature, Manchester Field, Calcasieu Parish, Louisiana (from Schmidt, 1971, and LaPlante, 1974).

temperature continues to rise. As the temperature passes 250°F (120°C) the rate of dehydration of montmorillonite decreases sharply, and diagenesis is completed. The loss of water from the shale continues, its porosity and permeability decline accordingly, and its thermal conductivity increases. When the conversion process ends, some 15 to 20 percent of the original montmorillonite remains unaltered and the hyperfiltration efficiency of the shale is largely preserved. The dissolved solids content of the clay pore water increases, osmotic forces opposing drainage grow, and resistance to compaction increases as porosity decreases.

Field data on the conversion of kerogen to hydrocarbon at depths below 3 km (9,600 ft) in samples from a well in the Manchester field, Calcasieu Parish, Louisiana, are given by LaPlante (1974). These data (fig. 57) show that less than one percent of the kerogen present has been converted to hydrocarbon at depths less than 3.1 km (9,920 ft) and temperatures less than 77°C (170°F). Below this depth, as temperature rises to about 112°C (234°F), conversion of kerogen progresses at a rate of about 1 percent for each 3°C temperature rise. The top of the geopressure zone is at a depth of 3.3 km (10,560 ft) and shale mineral diagenesis progesses rapidly below this depth with the montmorillonite content decreasing at a rate of about 1.2 percent for each 1°C of temperature rise. At a depth of 4.2 km (13,500 ft), about 13 percent of the kerogen has been converted to hydrocarbon; and the amount of expandable clay (montmorillonite) has been reduced from about 70 percent at a depth of 3.1 km to about 22 percent at 4.2 km.

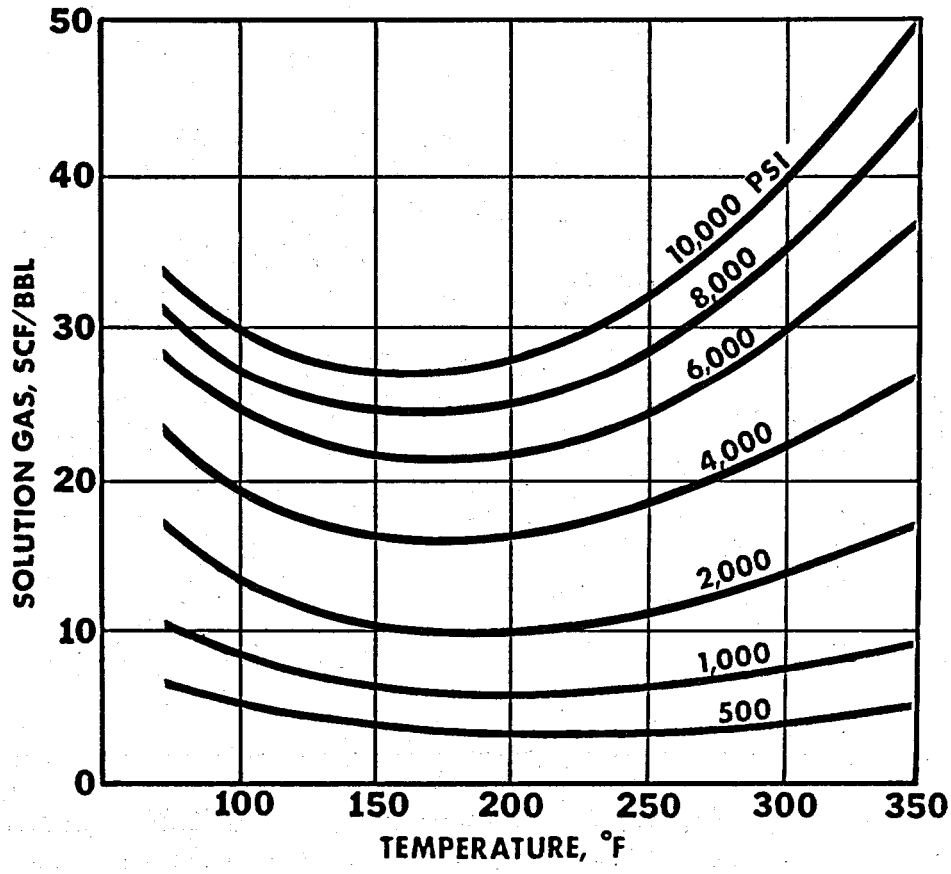

Figure 58. Solubility of methane in fresh water.

The curves shown in figure 57 indicate a direct relation between the rate of thermal diagenesis of montmorillonite and the rate of thermal maturation (generation) of hydrocarbons in a clay bed. Perhaps dissolution and removal of produced hydrocarbons from the vicinity of the maturing kerogen by water released by simultaneous clay mineral diagenesis enables kerogen conversion to continue.

The flush of water from shale source beds at the peak of the cycle of clay mineral dehydration sweeps dissolved bitumens from the source beds. The

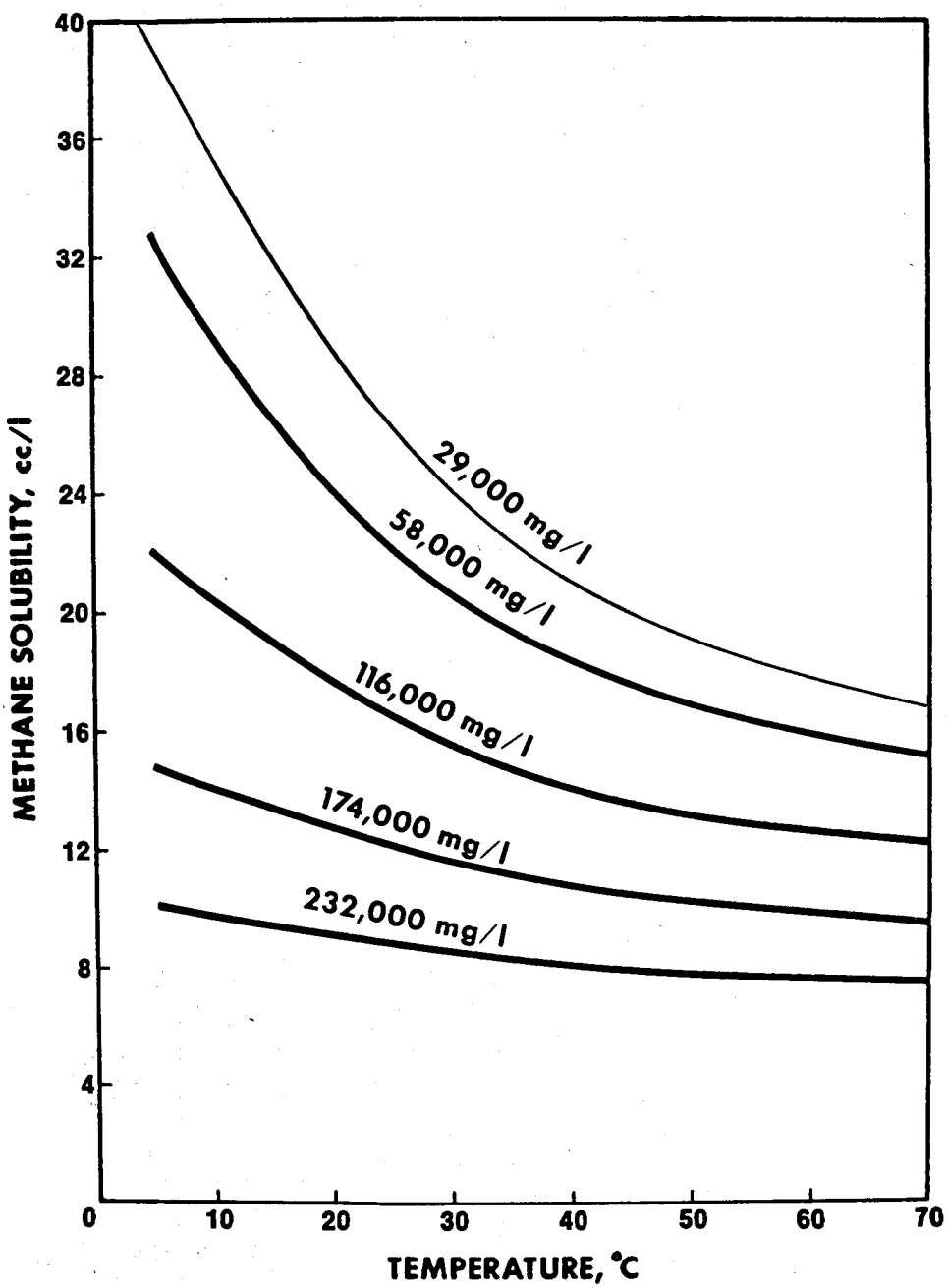

Figure 59. Solubility of methane in water as a function of salinity and temperature, at 1 atmosphere of pressure (from Mishnina, Avdeeva, & Bozkovskaya, 1961).

primary migration of petroleum hydrocarbons, to the extent that it can occur, is thus accomplished. Hydrocarbons and unaltered kerogen still trapped in the source bed are in a natural catalytic cracker and with increasing pressure and temperature they continue to break down into simpler compounds. Methane, a stable hydrocarbon gas that is very soluble in water at high temperature and pressure, is generated in enormous quantities and saturates the water in the geopressure zone. The solubility of methane in fresh water at pressures ranging up to 703 kg/cm^2 (10,000 psi) and temperatures ranging up to 177°C (350°F) is shown graphically in figure 58. Up to 50 standard cubic feet per barrel (scf/bbl) can be in solution at the maximum pressure and temperature shown on the graph.

The solubility of methane at a given pressure varies inversely with water salinity and temperature in the range from 10 to 70°C, as shown on the graphs in figure 59. Data on solubilities at higher temperatures and pressures are not available.

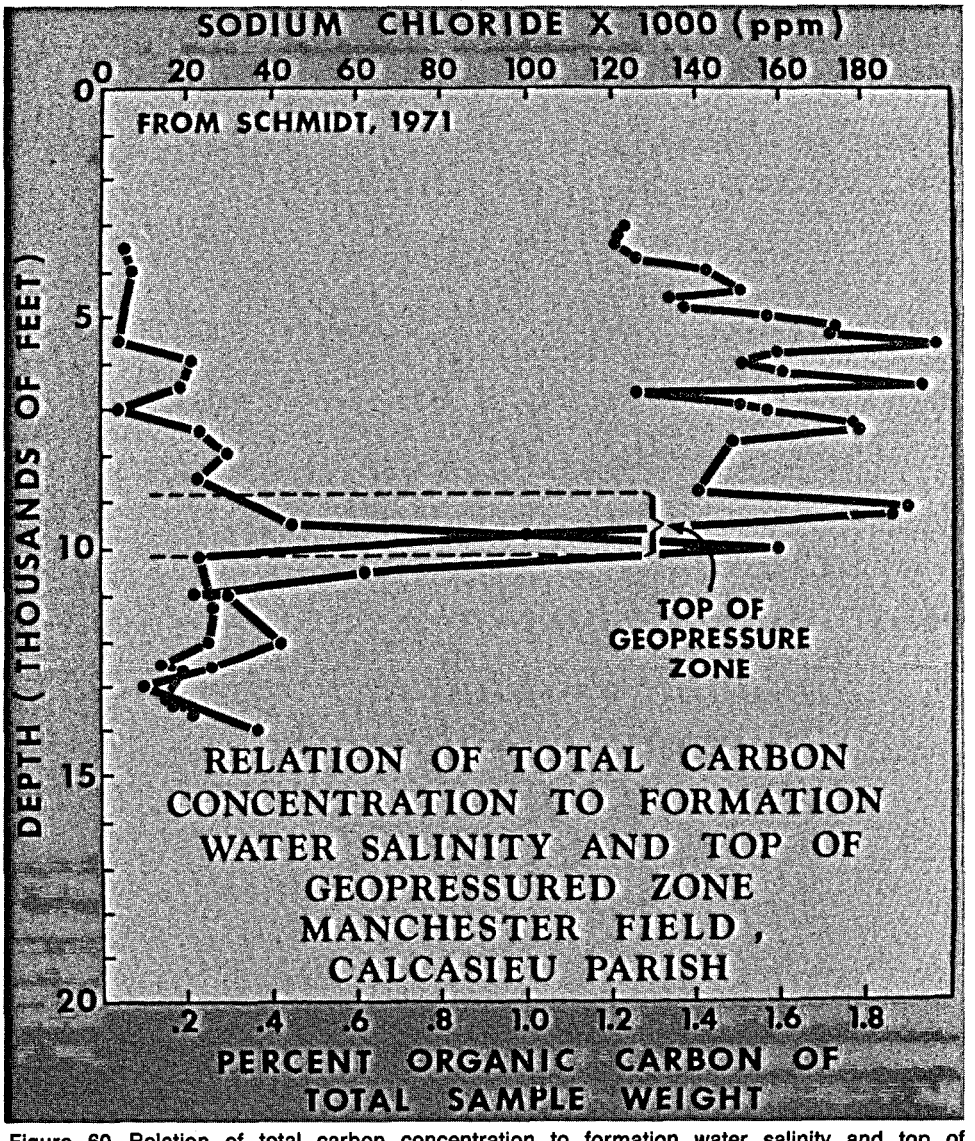

Figure 60. Relation of total carbon concentration to formation water salinity and top of geopressured zone, Manchester Field, Calcasieu Parish, Louisiana.

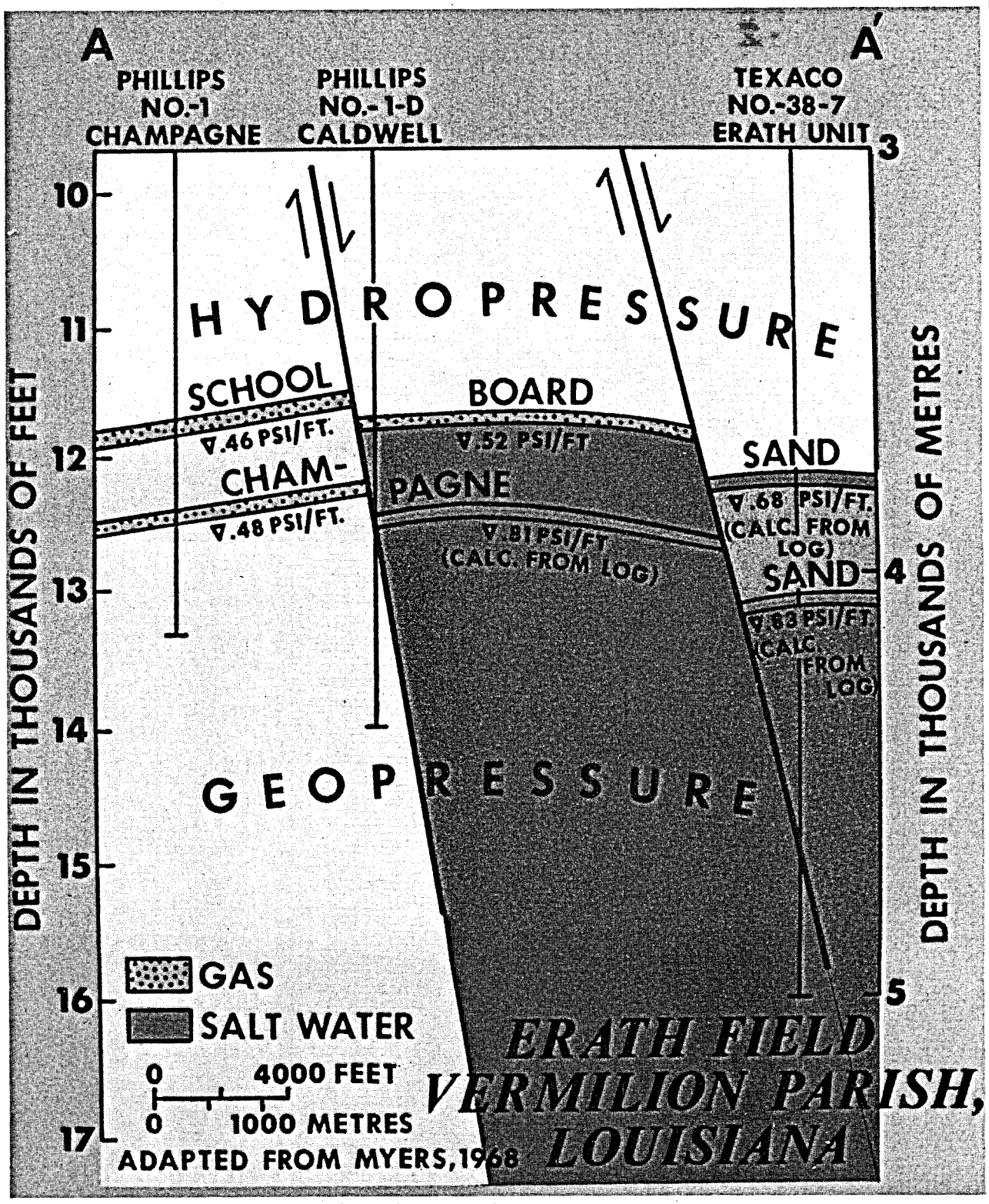

Figure 61. Relation of pressure drop near the top of the geopressure zone to the occurrence of commercial accumulations of natural gas in Vermilion Parish, Louisiana.

Petroleum hydrocarbons in water solution in the geopressure zone move with the water to avenues of escape through the overlying clay-bed seal, or growth faults, which cut through the seal. Water escaping upward through the clay-bed seal carries hydrocarbons into its basal part where they are trapped and accumulated, as shown in figure 60. Clay beds form excellent hydrocarbon seals in the Gulf basin, where oil and gas lie beneath such seals.

Petroleum hydrocarbons in water solution move with the water up fault planes into the transition zone between the geopressure zone and the overlying hydropressure zone. As the water enters sand beds cut by the fault, pressure drop causes dissolved hydrocarbons to come out of solution. If a structural trap is present along the flow path, a commercial accumulation of hydrocarbon fluid may be formed, as shown in figure 61.

The relationship of temperature and pressure decline in waters escaping from the geopressure zone, and the occurrence of commercial accumulations of oil and gas in the northern Gulf of Mexico basin is shown in figure 62. Timko

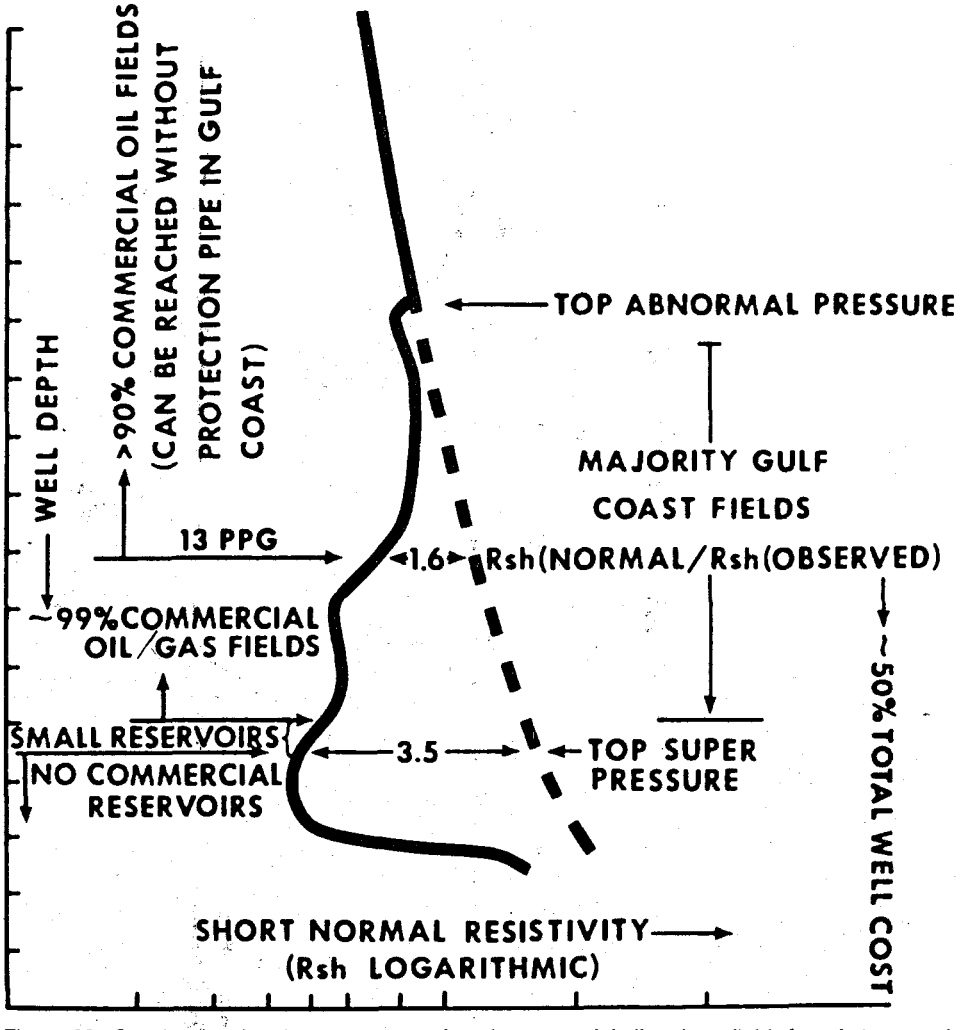

Figure 62. Graphs showing the percentage of total commercial oil and gas fields found at reservoir pressures resulting from gradients ranging from 0.50 to 0.68 psi/ft, and how these relate to the shale resistivity ratio (from Fertl & Timko, 1973),

and Fertl (1973) assert that 99 percent of the commercial oil and gas fields occurred (when discovered) in reservoirs at pressures resulting from gradients less than 0.68 psi/ft and that the majority of Gulf Coast oil and gas fields occurred (when discovered) at pressures resulting from gradients between 0.50 and 0.68 psi/ft. Exsolution of fluid hydrocarbons from water in this zone of pressure and temperature decline, and entrapment in the first favorable structure, fits this model very well.

A statistical study by Burst (1969), the results of which are shown in figure 63, identifies the depth at which the thermal diagenesis of montmorillonite occurs as the controlling factor of the depth of commercial oil-producing zones in the Gulf Coastal Plain. The elements of Gulf basin geology described above tend to support Burst's conclusion, and real data now available define the parameters that control the processes of maturation, primary migration in water solution,

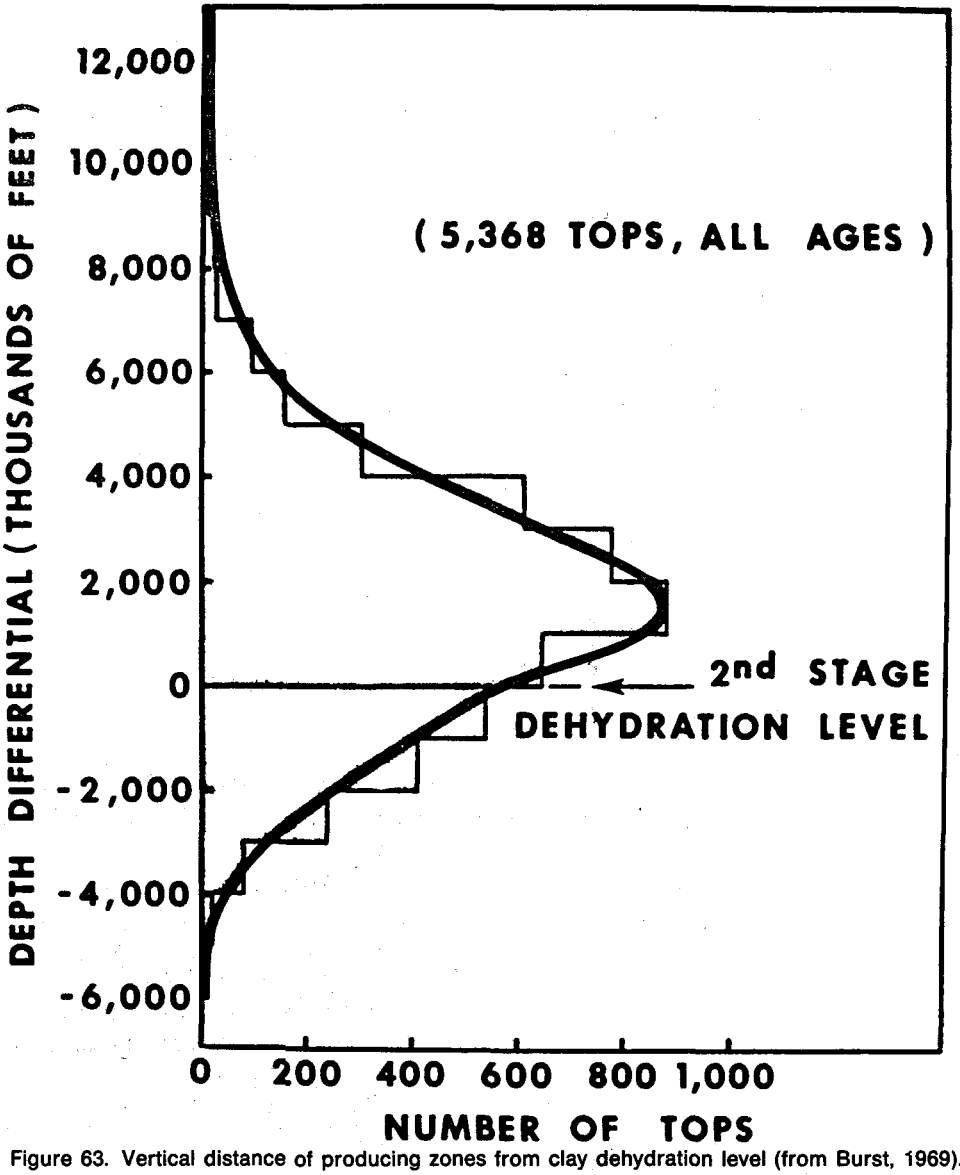

Figure 63. Vertical distance of producing zones from clay dehydration level (from Burst, 1969).

movement to areas of escape from the geopressure zone, escape and exsolution in the zone of transition from geopressure to hydropressure, and entrapment in favorable structures. All regimes described above—hydrodynamic, hydrothermal, hydrochemical, and hydrocarbon—play their parts in this process within the framework of sediment facies and geologic structure.

SUMMARY

The energy resources of the northern Gulf of Mexico basin—petroleum hydrocarbon and geothermal waters—are both derived from clay by the thermal metamorphism of two mineral components. This metamorphism occurs in the same temperature range, producing a solvent (fresh water) and a solute (petroleum hydrocarbons) that immediately become a solution. The metamorphism drastically reduces the load-bearing strength of the clay bed. The excess pore fluid is expelled or shares the overburden load. But Pascal's law states that pressure applied to an enclosed fluid is transmitted equally in all directions without loss, and exerts equal force on equal areas. The confining pressure decreases most rapidly upward, and the system in which the clay bed occurs drains in the direction of pressure release.

As solvent and solute move together out of the clay bed and through sand beds and fault planes in the direction of pressure release, pressure and temperature drop so low that the solute hydrocarbon can no longer remain in the solvent water. Fluid hydrocarbons then appear as a separate phase and, being less dense than water, seek the high points in the regional flow system—the structural traps.

Knowledge of hydrodynamic, hydrothermal, and hydrochemical regimes enables prediction of likely places for commercial accumulations of fluid hydrocarbons. This predictive capability lays the basis for a new method of exploration for oil and gas. Maps of geologic structure and sediment type supplemented by isothermal, isosaline, and isopressure maps describe important features of the fluid hydrocarbon regime and of the geothermal energy resources as well.

REFERENCES

Alger, R. P., Interpretation of electric logs in fresh water wells in unconsolidated formations: Schlumberger Well Surveying Corp., Houston, Texas, 25 p.

Anand, J., Somerton, W. H., and Gomaa, E., 1973, Predicting thermal conductivities of formations from other known properties: Jour. Petroleum Technology, Oct. 1973, p. 267-273.

Anderson, Don L., 1971, The San Andreas fault: Scientific American, Nov. 1971, p. 143-157.

Balk, R., 1949, Structure of Grand Saline salt dome, Van Zandt County, Tex.: Am. Assoc. Petroleum Geologists Bull., v. 33, no. 11, p. 1791-1829.

_____, 1953, Salt structure of Jefferson Island salt dome, Iberia and Vermilion Parishes, La.: Am Assoc. Petroleum Geologists Bull., v. 37, no. 11, p. 2455-2474.

Barton, D. C., Ritz, C. H., and Hickey, Maude, 1933, Gulf Coast geosyncline: Am. Assoc. Petroleum Geologists Bull., v. 17, p. 1446-1458.

Berg, J. W., Jr., 1952, Conductivity study of Aqueous Kaolin NaDl mixtures: Producers Monthly 16, Jan. 1952, p. 36-41.

Binder, C. R., 1965, Electron spin resonance: its application to the study of thermal and natural histories of organic sediments: Ph.D. thesis, Penn. State Univ., Univ. Park, Pa., 129 p.

Bogomolov, Y. G., 1967, Geotemperature regime: Int. Assoc. Scientific Hydrology Bull., Dec., p. 86-91.

Boyd, D. R., and Dyer, B. F., 1964, Frio barrier bar system of South Texas: Trans. Gulf Coast Assoc. Geol. Societies, v. 14, p. 309-322.

Bruce, C. H., 1973, Pressured shale and related sediment deformation: mechanism for development of regional contemporaneous faults: Am. Assoc. Petroleum Geologists Bull., v. 57, p. 878-886.

Bullard, Sir Edward, 1971, The origin of the oceans: Scientific American, Sept. 1971, p. 88-97.

Burst, J. F., 1969, Diagenesis of Gulf Coast clayey sediments and its possible relation to petroleum migration: Am. Assoc. Petroleum Geologists Bull. 53, no. 1, p. 73-93.

Clabaugh, P. S., 1962, Petrofabric study of deformed salt: Science, v. 136, no. 3514, p. 389-391.

Cordell, R. J., 1972, Depths of oil origin and primary migration: a review and critique: Am. Assoc. Petroleum Geologists Bull., V. 56, p. 2029-2067.

_____,1974, Depth of oil origin and primary migration: a review and critique: Discussion, Am. Assoc. Petroleum Geologists Bull., v. 58, no 1, p. 151-154.

Dickey, Parke A., 1966, Patterns of chemical composition in deep subsurface waters: Am. Assoc. Petroleum Geologists Bull., v. 50, p. 2472-2478.

Dickinson, George, 1953, Reservoir pressures in Gulf Coast Louisiana: Am. Assoc. Petroleum Geologists Bull., v. 37, p. 410-432.

Dietz, Robert S., and Holden, John C., 1970, The breakup of Pangaea: Scientific American, Oct. 1970, p. 124-132.

Fertl, Walter H. and Timko, Donald J., How downhole temperatures, pressures affect drilling, reprinted from June 1972-March 1973 from World Oil, A Gulf Publishing Company Publication, Copyright 1973.

Garrison, Louis E., and Martin, Ray G., Jr., 1973, Geologic structures in the Gulf of Mexico basin: U.S. Geol. Survey Prof. Paper 773, p. 1-29.

George, Rush, 1959, Approximate formation pressure from resistivity logs in south Louisiana: Schlumberger Well Surveying Corp., New Orleans, La., (log interpretation chart).

Hanna, Marcus, 1958, Salt-dome structures: Gulf Oil Corp. Manual, 45 p., 34 figs.

Hardin, George C., Jr., 1961, Subsurface geology, *in* "Geology of Houston and Vicinity, Texas," Houston Geol. Soc., p. 21-26.

_____, 1962, Notes on Cenozoic sedimentation in the Gulf Coast geosyncline, U.S.A., *in* "Geology of the Gulf Coast and Central Texas," Houston Geol. Soc. Guidebook, 1.

Hill, H. J., and Milburn, J. D., 1956, Effect of clay and water salinity on electrochemical behavior of reservoir rocks: Petroleum Trans. AIME, v. 207, p. 65-72.

Hottman, C. E., and Johnson, R. K., 1965, Estimation of formation pressure from log-derived shale properties, J. Petrol. Tech. 17, p. 717-722.

Hunt, J. M., 1968, How gas and oil form and migrate: World Oil, Oct., p. 140, 145, 148-150.

Joffé, A. F., 1928, The physics of crystals: L. B. Loeb, ed.; MGraw-Hill, New York, 198 p.

Jones, P. H., 1969, Hydrology of Neogene deposits in the northern Gulf of Mexico basin: Bull. Louisiana Water Resour. Res. Inst., GT-2.

_____, 1969b, Hydrodynamics of geopressure in the northern Gulf of Mexico basin: Jour. Petroleum Technology, v. 21, p. 803-810.

Jones, Paul H. and Wallace, Raymond H., Jr., 1974, Hydrogeologic aspects of structural deformation in the northern Gulf of Mexico basin: Jour. of Research, U.S. Geol. Survey, Sept-Oct. 1974, p. 511-517.

Kehle, R. O., 1971, Geothermal survey of North America, 1971 annual progress report: unpublished duplicated report, Research Committee, Am. Assoc. Petroleum Geologists, Tulsa, Okla., 31 p.

Keller, G. V., 1952, The role of clays in the electrical conductivity of the Bradford Sand: Producers Monthly 15, p. 23-28.

Langseth, M. G., 1965, Techniques of measuring heat flow through the ocean floor: Terrestrial Heat Flow, Geophys. Monograph 8, AGU (1965), p. 58-77.

LaPlante, R. E., 1972, Petroleum generation in Gulf Coast tertiary sediments: Am. Assoc. Petroleum Geologists Bull., v. 56, no. 3, 635 p. (abs).

Lapwood, E. R., 1948, Convection of a fluid in a porous medium: Proc. Camb. Phil. Soc., v. 44, p. 508-521.

Lee, W. H. K., 1968, Effects of selective fusion on the thermal history of the Earth's mantle: Earth and Planetary Science Letters 4 (1968), p. 270-276.

Lehner, P., 1969, Salt tectonics and Pleistocene stratigraphy on Continental Slope of northern Gulf of Mexico: Am. Assoc. Petroleum Geologists Bull. 53, 2431 p.

Lewis, C. R., Rose, S. C., 1969, A theory relating high temperatures and overpressures: J. Soc. Petrol. Engers., SJPE 2564.

Marshall, C. E., and Krinbill, C. A., 1942, The clays as colloidal electrolytes: Jour. Phys. Chem. 46, 1077 p.

Meyerhoff, A. A. (ed), 1968, Geology of natural gas in south Louisiana, *in* "Natural Gases of North America," Mem. Amer. Ass. Petrol. Geol., 1, p. 376.

Milne, I. H., and Earley, J. W., 1958, Effect of source and environement on clay minerals: Am. Assoc. Petroleum Geologists Bull., v. 42, p. 328-338.

Moses, P. L., 1961, Geothermal gradients now known in greater detail: World Oil, v. 152, no. 6, p. 79-82.

Muehlberger, W. R., and Clabaugh, P. S., 1965, Internal structure and growth of salt domes (abs): Am. Assoc. Petroleum Geologists Bull., v. 49, no. 3, pt. 1, p. 352-353.

Murray, G. E., 1961, Geology of Atlantic and Gulf coastal province of North America: New York, Harper Brothers, 692 p.

Nichols, E. A., 1947, Geothermal gradients in Mid-Continent and Gulf Coast oil fields: Am. Inst. Min. Met. Engrs. Trans., v. 170, 44 p.

OCamb, R. D., 1961, Growth faults of south Louisiana: Gulf Coast Assoc. of Geol. Socs. Trans., v. 11, p. 139-175.

Pennebaker, E. S., 1969, The use of geophysics in abnormal pressure applications: Soc. of Exploration Geophysicists, preprint SPE-2165, 8 p., 8 figs.

Perry, E. A. and Hower, J., 1972, Late-stage dehydration in deeply buried pelitic sediments: Am. Assoc. Petroleum Geologists Bull., v. 56, no. 10, p. 2013-2021.

Philippi, G. T., 1965, On the depth time, and mechanism of petroleum generation, Geochim. et Cosmochina: Acta, v. 29, p. 1021-1049.

_____, 1968, Essentials of the petroleum formation process are organic source material and a subsurface temperature controlled chemical reaction mechanism, *in* Proceedings of the 4th International Meeting on Organic Geochemistry, Amsterdam, Sept. 16-18, 1968. p. 25-46. Oxford, Pergamon Press, 1969.

_____, 1974, Depth of oil origin and primary migration: review and critique: Discussion, Am. Assoc. Petroleum Geologists Bull.,v. 58, no. 1, p. 149-150.

Powers, M. C., 1967, Fluid release mechanisms in compacting marine mudrocks and their importance in oil exploration: Am. Assoc. Petroleum Geologists Bull. 51, p. 1240-1254.

Price, Leigh Charles, 1973, The solubility of hydrocarbons and petroleum in water as applied to the primary migration of petroleum: Ph.D. dissertation, Univ. of California, Riverside, March 1973, 298 p.

Pusey, W. C., 1973, Paleotemperatures in the Gulf Coast using the ESR-kerogen methods: Gulf Coast Assoc. Geol. Soc. Trans., v. 23, p. 195-202.

Raleigh, Cecil B., and Patterson, Charles M., 1965, The experimental deformation of serpentine and its technical implications: Jour. Geophysical Research, v. 70, p. 3965-3985.

Rubey, W. W., and Hubbert, M. K., 1959, Role of fluid pressure in mechanics of overthrust faulting, II overthrust belt in geosynclinal area of western Wyoming in light of fluid pressure hypothesis: Geol. Soc. America Bull., v. 70, p. 167-206.

Sherborne, J. E., and Newton, W. M., 1972, Factors influencing electrical resistivity of drilling muds: Petroleum Trans. AIME 1466, Jour. Petroleum Technology, March 1942.

Silverman, S. R., 1965, Investigation of petroleum origin and evolution mechanisms by carbon isotope studies, *in* Isotopic and Cosmic Chemistry, p. 92-102, Craig, H., Miller, S. L., and Wasserberg, G. J., Editors: North Holland Publishing Co., Amsterdam.

Smits, L. M. J., 1968, SP log interpretation in shaly sands: Jour. Soc. Petroleum Engineers, June 1968, p. 123-136.

Staplin, F. L., 1969, Sedimentary organic matter, organic metamorphism, and oil and gas occurrence: Bul. Can. Petrol. Geol. v. 17, no. 1, p. 47-67.

Stuart, Charles A., 1970, Geopressures, *in* Proceedings of the Second Symposium on Abnormal Subsurface Pressure, Louisiana Sate Univ., Baton Rouge, La., Jan. 1970: 121 p.

Tissot, B., et al., 1971, Origin and evolution of hydrocarbons in early Toarcian shales, Paris Basin, France: Am. Assoc. Petroleum Geologists Bull., v. 55, no. 12, p. 2177-2193.

Wallace, R. H., Jr., 1970, Abnormal pressures and potential geothermal resources in the Rio Grande embayment of Texas, *in* Proceedings of the Second Symposium on Abnormal Subsurface Pressure, La. State Univ. Baton Rouge, La.: p. 87-116.

Wallace, W. E. 1965, Application of electric log measured pressures to drilling problems and a new simplified chart for well site pressure computation: The Log Analyst, 4.

Waxman, M. H., and Smits, L. J. M., 1968, Electrical conductivities in oil-bearing shaly sands: Jour. Soc. Petroleum Engineers, June 1968, p. 107-122.

Welte, D. H., 1965, Relation between petroleum and source rock: Am. Assoc. Petroleum Geologists Bull., v. 49, no. 12, p. 2246-2268.

White, D. E., 1965, Saline waters of sedimentary rocks, *in* Fluids in Subsurface Environments: Am. Assoc. Petroleum Geologists Mem. 4, p. 342-366.

Wilhelm, Oscar, and Ewing, Maurice, 1972, Geology and history of the Gulf of Mexico: Geol. Soc. America Bull., v. 83, p. 575-600.

Winsauer, W. O., and McCardell, W. M., 1953, Ionic double-layer conductivity in reservoir rocks: Petroleum Trans. AIME, v. 198, p. 129–134.

Worzel, J. L., and Watkins, J. S., 1973, Evolution of the northern Gulf Coast deduced from geophysical data: Gulf Coast Assoc. Geol. Soc. Trans., v. 23, p. 84–91.

Zierfuss, H., and van der Vliet, G., 1956, Laboratory measurements of heat conductivity of sedimentary rocks: Am. Assoc. Petroleum Geologists Bull., v. 40, no. 10, Oct. 1956, p. 2475–2488.